













# Sentinel-6 MF validation and cross calibration activities 2024 Annual Report



Reference: CLS-ENVP-RP-25-0111

Issue: 1/3

Date: October 21, 2025

EUMETSAT Eumetsat-Allee 1, D-64295 Darmstadt, Germany

Tel: +49 6151 807-7 Fax: +49 6151 807 555 http://www.eumetsat.int

Document Reference:	CLS-ENVP-RP-25-0111
Date:	October 21, 2025
Issue	1.3

Project:	MISSION PERFORMANCE	SERVICE FOR SENTINEL-6 MISSION
Title:	Sentinel-6 MF validation and cross calibration activities	
	2024 Annual Report	
	Name	Company
Author(s):	B. Courcol	CLS
	T. Krzemien	Celad
	E. Cadier	CLS
Approved by:	M. Raynal	CNES
Application authorized by :	S. Dinardo	EUMETSAT

# **Change Log**

Version	Date	Changes
1.0	30/05/2025	First Draft
1.1	04/06/2025	Addition of the executive summary
1.2	26/06/2025	CNES review taken into account
1.3	17/10/2025	EUMETSAT review taken into account

## **Acronyms**

AMR Advanced Microwave Radiometer

**CLS** Collecte Localisation Satellites

**CMEMS** Copernicus Marine Service

**CNES** Centre National d'Etudes Spatiales

**DUACS** Data Unification and Altimeter Combination System

**DV** Default Value

**ECMWF** European Centre for Medium-range Weather Forecasting

**EUMETSAT** European Organisation for the Exploitation of Meteorological Satellites

**ESA** European Space Agency

Global Ionosphere Maps

GDR Geophysical Data Record

GMSL Global Mean Sea Level

HR High Resolution Mode, also called Synthetic Aperture Radar (SAR) or Delay Doppler

Altimetry (DDA)

**HRMR** High Resolution Microwave Radiometer

**LR** Low Resolution Mode (=LRM)

**LUT** Look-Up Table

MLE Maximum Likelihood Estimator

MQE Mean Quadratic Error

MSS Mean Sea Surface

NASA National Aeronautics and Space Administration

NOAA National Oceanic and Atmospheric Administration

NR Numerical Retracker

NTC Non Time Critical

PB Processing Baseline

**RMC** Range Migration Correction

**SAMOSA** SAR Altimetry MOde Studies and Applications

SSH Sea Surface Height

SSHA Sea Surface Height Anomaly(=SLA)

**SLA** Sea Level Anomaly(=SSHA)

SSB Sea State Bias

**STD** Standard Deviation

**SWH** Significant Wave Height

**VWM** Vertical Wave Motion

WTC Wet troposphere Correction

## **Table of Content**

1	Introduction           1.1. History	
2	Executive Summary	3
3	Processing Status 3.1. Data used	8 9
4	Data coverage and edited measurements4.1. Missing measurements	
5	Monitoring of altimeter and radiometer parameters  5.1. 20 Hz range measurements  5.2. Off nadir angle from waveform  5.3. Range  5.4. Significant wave height  5.5. Backscatter coefficient  5.6. Wind speed  5.7. Sea state bias  5.8. Ionospheric correction  5.9. Radiometer wet troposphere correction	49 51 55 59 62 66 69
6	SSH crossover analysis 6.1. Overview 6.2. Mono-mission SSH crossovers 6.3. Multi-mission SSH crossovers 6.4. Pseudo time tag bias 6.5. Transponder analysis	77 80 82
7	SSHA along-track analysis 7.1. Overview	86 88
8	Mean Sea Level trends8.1. Computation of the Mean Sea Level	<b>91</b> 91 93
9	Conclusions	95
10	References	96

# **List of Figures**

1	Percentage of available data over ocean for NTC Sentinel-6 MF LR (blue) and HR (red) per cycle over the year 2024	4
2	Mean (left) and standard deviation (right) SSHA by day for LR MLE4 (blue), LR NR (green), HR SAMOSA (red), HR NR (purple) and Jason-3 (black). Computed over the year 2024	4
3	Maps of Sentinel-6 MF SSHA difference for LR NR - LR MLE4 (top left) and HR NR - HR SAMOSA (top right), and the corresponding mean as a function of ERA 5 model SWH (bottom).	5
4	Monitoring of SSH difference at mono-mission crossover for Sentinel-6 MF LR MLE4 (blue), LR NR (green), HR SAMOSA (red), HR NR (purple) and Jason-3 (black). Mean (left) and error (right) per cycle are computed over the year 2024. Only data with  latitude  < 50 °, bathymetry < -1000 m and low oceanic variability were selected	5
5	Sentinel-6 MF - Jason-3 SSH difference at crossover: maps over year 2024 for LR MLE4 (top left), LR NR (top right), HR SAMOSA (middle left) and HR NR (middle right), and corresponding cyclic monitoring (bottom). Only data with  latitude  < 50 °, bathymetry < -1000 m and low oceanic variability were selected.	6
6	Global (left) and regional (right) MSL trends from 1993 onwards	7
7	Percentage of available data over all surfaces for both LR (blue) and HR (red) per cycle	11
8	Percentage of available data over ocean for both LR (blue) and HR (red) per cycle	12
9	Percentage of edited data over ocean for LR MLE4 (blue), LR NR (green), HR SAMOSA (red) and HR NR (purple) per day over the entire mission lifetime (left) and 2024 only (right).	13
10	Maps of average percentage of edited ocean data for LR MLE4 (top left), LR NR (top right), HR SAMOSA (bottom left) and HR NR (bottom right), computed on year 2024	15
11	Percentage of data edited on ice criterion per day over the entire mission lifetime (left) and 2024 only (right)	16
12	Percentage of data edited on threshold criteria for LR MLE4 (blue), LR NR (green), HR SAMOSA (red) and HR NR (purple) per day, for out of bounds (top) and default value (bottom) indicators over the entire mission lifetime (left) and 2024 only (right)	19
13	Percentage of data edited on range number threshold for LR MLE4 (blue), LR NR (green), HR SAMOSA (red) and HR NR (purple) per day, for out of bounds (top) and default value (bottom) over the entire mission lifetime (left) and 2024 only (right)	20
14	Maps of average percentage of data edited on range number threshold for both LR MLE4 (top left), LR NR (top right), HR SAMOSA (bottom left) and HR NR (bottom right), for out of bounds, computed on year 2024	21
15	Percentage of data edited on sigma0 number threshold for LR MLE4 (blue), LR NR (green), HR SAMOSA (red) and HR NR (purple) per day, for out of bounds (top) and default value (bottom) over the entire mission lifetime (left) and 2024 only (right)	21
16	Maps of average percentage of data edited on sigma0 number threshold for both LR MLE4 (top left), LR NR (top right), HR SAMOSA (bottom left) and HR NR (bottom right), for out of bounds, computed on year 2024	22

17	Percentage of data edited on range std threshold for both LR MLE4 (blue), LR NR (green), HR SAMOSA (red) and HR NR (purple) per day, for out of bounds (top) and default value (bottom) over the entire mission lifetime (left) and 2024 only (right)	23
18	Maps of average percentage of data edited on range std threshold for both LR MLE4 (top) and LR NR (bottom), for out of bounds (left) and default value (right), computed on year 2024.	24
19	Maps of average percentage of data edited on range std threshold for both HR SAMOSA (top) and HR NR (bottom), for out of bounds (left) and default value (right), computed on year 2024	24
20	Percentage of data edited on sigma0 std threshold for LR MLE4 (blue), LR NR (green), HR SAMOSA (red) and HR NR (purple) per day, for out of bounds (top) and default value (bottom) over the entire mission lifetime (left) and 2024 only (right)	25
21	Maps of average percentage of data edited on sigma0 std threshold for both LR MLE4 (top) and LR NR (bottom), for out of bounds (left) and default value (right), computed on year 2024.	25
22	Maps of average percentage of data edited on sigma0 std threshold for both HR SAMOSA (top) and HR NR (bottom), for out of bounds (left) and default value (right), computed on year 2024.	26
23	Percentage of data edited on sigma0 threshold for LR MLE4 (blue), LR NR (green), HR SAMOSA (red) and HR NR (purple) per day, for out of bounds (top) and default value (bottom) over the entire mission lifetime (left) and 2024 only (right)	27
24	Maps of average percentage of data edited on sigma0 threshold for both LR MLE4 (left) and LR NR (right), for out of bounds (top) and default value (bottom), computed on year 2024	27
25	Maps of average percentage of data edited on sigma0 threshold for both HR SAMOSA (left) and HR NR (right), for out of bounds (top) and default value (bottom), computed on year 2024.	28
26	Percentage of data edited on SWH threshold for LR MLE4 (blue), LR NR (green), HR SAMOSA (red) and HR NR (purple) per day, for out of bounds (top) and default value (bottom) over the entire mission lifetime (left) and 2024 only (right)	29
27	Maps of average percentage of data edited on SWH threshold for both LR MLE4 (top) and LR NR (bottom), for out of bounds (left) and default value (right), computed on year 2024	30
28	Maps of average percentage of data edited on SWH threshold for both HR SAMOSA (top) and HR NR (bottom), for out of bounds (left) and default value (right), computed on year 2024.	30
29	Percentage of data edited on wind speed threshold for LR MLE4 (blue), LR NR (green), HR SAMOSA (red) and HR NR (purple) per day, for out of bounds (top) and default value (bottom) over the entire mission lifetime (left) and 2024 only (right)	31
30	Maps of average percentage of data edited on wind speed threshold for LR MLE4 (top left), LR NR (right top), HR SAMOSA (bottom left) and HR NR (bottom right), for default value, computed on year 2024	32
31	Percentage of data edited on SSB threshold for LR MLE4 (blue), LR NR (green), HR SAMOSA (red) and HR NR (purple) per day, for out of bounds (top) and default value (bottom) over the entire mission lifetime (left) and 2024 only (right)	33
32	Maps of average percentage of data edited on SSB threshold for both LR MLE4 (top left), LR NR (top right), HR SAMOSA (bottom left) and HR NR (bottom right) for default value, computed on year 2024	33

33	Percentage of data edited on filtered ionospheric correction threshold for LR MLE4 (blue), LR NR (green), HR SAMOSA (red) and HR NR (purple) per day, for out of bounds (top) and default value (bottom) over the entire mission lifetime (left) and 2024 only (right)	34
34	Maps of average percentage of data edited on LR filtered ionospheric correction threshold for both LR MLE4 (top) and LR NR (bottom), for out of bounds (left) and default value (right), computed on year 2024	35
35	Percentage of data edited on square off nadir angle threshold for both LR MLE4 (blue) and LR NR (green) per day, for out of bounds (top) and default value (bottom) over the entire mission lifetime (left) and 2024 only (right).	36
36	Maps of average percentage of data edited on square off nadir angle threshold for both LR MLE4 (top) and LR NR (bottom), for out of bounds (left) and default value (right), computed on year 2024	36
37	Map of model dry tropospheric correction set to default value. Computed for 1 cycle of HR NTC data	37
38	Percentage of data edited on equilibrium tide threshold for LR (blue) and HR (red) per day, for out of bounds (top) and default value (bottom) over the entire mission lifetime (left) and 2024 only (right)	38
39	Percentage of data edited on ocean tide threshold for LR (blue) and HR (red) per day, for out of bounds (top) and default value (bottom) over the entire mission lifetime (left) and 2024 only (right).	39
40	Maps of average percentage of data edited on ocean tide threshold for LR (left) and HR (right), for default value, computed on year 2024	39
41	Percentage of data edited on wet tropospheric correction threshold for LR (blue) and HR (red) per day, for out of bounds (top) and default value (bottom) over the entire mission lifetime (left) and 2024 only (right)	40
42	Maps of average percentage of data edited on radiometer wet tropospheric correction threshold, for out of bounds (left) and default value (right), computed on year 2024	40
43	Percentage of data edited on SSH threshold for LR MLE4 (blue), LR NR (green), HR SAMOSA (red) and HR NR (purple) per day, for out of bounds (top) and default value (bottom) over the entire mission lifetime (left) and 2024 only (right)	41
44	Maps of average percentage of data edited on SSH threshold for LR MLE4 (left), LR NR (right), for default value, computed on year 2024	41
45	Percentage of data edited on SLA threshold for LR MLE4 (blue), LR NR (green), HR SAMOSA (red) and HR NR (purple) per day, for out of bounds (top) and default value (bottom) over the entire mission lifetime (left) and 2024 only (right)	42
46	Maps of average percentage of data edited on SLA threshold for both LR MLE4 (top) and LR NR (bottom), for out of bounds (left) and default value (right), computed on year 2024	42
47	Maps of average percentage of data edited on SLA threshold for both HR SAMOSA (top) and HR NR (bottom), for out of bounds (left) and default value (right), computed on year 2024.	43
48	Mean number of 20Hz range measurements for LR MLE4 (blue), LR NR (green), HR SAMOSA (red) and HR NR (purple) per day, in Ku-band (left) and C-band (right, LR MLE3 only)	46

49	Centred maps of mean number of 20Hz range measurements. Top: maps for Sentinel-6 MF LR Ku band (left: MLE4, right: NR), middle: maps for Sentinel-6 MF HR (left: SAMOSA, right: NR), bottom: map for Jason-3 Ku band. Computed on year 2024	46
50	Centred maps of mean number of 20Hz range measurements in C band for Sentinel-6 MF (left) and Jason-3 (right)	47
51	Mean STD of 20Hz range measurements for LR MLE4 (blue), LR NR (green), HR SAMOSA (red) and HR NR (purple) per day, in Ku-band (left) and C-band (right, LR MLE3 only, in blue).	47
52	Maps of mean STD of 20Hz range measurements for Ku-band LR MLE4 (top left), LR NR (top right), HR SAMOSA (middle left), HR NR (middle right) and C band (bottom). Computed on year 2024	48
53	Mean square off nadir angle per day for LR MLE4 (blue) and LR NR (green)	49
54	Map of mean square off nadir angle for LR MLE4 (left) and LR NR (right). Computed on year 2024.	49
55	Square off nadir angle wrt SWH for MLE4 (blue) and NR (green)	50
56	Histogram of square off nadir angle for Sentinel-6 MF MLE4 (blue), NR (green) and Jason-3 (black).	50
57	HR SAMOSA - LR MLE4 (black) and HR NR - LR NR (grey) differences in range per day	51
58	HR SAMOSA - LR MLE4 (black) and HR NR - LR NR (grey) range differences as a function of ERA5 model SWH	51
59	Maps of HR SAMOSA - LR MLE4 difference in range, for ascending tracks (top left) and descending tracks (top right). Bottom left: difference of the two maps above. Bottom right: along-track wind from model. Computed on year 2024	52
60	Maps of HR NR - LR NR difference in range, for ascending tracks (top left) and descending tracks (top right). Bottom left: difference of the two maps above. Bottom right: along-track wind from model. Computed on year 2024.	52
61	Histogram of HR SAMOSA - LR MLE4 (blue) and HR NR - LR NR (red) differences in range.	53
62	Time monitoring of Sentinel-6 MF LR NR - LR MLE4 (blue) and HR NR - HR SAMOSA (red) range difference per cycle, for the mean (left) and the standard deviation (right)	53
63	HR-LR differences for Ku-band range for HR NR - HR SAMOSA (top left) and LR NR - LR MLE4 (top right). Bottom: difference with respect to ERA5 SWH	54
64	Maps of mean SWH for Ku band LR MLE4 (top left), LR NR (top right), HR SAMOSA (middle left), HR NR (middle right) and C band (bottom). Computed in the year 2024	55
65	Top: Histogram of Ku-band SWH for Sentinel-6 MF LR MLE4 (blue), LR NR (green), HR SAMOSA (red), HR NR (purple) and Jason-3 (black). Bottom: daily monitoring of SWH mean in Ku-band (left) and C-band (right)	56
66	HR-LR differences for Ku-band SWH for SAMOSA - MLE4 (black) and NR (grey). Top left: mean per cycle over side B, top right: mean per day over 2024. Bottom: difference with respect to ERA5 SWH	57

67	HR-LR NR Ku-band SWH difference. Top left: map for HR NR without VWM correction. Top right: map for HR NR with VWM correction. Bottom: corresponding curves with respect to ERA5 SWH in black and red respectively and for HR SAMOSA in blue. Computed over 1 month of F09 data.	57
68	Ku-band SWH differences for LR NR - LR MLE4 (blue) and HR SAMOSA - HR NR (red). Top left: mean per cycle over side B, top right: mean per day over 2024. Bottom: difference with respect to ERA5 SWH	58
69	Cyclic mean of the altimeter minus ERA5 model SWH difference for LR MLE4 (blue), LR NR (green), HR SAMOSA (red) and HR NR (purple). Computed over side B	58
70	Daily monitoring of Sigma0 mean in Ku-band (left) for Sentinel-6 MF LR MLE4 (blue), LR NR (green), Sentinel-6 MF HR (red) and Jason-3 (black) and C-band (right)	59
71	Maps of mean sigma0 for Ku-band LR MLE4 (top left), LR NR (top right), HR SAMOSA (middle left), HR NR (middle right) and C band (bottom). Computed on year 2024	60
72	Monitoring of the LR NR - MLE4 (blue) and HR NR - SAMOSA (red) sigma0 differences per day, over 2024 (left) and since F09 update (right)	61
73	Daily monitoring of the HR SAMOSA - LR MLE4 (black) and HR NR - LR NR (grey) sigma0 difference, over 2024 (left) and since F09 update (right)	61
74	Maps of mean wind speed for LR MLE4 (top left), LR NR (top right), HR SAMOSA (middle left), HR NR (middle right) and Jason-3 (bottom). Computed on year 2024	62
75	Mean (left) and standard deviation (right) wind speed per day for LR MLE4 (blue), LR NR (green), HR SAMOSA (red), HR NR (purple) and Jason-3 (black).	63
76	Histogram of wind speed for Sentinel-6 MF LR MLE4 (blue), LR NR (green), HR SAMOSA (red), HR NR (purple) and Jason-3 (black). Computed over 2024	63
77	Monitoring per day (top left), correlation to model SWH (top right) and maps (bottom panels) of the LR NR - MLE4 and HR NR - SAMOSA wind speed differences.	64
78	Mean (left) and standard deviation (right) HR SAMOSA - LR MLE4 (black) and HR NR - LR NR (grey) wind speed difference per day.	64
79	Mean per cycle over side B (left) and per day over 2024 only (right) wind speed difference wrt model for LR MLE4 (blue), LR NR (green), HR SAMOSA (red), HR NR (purple) and Jason-3 (grey)	65
80	Maps of mean SSB for LR MLE4 (top left), LR NR (top right), HR SAMOSA (middle left), HR NR (middle right) and Jason-3 (bottom). Computed on year 2024.	66
81	Top: Histogram of Ku-band SSB for Sentinel-6 MF LR MLE4 (blue), LR NR (green), HR SAMOSA (red), HR NR (purple) and Jason-3 (black), over 2024. Bottom: daily monitoring of SSB mean in Ku-band (left) and C-band (right).	67
82	Monitoring per day (top left), correlation to model SWH (top right) and maps (bottom panels) of the LR NR - MLE4 and HR NR - SAMOSA SSB differences	68
83	Mean (left) and standard deviation (right) HR-LR MLE4 SSB difference per day	68
84	Monitoring of filtered ionospheric correction for Sentinel-6 MF LR MLE4 (blue), LR NR (green) and Jason-3 (black). Left: Mean per day. Right: Histogram computed 2024	69

85	Maps of mean filtered ionospheric correction for Sentinel-6 MF LR MLE4 (left) and LR NR (right). Computed on year 2024	69
86	Time monitoring of the NR - MLE4 filtered ionospheric correction difference per day in cm	70
87	Mean per cycle over side B (left) and per day over 2024 only (right) filtered iono - GIM iono for Sentinel-6 MF LR MLE4 (blue), LR NR (green) and Jason-3 (black)	70
88	Maps of mean filtered ionospheric correction - GIM iono for Sentinel-6 MF LR MLE4 (left), LR NR (right) and Jason-3 (bottom). Computed on year 2024	71
89	Maps of mean brightness temperature for channels 18.7 GHz (top left), 23.8GHz (top right), 34.0GHz(bottom left) in K and mean wet tropospheric correction (bottom right) in m. Computed on year 2023.	72
90	Histogram of wet tropospheric correction in m for Sentinel-6 MF (blue) and Jason-3 (black) computed over 2024	73
91	Mean (left) and standard deviation (right) HRMR+AMR wet troposhperic correction - ECMWF model per day for Sentinel-6 MF (blue) and Jason-3 (black)	74
92	Maps of mean HRMR+AMR wet troposhperic correction - ECMWF model for Sentinel-6 MF (left) and Jason-3 (right)	74
93	Mean (HRMR+AMR) - AMR wet tropospheric correction difference per day for Sentinel-6 MF in m. Right panel: computed for open ocean (distance to coast larger than 200 km) in dark blue, and for coastal measurement (distance to coast smaller than 200 km) in light blue	75
94	Map of mean (HRMR+AMR) - AMR wet tropospheric correction difference for Sentinel-6 MF in mm	75
95	Variance of SSHA computed with HRMR+AMR derived WTC minus variance of SSHA computed with AMR derived WTC, as a function of the distance from the coast for Sentinel-6 MF in $mm^2$	76
96	Mean SSH differences at crossovers by cycle for Sentinel-6 MF LR MLE4 (blue), LR NR (green), HR SAMOSA (red) and HR NR (purple) and Jason-3 (black). Computed on year 2024.	77
97	Error of SSH differences at crossovers by cycle for Sentinel-6 MF LR MLE4 (blue), LR NR (green), HR SAMOSA (red) and HR NR (purple) and Jason-3 (black). Computed on year 2024.	78
98	Mean (left) and error (right) SSH differences at crossovers by cycle for Sentinel-6 MF LR MLE4 (blue), LR NR (green), HR SAMOSA (red) and HR NR (purple) and Jason-3 (black), using model wet tropospheric correction. Computed on year 2024	78
99	Maps of mean SSH differences at mono-mission crossovers in m for LR MLE4 (top left), LR NR (top right), HR SAMOSA (bottom left) and HR NR (bottom right) computed on year 2024.	79
100	Mean multimission SSH differences at crossovers by cycle for Sentinel-6 MF LR MLE4/Jason-3 (blue), LR NR/Jason-3 (green), HR SAMOSA/Jason-3 (red) and HR NR/Jason-3 (purple). Computed on year 2024	80
101	STD multimission SSH differences at crossovers by cycle for Sentinel-6 MF LR MLE4/Jason-3 (blue), LR NR/Jason-3 (green), HR SAMOSA/Jason-3 (red) and HR NR/Jason-3 (purple). Computed on year 2024.	80

102	Mean (left) and standard deviation (right) of multimission SSH differences at crossovers by cycle for Sentinel-6 MF LR MLE4 / Jason-3 (blue), LR NR / Jason-3 (green), HR SAMOSA/Jason-3 (red) and HR NR/Jason-3 (purple). Computed on year 2024 using model WTC for SSH	
103	Maps of multimission mean SSH differences at crossovers for LR MLE4/Jason-3 (top left), LR NR/Jason-3 (top right), HR SAMOSA (bottom left) and HR NR (bottom right) computed on year 2024	81
104	Pseudo time tag bias by cycle for LR MLE4 (blue), LR NR (green), HR SAMOSA (red) and HR NR (purple). Computed on year 2024	82
105	Monitoring of the range bias at CDN1 transponder, up to cycle 152	83
106	Monitoring of the datation bias at CDN1 transponder, up to cycle 152	83
107	Histograms of SSHA in m for Sentinel-6 MF LR MLE4 (blue), LR NR (green), HR SAMOSA (red), HR NR (purple) and Jason-3 (black).	84
108	Mean (left) and standard deviation (right) SSHA by day for LR MLE4 (blue), LR NR (green), HR SAMOSA (red), HR NR (purple) and Jason-3 (black).	85
109	Mean (left) and standard deviation (right) SSHA with wet tropospheric correction from model by day for LR MLE4 (blue), LR NR (green), HR (red) and Jason-3 (black)	85
110	Time monitoring of Sentinel-6 MF LR NR - LR MLE4 SSHA in meters, without the Caspian Sea. Left: mean per cycle, Right: standard deviation per cycle	86
111	Map of Sentinel-6 MF LR NR - LR MLE4 SSHA in meters (left), and its mean as a function of ERA 5 model SWH (right)	87
112	Distributions of Sentinel-6 MF LR NR - LR MLE4 SSHA difference for side B	87
113	Map of Sentinel-6 MF HR NR - HR SAMOSA SSHA in meters (left), and its mean as a function of ERA 5 model SWH (right)	88
114	Distributions of Sentinel-6 MF HR NR - HR SAMOSA SSHA difference for side B	88
115	Mean per cycle over side B (left) and per day over 2024 (right) of the HR SAMOSA - LR MLE4 (black) and HR NR - LR NR (grey) SSHA difference	89
116	Maps of mean SSHA HR SAMOSA - LR MLE4 (left panel) and HR NR - LR NR (right panel) difference in meters. Computed on year 2024.	90
117	Global (left) and regional (right) MSL trends from 1993 onwards	92
118	GMSL from Sentinel-6 MF LR data (top left), Sentinel-6 MF HR data (top right) and from Jason-3 GDR-F data with a 1.645 sigma confidence interval. Computed over Sentinel-6 MF POS4-B period, i.e. from cycle 32 onwards	94

## **List of Tables**

1	Events on Sentinel-6 MF	9
2	List of missing passes in LR over 2024	11
3	List of missing passes in HR over 2024	11
4	Table of parameters used for editing and the corresponding percentages of edited measure-	
	ments for each parameter for Sentinel-6 MF LR and HR	18
5	Table of parameters used for the editing on the SSHA pass statistics. These parameters are	
	identical in HR and LR	44
6	Mean and error of monomission SSH crossover differences for Sentinel-6 MF LR and HR	
	and Jason-3	79
7	GMSL trend values and corresponding 1 sigma uncertainties for Sentinel-6 MF LR, HR and	
	Jason-3 (on the Sentinel-6 MF period), with radiometer and model wet tropospheric correc-	
	tions. Computed over POS4-B period, i.e. from cycle 32 onwards.	93

## 1 Introduction

Sentinel-6 is a collaborative Copernicus mission, implemented and co-funded by the European Commission, ESA, EUMETSAT and the USA through NASA and NOAA.

EUMETSAT is responsible for the Sentinel-6 operations as part of the Copernicus component of the EU Space Programme. The Sentinel-6 Quality Assessment reports are generated by CNES in the frame of a EUMETSAT CNES agreement in the context of Copernicus.

This document presents the synthesis report concerning validation activities of Sentinel-6 data for the year 2024.

## 1.1. History

Sentinel-6 MF satellite was successfully launched on the 21th of November 2020. On November 30th, its Poseidon-4 altimeter was switched on, and since December 17th 2020, Sentinel-6 MF is on its operational orbit to continue the long-term climate data record on the primary TOPEX, Jason-1, Jason-2 and Jason-3 ground track.

To calibrate both altimeters, POS4 was switched to its redundant side (POS4-B) on the 14th of September 2021. It remains in this configuration from this date onwards.

Up until April 7, 2022, Sentinel-6 MF and Jason-3 operated in tandem flight, maintaining a separation of only 30 seconds. Following this period, Jason-3 was transferred to the same interleaved orbit previously utilized by TOPEX between 2002 and 2005, Jason-1 from 2009 to 2012, and Jason-2 from 2016 to 2017.

After the tandem phase with Jason-3, Sentinel-6 MF has become the reference mission in the CMEMS multi-missions Ocean topography products.

During 2024, the most significant development for Sentinel-6 MF processors was the update of the processing baseline to version F09, which was implemented on April 13, 2024. Notably, this update introduced Numerical Retracking (NR) within the High Resolution (HR) mode.

Since the beginning of the mission, Sentinel-6 data is monitored on a cyclic frequence to assess its products' quality. Cyclic reports are available through Eumetsat website. Please note that analyses are done over ocean only, no assessment is done over hydrological targets. This encompasses several points, which are either part of Cal/Val routine activities or following mission events:

- mono-mission validation and monitoring,
- accuracy and stability of SLA measurements check,
- · specific studies and investigations.

#### 1.2. Overview

The present document assesses Sentinel-6 MF data quality and performance over ocean. After an executive summary in the next page, dedicated sections of this report deal with:

- · description of data processing,
- · data coverage / availability,
- · monitoring of rejected spurious data,
- analysis of relevant parameters derived from instrumental measurements and geophysical corrections,
- · system performance via analyses at crossover points,
- system performance via along-track Sea Level Anomalies monitoring,
- · GMSL analysis.

Over all these parts, the document also presents some Sentinel-6 MF/Jason-3 cross-calibrations. However, the full tandem flight phase (November 21st 2020 to April 7th 2022) analysis can be found in the Processing Baseline F08 reprocessing CalVal assessment.

# 2 Executive Summary

Sentinel-6 MF onboard altimeter (POS4) allows for simultaneous low and high resolution observations due to its innovative design. This is referred as **interleaved mode** in which hence the instrument acquires data at same time in :

- Low Resolution Mode, hereafter "LR", which is the historical mode used by previous altimeters in the Topex/Jason satellites.
- High Resolution Mode, hereafter "HR", commonly called Synthetic Aperture Radar (SAR) or Delay Doppler Altimetry (DDA), already used on Cryosat-2 and on the Sentinel-3 satellites.

Over the year 2024, POS4 altimeter operated in Range Migration Correction and open loop tracking for most of the globe.

In April 2024, Sentinel-6 MF Processing Baseline was updated from F08 to F09 version. A detailed product notice on the changes between baselines is available at EUMETSAT's product release note. F09 major improvements benefited the HR processing, with the addition of:

- a Numerical Retracking (NR) in HR mode, which includes skewness parameter set at 0.1 (similar to Jason-3 and Sentinel-6 MF processings),
- the **range walk correction** in ALT L1 HR processing, improving the two HR retrackers retrievals (SAMOSA and NR).
- a **Vertical Wave Motion (VWM) correction** in ALT L2 HR products applied to NR Significant Wave Heights (SWH).

During each cycle, missing measurements were monitored, spurious data were edited, and relevant parameters derived from instrumental measurements and geophysical corrections were analysed. Please note that these analyses are done **over ocean** only, no assessment is done over hydrological targets. This summary focuses on the performances over the year 2024.

## 1/ Data availability

In 2024, data availability over ocean was excellent for both Sentinel-6 MF LR and HR products (figure 8), with respectively 99.99 % and 99.81 % of available data. Over this year, **no important event impacting data availability occurred.** 

#### Percentage of available points (ocean)

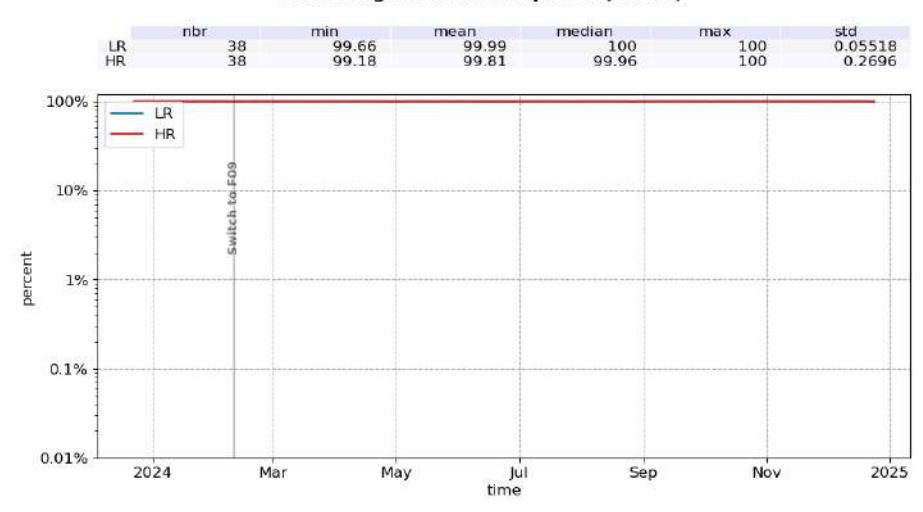


Figure 1: Percentage of available data over ocean for NTC Sentinel-6 MF LR (blue) and HR (red) per cycle over the year 2024.

#### 2/ Sea Level Anomalies

In 2024 Sentinel-6 MF and Jason-3 SSHA followed identical seasonal cycles and variations (figure 2), with mean values of 5.9 cm for Sentinel-6 MF LR MLE4, 5.5 cm for LR NR, 4.7 cm for HR SAMOSA, 5.7 cm for HR NR and 3.6 cm for Jason-3. Excluding the Caspian Sea, Sentinel-6 MF SSHA daily standard deviation shows to be similar between all datasets.

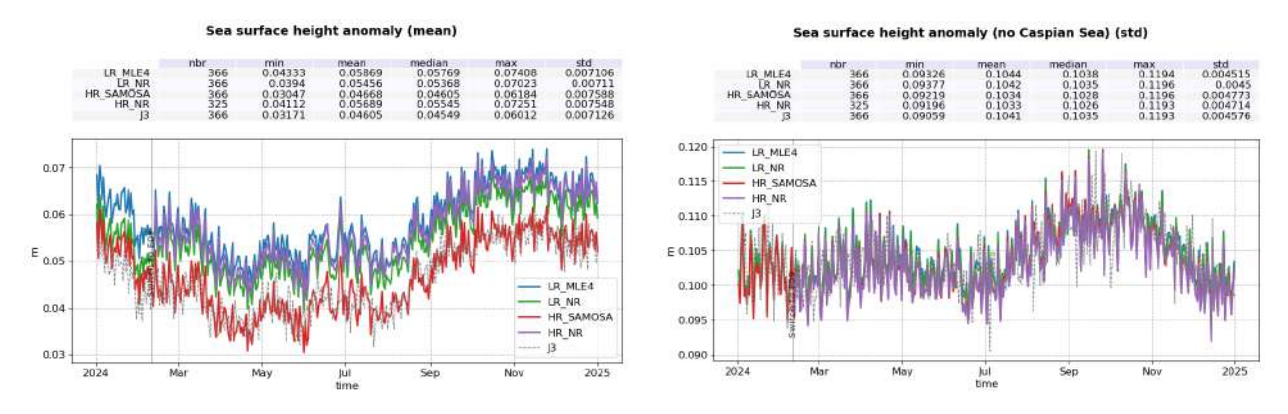


Figure 2: Mean (left) and standard deviation (right) SSHA by day for LR MLE4 (blue), LR NR (green), HR SAMOSA (red), HR NR (purple) and Jason-3 (black). Computed over the year 2024.

The comparison between LR MLE4 and LR NR SSHA, as shown in figure 3, confirms that the numerical retracker delivers notable improvements, as already cited in the previous annual report (thanks to PB F08 addition of LR NR). Still, there is a clear correlation with SWH visible in both the spatial map and the SWH-dependent curve. Unlike MLE4, the NR's outputs do not rely on instrumental LUTs. As a result, the NR results are not affected by any inaccuracies that might arise from LUT approximations, making its retrievals more robust to SWH variations.

In PB F09, HR retrievals were improved thanks to range walk and the addition of the NR. The availability of NR allows for better accountability of instrumental aging through the use of the in-flight point target response (PTR). The improvement of HR long-term stability will require further data and is not possible with 2024 results alone. In the meantime, HR NR SSHA comparison to HR SAMOSA highlights a strong correlation to sea state, and inital investigations indicate that this may be due to the absence of skewness parameter in SAMOSA. This is under investigation.

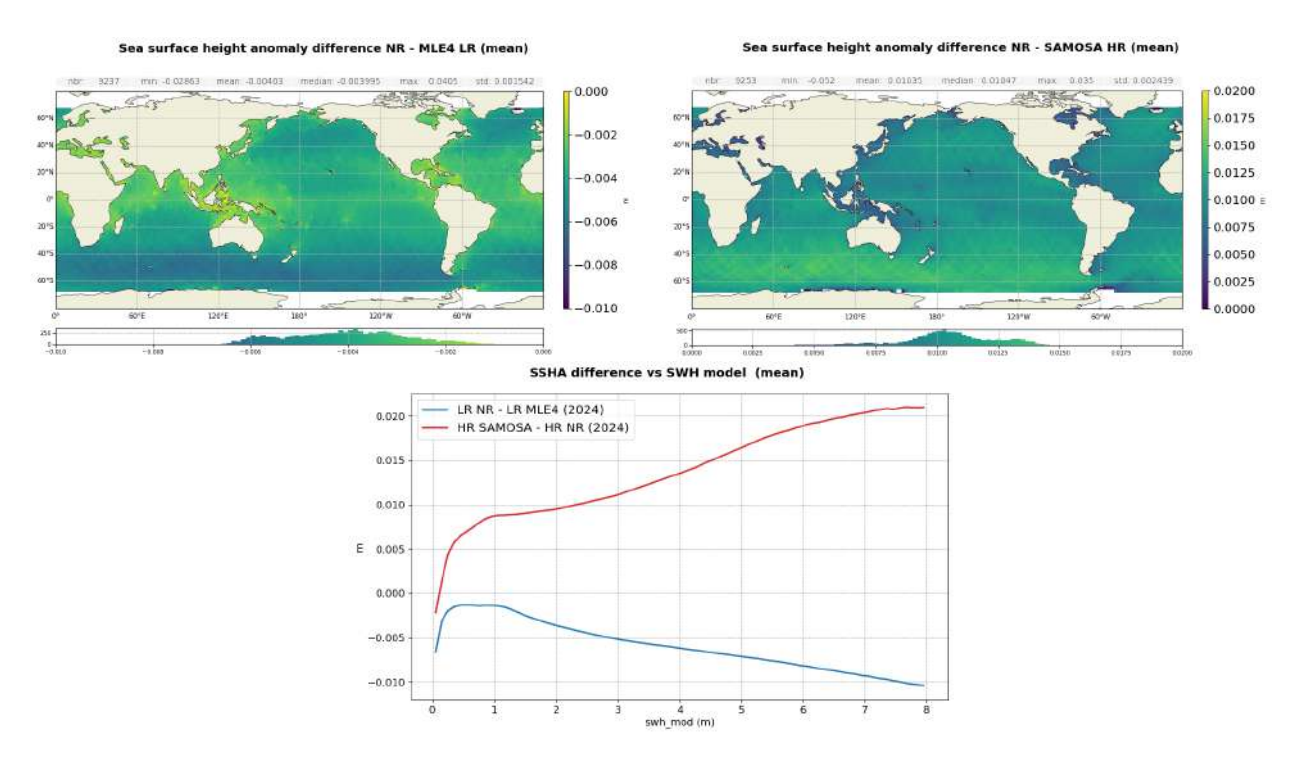


Figure 3: Maps of Sentinel-6 MF SSHA difference for LR NR - LR MLE4 (top left) and HR NR - HR SAMOSA (top right), and the corresponding mean as a function of ERA 5 model SWH (bottom).

## 3/ Performance at crossover points

Looking at SSH difference at mono-mission crossovers, mean values are well centred around 0 for all modes and retrackers (figure 4 left panel).

Concerning the SSH error at mono-mission crossovers ( $STD/\sqrt{2}$ ), Sentinel-6 MF shows very good and stable performance with an error of 3.4 cm in LR and 3.3 cm in HR, which is similar to Jason-3 error (figure 4 right panel). A slight increase is observed for Sentinel-6 MF from mid-September to mid-October due to punctual crossover points with higher SSH difference.

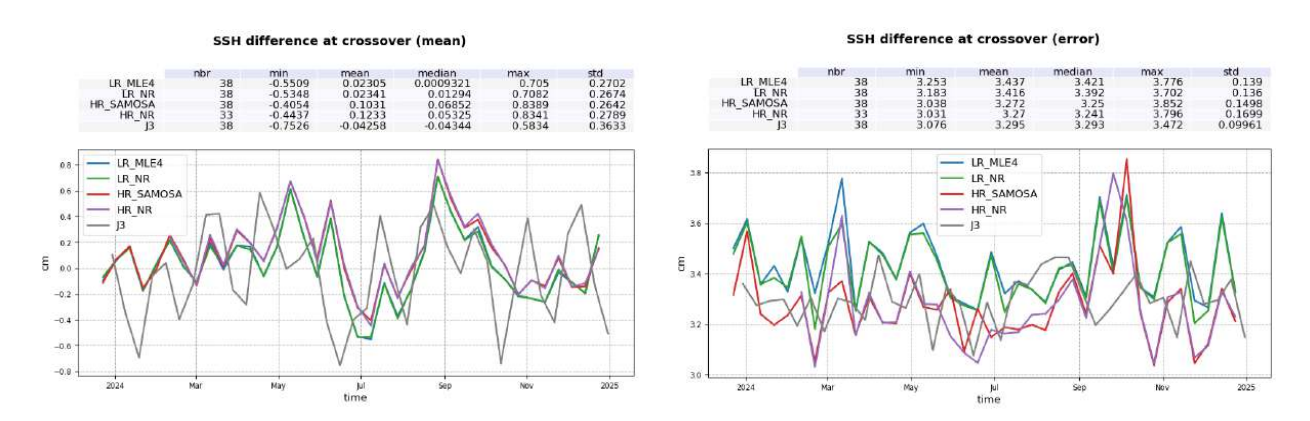


Figure 4: Monitoring of SSH difference at mono-mission crossover for Sentinel-6 MF LR MLE4 (blue), LR NR (green), HR SAMOSA (red), HR NR (purple) and Jason-3 (black). Mean (left) and error (right) per cycle are computed over the year 2024. Only data with |latitude| < 50 °, bathymetry < -1000 m and low oceanic variability were selected.

As shown in figure 4, the mean differences in sea surface height (SSH) at Sentinel-6 MF and Jason-3 crossover points exhibit consistent behavior across all four Sentinel-6 MF retrieval types throughout 2024. There is no evidence of drift or recurring patterns over the year. The observed mean SSH differences are

minimal: -1.3 cm for LR MLE4, -0.9 cm for LR NR, -0.1 cm for HR SAMOSA, and -1.2 cm for HR NR. No significant regional pattern can be seen on the corresponding maps for LR MLE4, LR NR and HR NR (figure 5 top and middle right panels). The HR SAMOSA map (middle left panel) highlights the absence of skewness parameter in the HR SAMOSA processing, leading to correlation with sea state conditions in the comparison with Jason-3. Thanks to the addition of this parameter to the HR NR processing, such patterns are not visible on the HR NR SSH comparison to Jason-3.

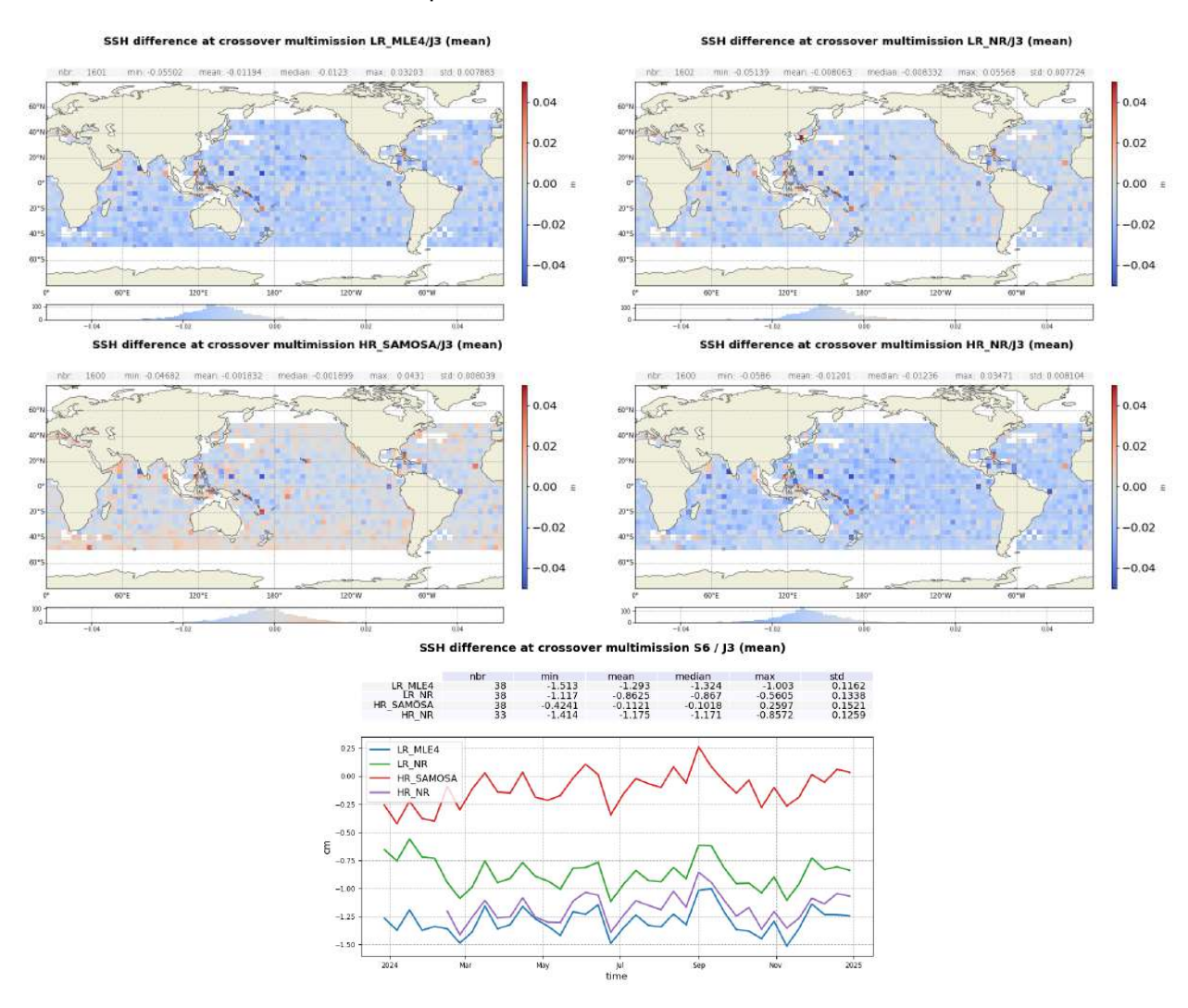


Figure 5: Sentinel-6 MF - Jason-3 SSH difference at crossover: maps over year 2024 for LR MLE4 (top left), LR NR (top right), HR SAMOSA (middle left) and HR NR (middle right), and corresponding cyclic monitoring (bottom). Only data with |latitude| < 50 °, bathymetry < -1000 m and low oceanic variability were selected.

#### 4/ Contribution to Global Mean Sea Level

Regional and global biases between missions have to be precisely estimated in order to ensure the quality of the reference GMSL series as seen on Figure 6. For more details, see the dedicated section on AVISO+ website<sup>1</sup>.

Sentinel-6 MF GMSL may be impacted by two known effects:

- The instrumental aging consisting in the evolution of the PTR shape in range direction. It impacts both
  range and SWH estimates in the analytical models as is the case of LR MLE4 and HR SAMOSA. Note
  that numerical models account for the in-flight instrument aging and hence they are not affected at all
  by these impacts.
- The evolution of the PTR shape in the azimuth direction, impacting the range variations within a burst, in HR only. It is corrected thanks to the range walk correction, that is available in PB F09.

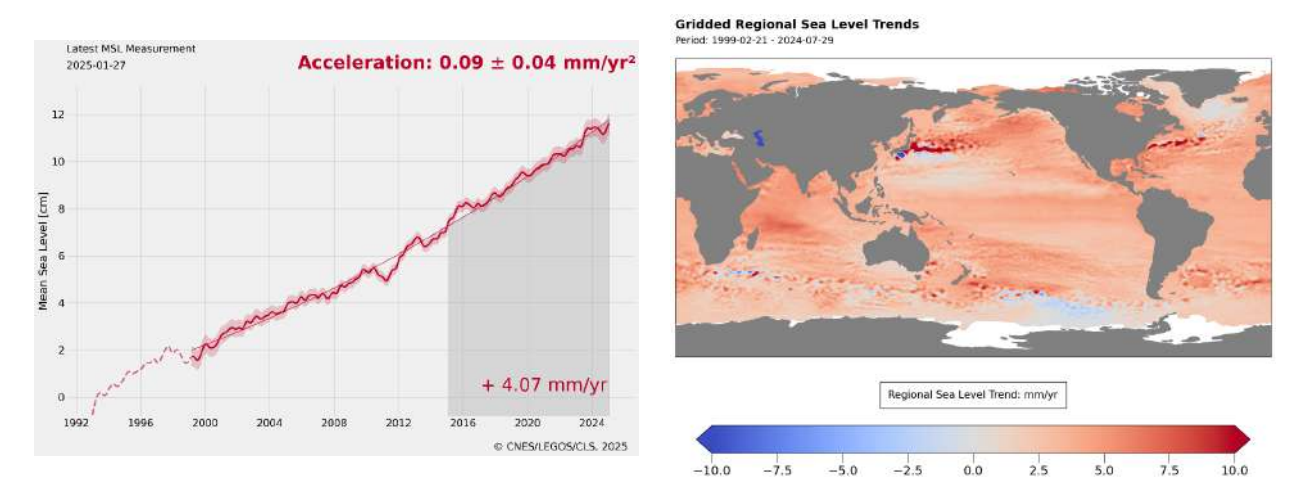


Figure 6: Global (left) and regional (right) MSL trends from 1993 onwards.

<sup>&</sup>lt;sup>1</sup>https://www.aviso.altimetry.fr/en/data/products/ocean-indicators-products/mean-sea-level.html

## 3 Processing Status

#### 3.1. Data used

#### Sentinel-6 MF

The metrics provided in this document are based on Sentinel-6 MF dataset over 2024 for L2 NTC 1Hz products. Additionally, some long-term monitoring include data that encompasses the entire POS4-B period, starting from cycle 31 pass 109 (corresponding to September 14th, 2021), or the entire mission lifetime.

Sentinel-6 MF data processing has evolved over time. Initially, from the start of the mission on December 17, 2020 through October 5, 2023 (covering cycle 107, pass 7), all data were reprocessed using the original Processing Baseline (PB) F08. Following this, from October 5, 2023 to February 10, 2024 (up to cycle 119, pass 254), a patched version of PB F08 was utilized. Beginning February 10, 2024, data have been processed with the updated PB F09. For further details about these processing baselines, please refer to section 3.4..

"Ocean" retrackers were used, being MLE4 and NR for LR mode and, for HR mode, SAMOSA and NR. A detailed description of the products can be found in the Sentinel-6 MF product notices for PB F08 [3] and F09 [5].

#### Jason-3

Comparison with Jason-3 uses L2 1 Hz GDR-F ([2]) products with MLE4 retracking on the same period as Sentinel-6 MF.

Sentinel-6 MF F08 and Jason-3 GDR-F share the same standard in terms of geophysical corrections: same tide models, same mean surface height, etc. (see [11] Appendix A for more details). In particular:

- for the wind speed, Collard algorithm is used on both missions
- for the sea state bias, Sentinel-6 MF processing uses sea state bias parametrization derived from Jason-3 GDR-F data, both in LR and in HR.

#### 3.2. List of events

The following table shows the major events that occurred over 2024.

Date start	Date end	Cycle	System	Event
21/01/2024 00:54:50	21/01/2024 00:54:50	117	AMR-C	AMR deep sky calibration
19/02/2024 15:20:46	19/02/2024 15:20:46	120	AMR-C	AMR deep sky calibration
29/02/2024 09:12:00	29/02/2024 09:18:00	121	Platform	Station keeping maneuver
19/03/2024 00:10:00	19/03/2024 00:10:00	123	AMR-C	AMR deep sky calibration
16/04/2024 19:44:03	16/04/2024 19:44:03	126	AMR-C	AMR deep sky calibration
07/05/2024 13:42	08/05/2024 05:32	128	DORIS	DORIS restart
14/05/2024 06:08:46	14/05/2024 06:08:46	129	AMR-C	AMR deep sky calibration
28/05/2024 09:45:59	28/05/2024 09:52:25	130	Platform	Station keeping maneuver
13/06/2024 18:56:23	13/06/2024 18:56:23	132	AMR-C	AMR deep sky calibration
12/07/2024 02:16:00	12/07/2024 02:16:00	135	AMR-C	AMR deep sky calibration
10/08/2024 20:13:38	10/08/2024 20:13:38	138	AMR-C	AMR deep sky calibration

10/09/2024 05:51:04	10/09/2024 05:51:04	141	AMR-C	AMR deep sky calibration	
18/09/2024 01:51:00	18/09/2024 01:59:00	142	Platform	Station keeping maneuver	
09/10/2024 16:41:14	09/10/2024 16:41:14	144	AMR-C	AMR deep sky calibration	
08/11/2024 01:52:17	08/11/2024 01:52:17	147	AMR-C	AMR deep sky calibration	
07/12/2024 19:50:52	07/12/2024 19:50:52	150	AMR-C	AMR deep sky calibration	
12/12/2024 08:04:00	12/12/2024 08:12:00	150	Platform	Station keeping maneuver	

Table 1: Events on Sentinel-6 MF.

## 3.3. Tracking and acquisition mode

Sentinel-6 MF altimeter, Poseidon-4, always operates in interleaved mode, which enables simultaneous measurements in :

- Low Resolution Mode, hereafter "LR", which is the historical mode used by previous altimeters in the Topex/Jason satellites. Please note that while Topex/Jason altimeters were acquiring data with a 2kHz PRF, Sentinel-6 LR mode uses a 9kHz PRF.
- High Resolution Mode, hereafter "HR", commonly called Synthetic Aperture Radar (SAR) or Delay Doppler Altimetry (DDA), already used on Cryosat-2 and on the Sentinel-3 satellites.

The LR and HR modes use separate retrackers (MLE4/NR and SAMOSA/NR respectively) and the resulting data are available in distinct products.

Please note that while LR products contain both Ku and C bands, there is no C band measurements in HR and therefore HR products contain only Ku band data.

Over the year 2024, POS4 altimeter operates in open loop.

## 3.4. Processing versions

Before 2024-02-10, data were processed using the processing baseline F08, which brought the addition of numerical retracker (NR) retrievals in LR products for Ku band. Numerical retracking allows accounting for the PTR shape evolution thanks to the use of in-flight PTRs. Other changes in PB F08 include an update of the antenna aperture angle from 1.33 degrees to 1.34 degrees and the update of the total electron content (TEC) computation with a more appropriate scaling factor (0.881 instead of 0.925) to align the altimeter-derived TEC with the GPS-derived JPL GIM model. More details on the PB F08 can be found in the associated product notice [3].

Data prior to 2023-10-05, displayed in some long-term monitoring, were processed with an older version of PB F08 which included an anomaly on LR NR SWH (AR 2620). Due to an implementation error, LR NR negative measurements of SWH were mapped to their absolute value at 20Hz and mixed to actual positive SWH during compression. The anomaly will be retroactively corrected during the next reprocessing campaign (G01). Thanks to the 2023 reprocessing campaign [4], performed using the unpatched PB F08, older processing baselines are no longer present in the datasets. However, this reprocessing includes an anomaly on LR NR SWH (AR 2620): LR NR negative measurements of SWH were mapped to their absolute value at 20Hz and mixed with positive estimates during compression. This error leads to an overestimation of SWH in regions where the SWH is small. This error in PB F08 was patched and thus only

impact data prior to 2023-10-05.

From 2024/02/10 (cycle 120 pass 1), Sentinel-6 MF NTC data were processed using the processing baseline F09. The main changes brought by this PB were :

- Numerical Retracking (NR) in HR mode, which includes skewness parameter set at 0.1. Please note
  that these new retracker outputs do not replace but complement SAMOSA-derived parameters: NR
  and SAMOSA retrievals are both included in HR products.
- Range walk correction in ALT L1 processing for HR mode for both SAMOSA and NR.
- Vertical Wave Motion (VWM) correction in ALT L2 HR products applied to NR Significant Wave Heights (SWH).

The first two updates listed above aimed at improving the long-term stability of the HR retrievals, the latter at improving the SWH [14].

Furthermore, PB F09 also included a correction in the computation of the HR backscatter coefficient; a corrected definition of total power in LR MLE4, and an updated configuration parameter which improves LR NR in case of peaky waveforms and during maneuvers. More details on the PB F09 can be found in the associated product notice [5], on EUMETSAT user portal[https://user.eumetsat.int/resources/userguides/sentinel-6-altimetry-processing-baseline].

# 4 Data coverage and edited measurements

This section presents in each sub section the monitorings for the entire mission duration (shown on the left) and specifically for the year 2024 (shown on the right). For details on previous years, see the 2023 annual report [6].

## 4.1. Missing measurements

#### 4.1.1. Over land and ocean

Determination of missing measurements relative to the theoretically expected orbit ground pattern is an essential tool to detect missing telemetry or satellite events.

Figure 7 shows the percentage of available measurements for Sentinel-6 MF LR and HR modes for all surfaces observed. Global availability is excellent for both LR (99.16%) and HR (98.96%) over 2024.

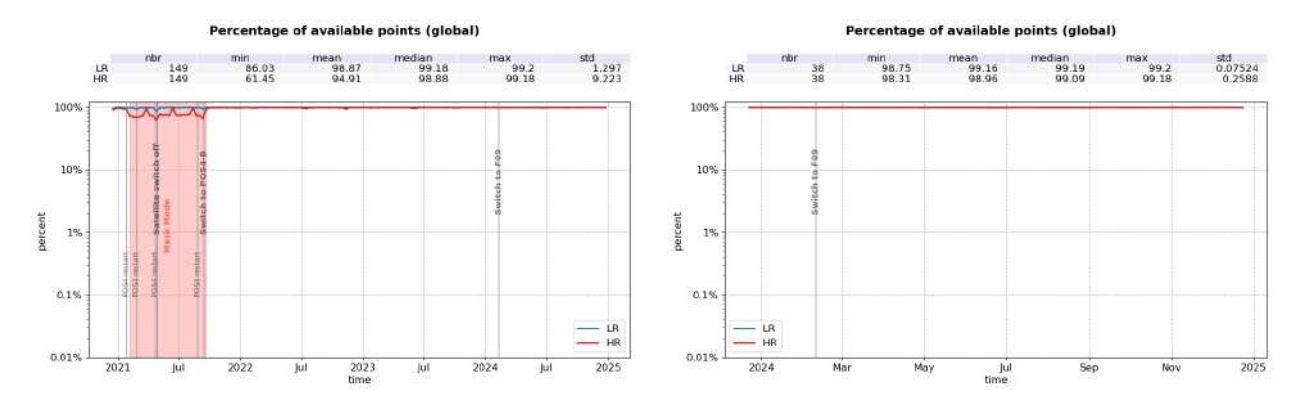


Figure 7: Percentage of available data over all surfaces for both LR (blue) and HR (red) per cycle.

Table 2 and 3 give the list of fully missing passes for LR and HR respectively, along with related events.

Cycle	Pass	Date	Comment
120	131	2024-02-15 17:03:48 to 18:00:00	UNS 10538

Table 2: List of missing passes in LR over 2024

Cycle	Pass	Date	Comment
120	131	2024-02-15 17:03:48 to 18:00:00	UNS 10538
128	196	2024-05-07 13:47:05 to 15:26:36	DORIS reboot, UNS 10711
133	170	2024-06-25 03:14:44 to 04:45:07	UNS 10948
134	138	2024-07-03 18:52:27 to 20:59:18	UNS 10976
140	14	2024-08-27 10:49:04 to 12:44:45	UNS 11166
152	168	2024-12-30 10:51:08 to 12:46:41	UNS 11645

Table 3: List of missing passes in HR over 2024

#### 4.1.2. Over ocean

Figure 8 shows the percentage of available measurements for Sentinel-6 MF LR and HR modes for ocean only. Availability over ocean is excellent for both LR (99.99%) and HR (99.81%) in 2024.

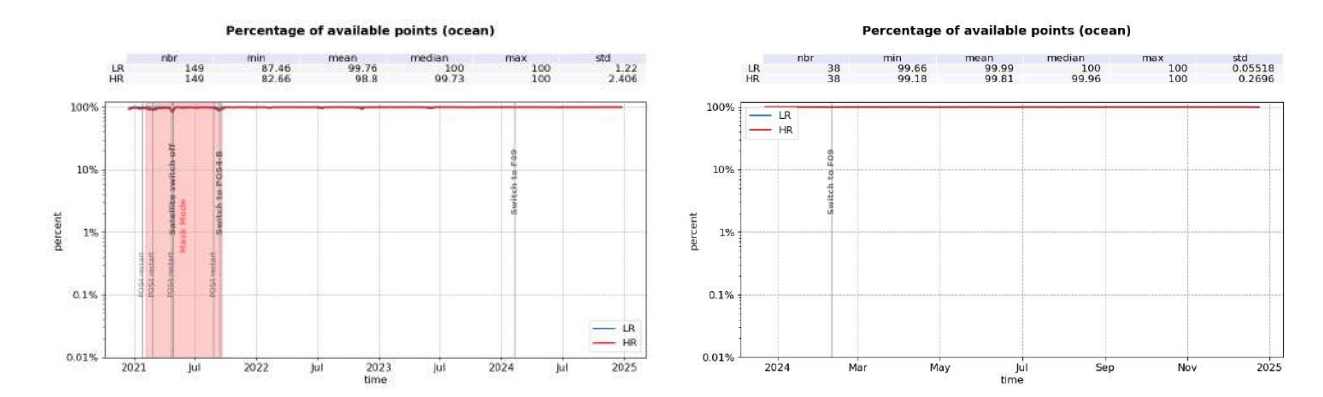


Figure 8: Percentage of available data over ocean for both LR (blue) and HR (red) per cycle.

#### 4.2.1. Overview

The outlier detection or editing step of the Cal/Val process is applied to remove any measurement that is considered erroneous. Thus, it helps to refine the various metrics which are provided in the specific sections dedicated to the performance over the ocean. The definition of an erroneous measurement, and of the accepted error level on the final sea level anomaly is of course a trade-off between accuracy and data coverage. The monitoring of the percentage of valid and edited measurements also provides relevant information about the mission performance.

A series of editing criteria are used to detect outliers over ocean. This process is divided into 4 main parts:

- removal of all measurements over land using a land/water mask,
- removal of all measurements affected by sea-ice (section 4.2.2.),
- removal of all measurements which exceed defined thresholds on different parameters (section 4.2.3.),
- further checks on along-track SLA consistency (section 4.2.4.).

For each step of the process, the number of outliers is routinely monitored at Cal/Val level. The number of removed data is used to detect processing anomalies which could be due to instrumental, geophysical or algorithmic changes. The process performed here is dedicated to ocean applications.

The percentage of edited data per day for HR and LR datasets over ocean in 2024 is monitored on figure 9. In average, slightly fewer data is edited in HR mode (9.9% in SAMOSA and 10.7% in NR starting in february) compared to LR (11.5% in MLE4 and 11.4% in NR).

An annual signal is visible: the total percentage of edited data is lower during March/April/May (6-7%), then increasing during May to July and remains around 14-15%, and start to slowly decrease in mid-September. This expected behaviour is related to sea ice coverage (see dedicated part 4.2.2.), and was already observed on previous altimetry missions such as Jason-3.

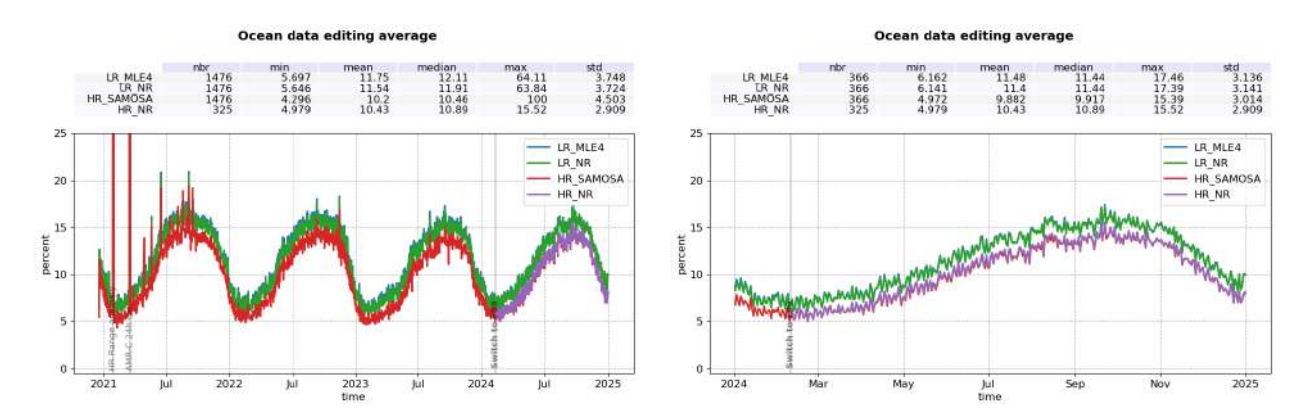


Figure 9: Percentage of edited data over ocean for LR MLE4 (blue), LR NR (green), HR SAMOSA (red) and HR NR (purple) per day over the entire mission lifetime (left) and 2024 only (right).

The maps of figure 10 represent the percentage of edited data for LR MLE4, LR NR, HR SAMOSA and HR NR, over the year 2024. Inter Tropical Convergence Zone (ITCZ) or zones with sea ice appear on the maps as regions with less valid data, as it is also the case for other altimeters: measurements are corrupted by rain or sea ice. They were therefore removed by editing. HR and LR maps are in line, except in wet zones

where less HR data are edited. A potential explanation for such a behaviour could be a better capability of HR processing to retrieve clean geophysical parameters over wet zones.

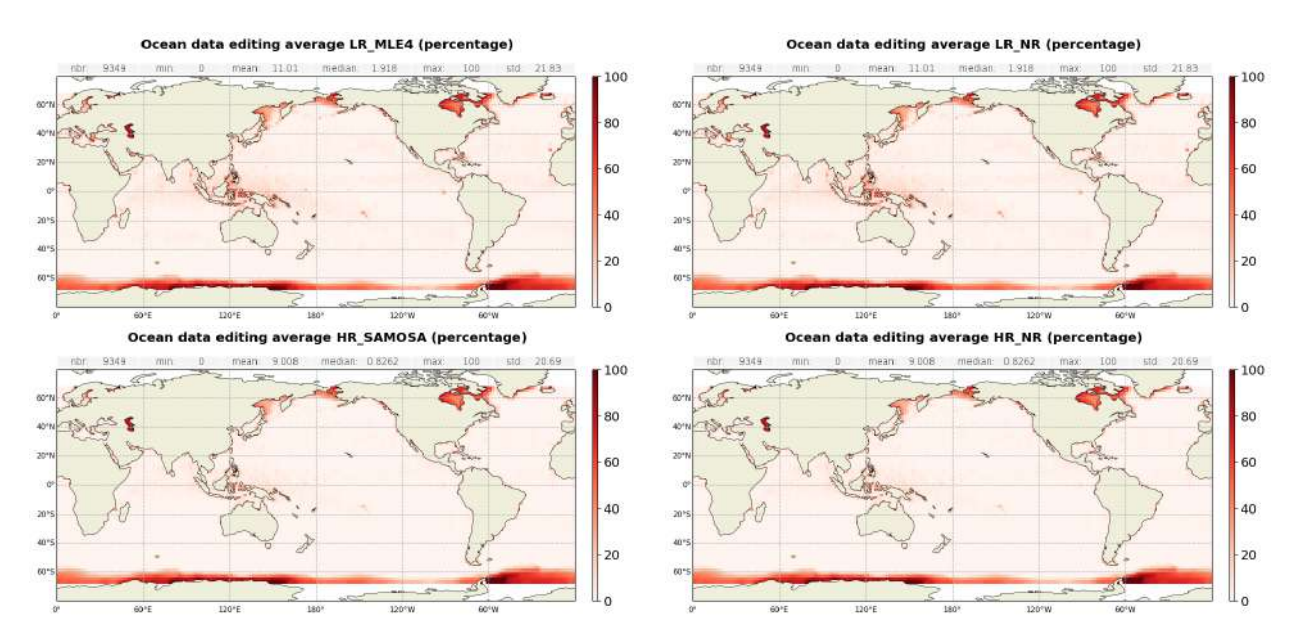


Figure 10: Maps of average percentage of edited ocean data for LR MLE4 (top left), LR NR (top right), HR SAMOSA (bottom left) and HR NR (bottom right), computed on year 2024.

#### 4.2.2. Flagging quality: ice

The first step of the editing process includes the removal of points where ice is detected. The ice flag (based on rad\_sea\_ice\_flag in L2 products) is used to remove measurements affected by sea ice within the altimeter footprint.

The percentage of measurements edited on the ice flag criterium over ocean is monitored on the figure 11.

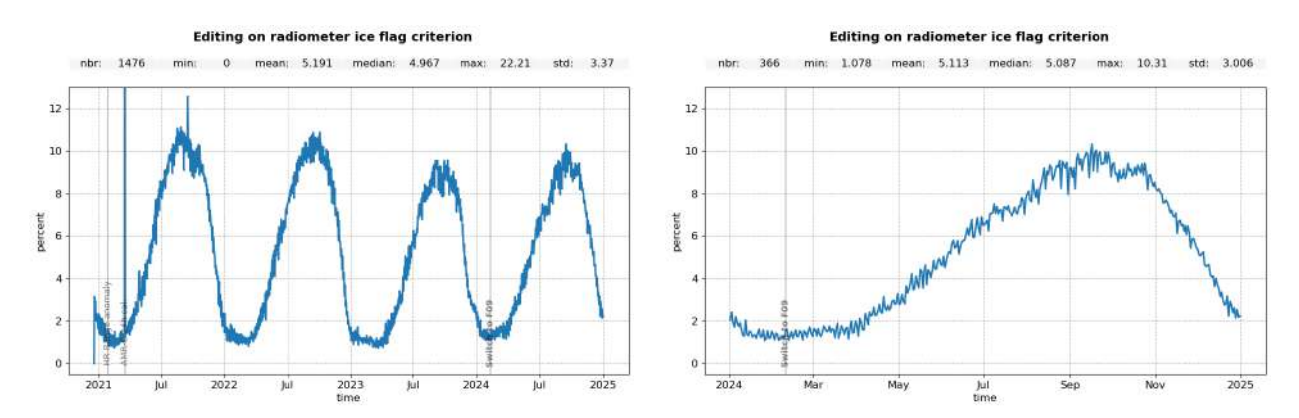


Figure 11: Percentage of data edited on ice criterion per day over the entire mission lifetime (left) and 2024 only (right).

Over the period shown, no anomalous trend is detected but the nominal annual cycle is visible. Indeed, the maximum number of points over ice is reached during the austral winter (i.e. July - September). As Sentinel-6 MF satellite has an inclination of  $66^{\circ}$ , it does not detect thawing of sea ice (due to global warming), which takes place especially in Northern Hemisphere over  $66^{\circ}$ .

Note that the percentage of edited data on ice criterion is lower for Sentinel-6 MF (5.2 % in average) than on Jason-3 (9.3 % in average [7]). Such a difference is due to the different definition of the ice flags used for this editing step. On Jason-3, the ice flag (ice\_flag in L2 product) is computed using a combination of radiometer and altimeter parameters. On Sentinel-6 MF, the sea ice flag is derived from radiometer outputs only. We recommend updating the ice flag with a computation similar to Jason-3 to improve its robustness.

#### 4.2.3. Thresholds

#### **4.2.3.1.** Overview

Once the measurements corrupted by sea ice surfaces are identified, the quality of the parameters retrieved by the altimeter, as well as that of the geophysical corrections are checked with respect to defined thresholds. These thresholds are detailed in table 4, with the corresponding percentage of detected outliers in LR MLE4, LR NR, HR SAMOSA and HR NR over 2024. These percentages are closely monitored cycle by cycle, day by day and pass by pass by CLS Cal/Val routines. A distinction is made between indicators at default value, and indicators out of bounds. For both cases, an individual measure may be edited by different criteria.

This allows detection of anomalies in the number of removed data, which could have instrumental, geophysical or algorithmic origins.

Parameters	Min thres.	Min thres. Max thres. Unit			% rejected			
				LR MLE4	LR NR	HR SAM.	HR NR	
Sea surface height anomaly	-2	2	m	3.45	2.78	3.06	2.53	
Sea surface height	-130	100	m	2.43	1.83	0.01	0.01	
Nb measurements of range	10	N/A		0.17	0.00	0.00	0.00	
Std. deviation of range	0	See (*)	m	2.72	1.10	0.94	1.24	
Backscatter coefficient	7	30	dB	2.14	0.12	0.17	0.21	
Nb measurements of sigma0	10	N/A		0.16	0.00	0.00	0.00	
Std. deviation of sigma0	0	1	dB	4.03	2.56	0.79	1.09	
Significant wave height	0	11	m	2.51	0.26	0.11	0.57	
Altimeter wind speed	0	30	m.s-1	2.29	0.91	1.29	0.94	
Sea State Bias	-0.5	0	m	2.13	0.01	0.00	0.00	
lonospheric correction fil- tered	-0.4	0.04	m	2.89	2.61	2.91	2.54	
Square off nadir angle	-0.2	0.64	deg2	0.83	1.49	N/A	N/A	
Equilibrium tide	-0.5	0.5	m	0.01	0.01	0.01	0.01	
Combined atmospheric cor- rection	-2	2	m	0.00	0.00	0.00	0.00	
Dry tropospheric correction	-2.5	-1.9	m	0.00	0.00	0.00	0.00	
Internal tide	-5	5	m	0.00	0.00	0.00	0.00	
Ocean tide	-5	5	m	0.04	0.04	0.04	0.04	
Pole tide	-15	15	m	0.00	0.00	0.00	0.00	
Earth tide	-1	1	m	0.00	0.00	0.00	0.00	
Radiometer wet tropospheric correction	-0.5	-0.001	m	0.11	0.12	0.11	0.11	
Global statistics of edited measurements by thresholds					6.3	4.8	4.9	

Table 4: Table of parameters used for editing and the corresponding percentages of edited measurements for each parameter for Sentinel-6 MF LR and HR.

(\*) The maximum threshold for range standard deviation is set as function of significant wave height as follow:

- In LR:

- for SWH  $\leq$  2m : 0.192

- for SWH > 2m : 0.018 \* SWH + 0.156

- In HR:

- for SWH  $\leq 2m$  : 0.087

- for SWH > 2m : 0.033 \* SWH + 0.121

The monitoring of edited data based on these thresholds criteria is shown on figure 12. On this monitoring, slightly different behaviours are observed between datasets. There are less data at default value in LR NR than in LR MLE4, as well as in HR NR than in SAMOSA. However, the opposite is true for criteria out of bounds. This indicates that more data are retrieved in NR (both LR and HR), but most of this additional data is of poor quality and then edited on threshold criteria. The total percentages of edited data based on the thresholds criteria are indeed almost identical between LR MLE4 and NR and between HR SAMOSA and NR.

Looking at data at default value (i.e. unavailable, bottom right panel), an annual signal is visible. Part of this signal can be linked to sea ice. Indeed, as stated above, Sentinel-6 MF radiometer sea ice flag definition does not allow to detect all measurements affected by sea ice. For the remaining measurements, MLE4, NR and SAMOSA retrackings failed to retrieve geophysical parameters, hence the default values detected here.

Looking at out-of-bounds data (top right panel), fewer data are edited in HR SAMOSA (1.8 %) and HR NR (2.4 %) than in LR (3.0 % in MLE4 and 3.8 % in NR). All monitorings are stable in time, with a small annual signal of about 1% amplitude.

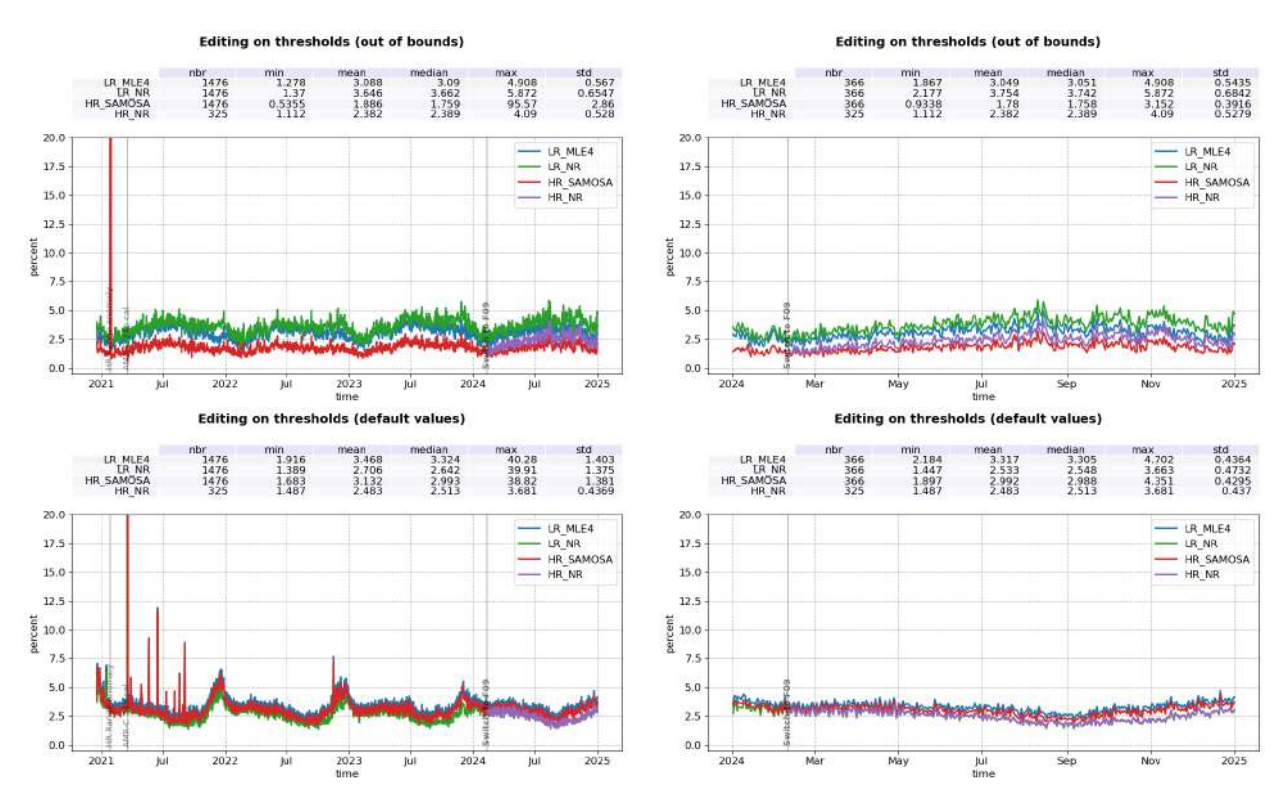


Figure 12: Percentage of data edited on threshold criteria for LR MLE4 (blue), LR NR (green), HR SAMOSA (red) and HR NR (purple) per day, for out of bounds (top) and default value (bottom) indicators over the entire mission lifetime (left) and 2024 only (right).

The overall percentage of edited data with this threshold step is of 6.4 % for LR MLE4, 6.3 % for LR NR, 4.8 % for HR SAMOSA and 4.9 % for HR NR (table 4). The difference is possibly caused by HR mode being less impacted by rain cells in wet zones.

#### 4.2.3.2. Individual thresholds

#### 20 Hz measurements number on range and sigma0

1 Hz range and sigma0 measurements computed with less than ten 20 Hz measurements are edited. Indeed, they are considered as not consistent to compute 1Hz resolution range.

In LR, such situation usually occurs in regions with disturbed sea state or heavy rain, as shown on figures 14 and 16. Indeed, waveforms are distorted by rain cells, which makes them often meaningless for SSH calculation. As a consequence, edited measurements due to several altimetric criteria are often correlated with wet areas. Over the year 2024, for the range, the average percentage of removed measurements using this criterion is 0.17% for Sentinel-6 MF LR MLE4 whereas it is less than of 0.01% for LR NR and HR (figure 13). For the sigma0, the average percentage of removed measurements using this criterion is 0.16% for Sentinel-6 MF LR MLE4 whereas it is less than of 0.01% for LR NR and HR (figure 15)

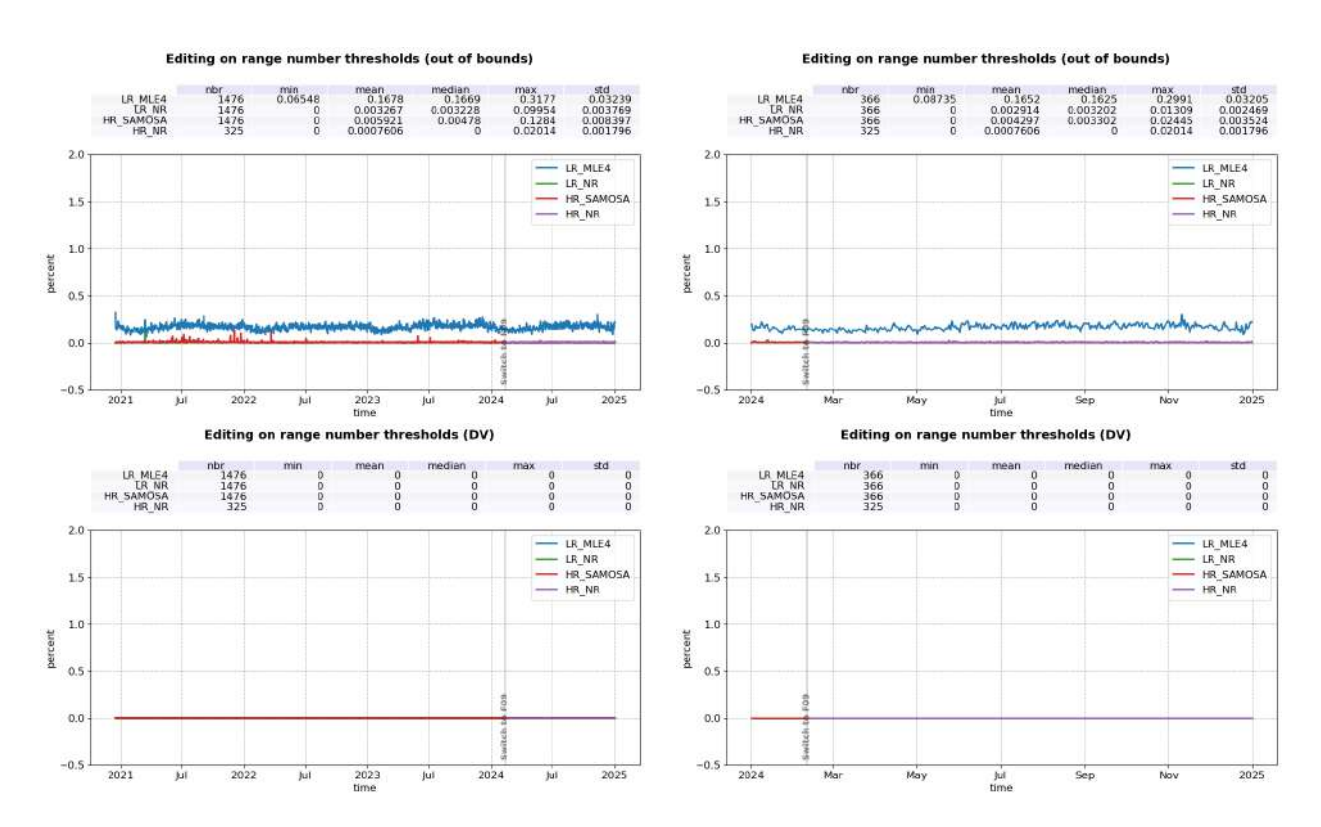


Figure 13: Percentage of data edited on range number threshold for LR MLE4 (blue), LR NR (green), HR SAMOSA (red) and HR NR (purple) per day, for out of bounds (top) and default value (bottom) over the entire mission lifetime (left) and 2024 only (right).

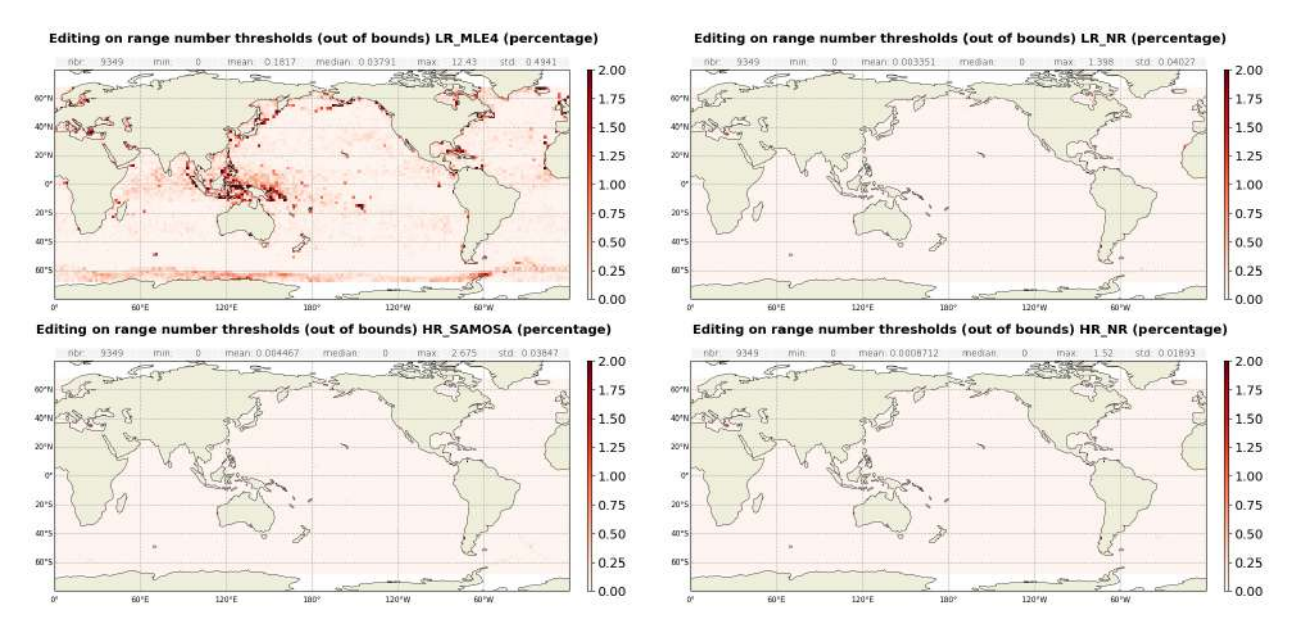


Figure 14: Maps of average percentage of data edited on range number threshold for both LR MLE4 (top left), LR NR (top right), HR SAMOSA (bottom left) and HR NR (bottom right), for out of bounds, computed on year 2024.

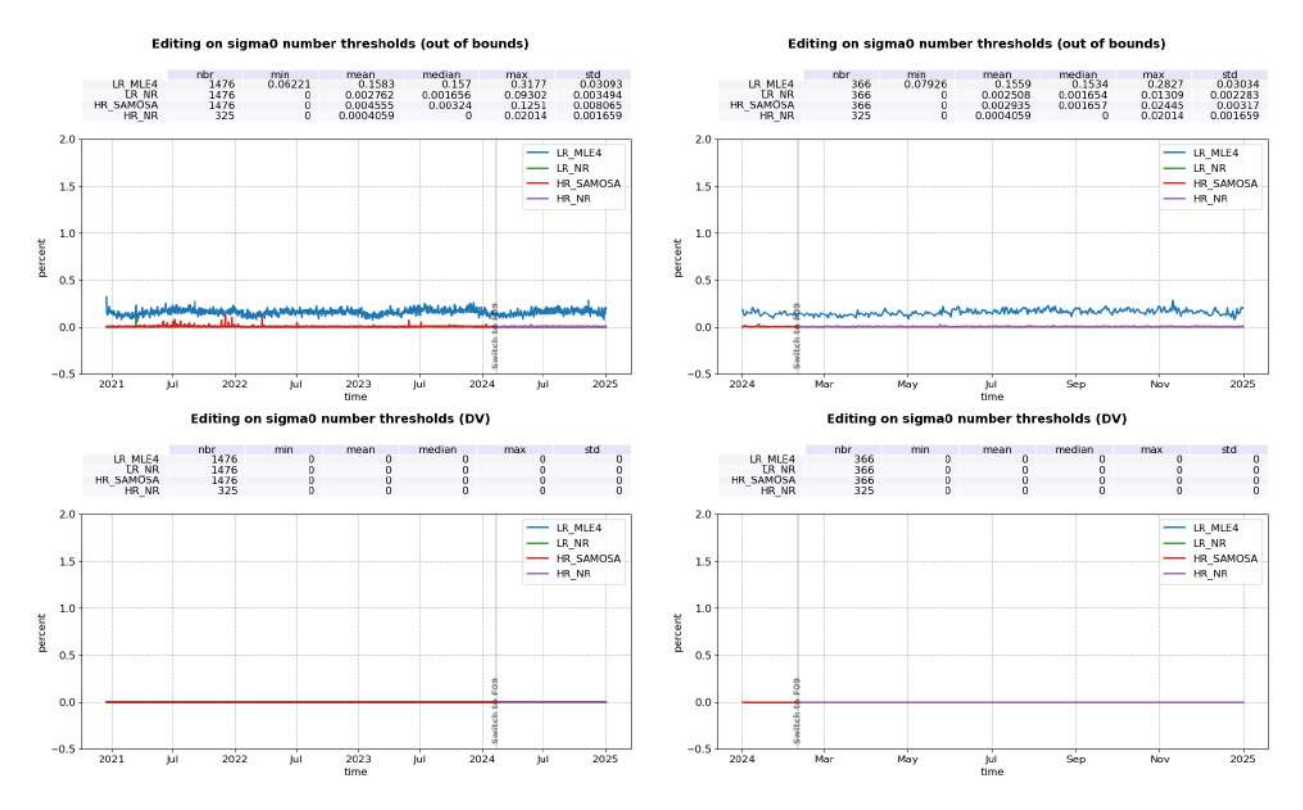


Figure 15: Percentage of data edited on sigma0 number threshold for LR MLE4 (blue), LR NR (green), HR SAMOSA (red) and HR NR (purple) per day, for out of bounds (top) and default value (bottom) over the entire mission lifetime (left) and 2024 only (right).

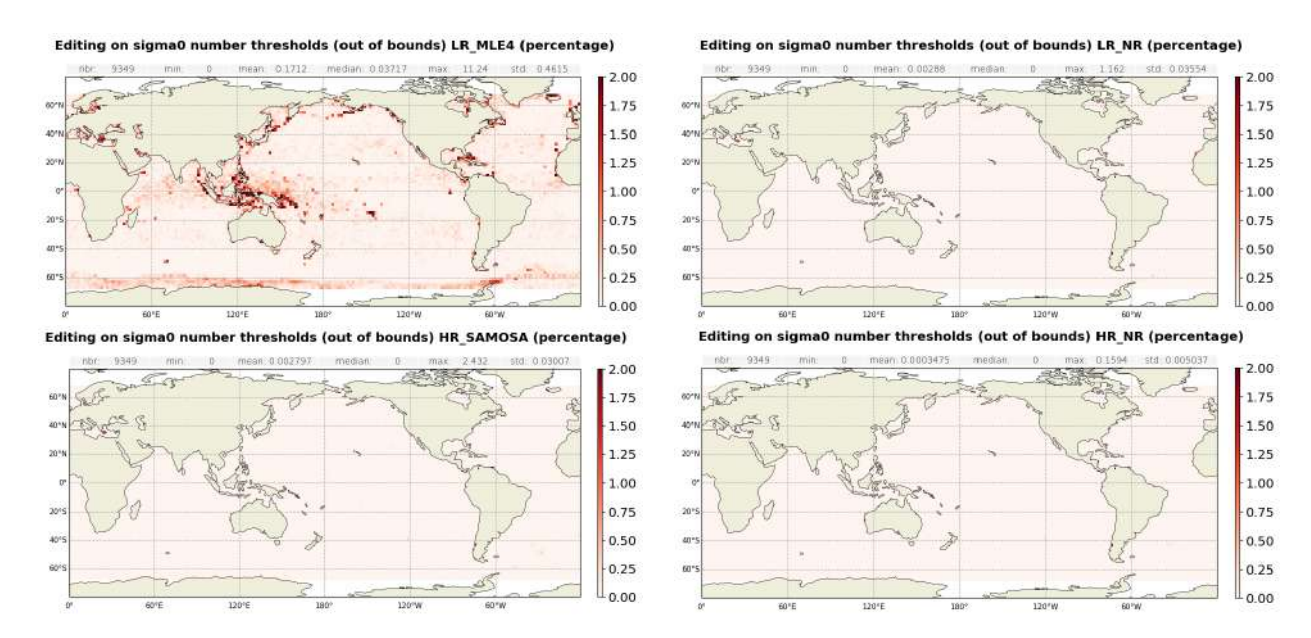


Figure 16: Maps of average percentage of data edited on sigma0 number threshold for both LR MLE4 (top left), LR NR (top right), HR SAMOSA (bottom left) and HR NR (bottom right), for out of bounds, computed on year 2024.

#### 20 Hz measurements standard deviation on range and sigma0

Using the threshold editing on 20Hz range measurements standard deviation (figure 17), 2.72% of data are removed in average in LR MLE4, higher than in LR NR, HR SAMOSA and HR NR (1.10 %, 0.94 and 1.24 % respectively). This difference is explained by a higher percentage of range standard deviation set to Default Value for LR MLE4 (figure 17, bottom panel). It highlights the LR NR and HR processings capabilities to retrieve geophysical parameters on icy regions.

Additionally, an annual signal appears here for all processings. As for 20Hz range measurements number, edited measurements are correlated with wet areas (figures 18 and 19).

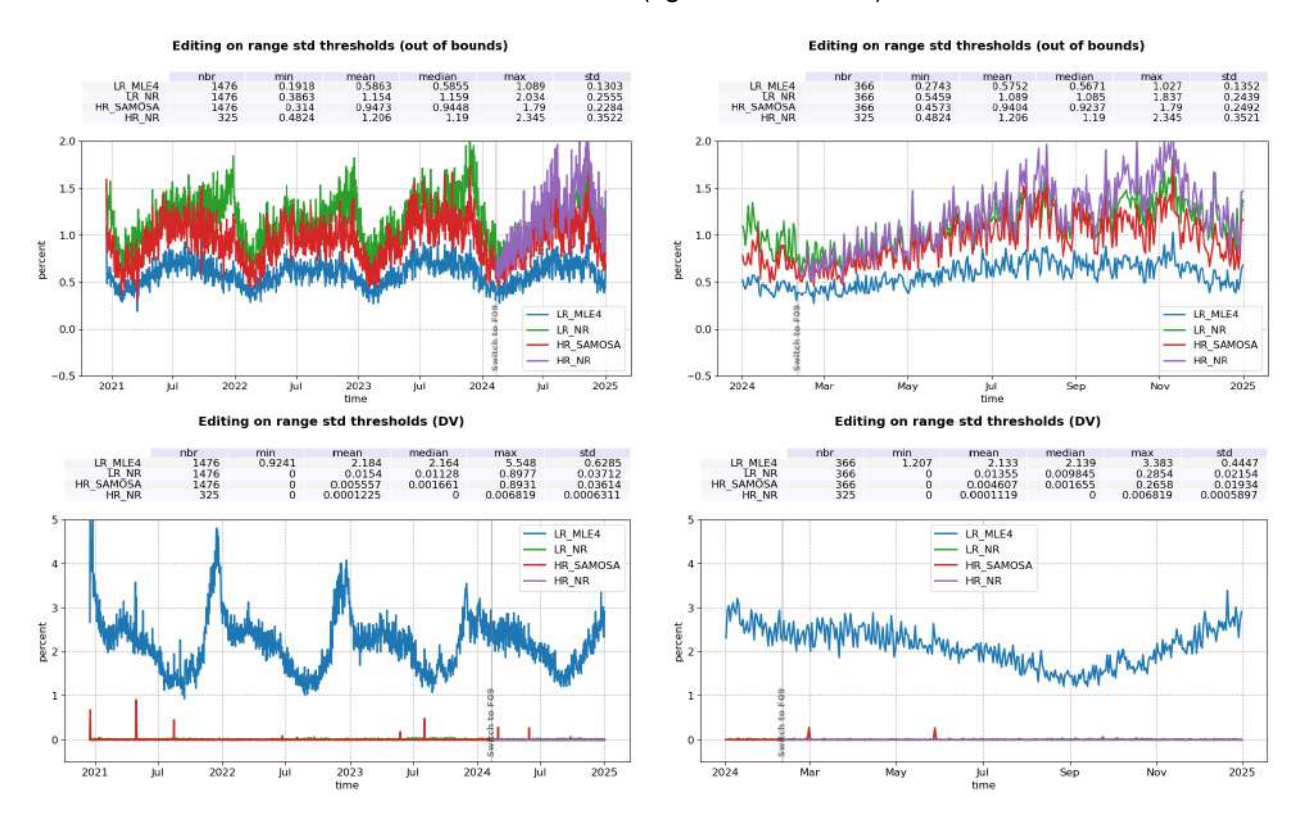


Figure 17: Percentage of data edited on range std threshold for both LR MLE4 (blue), LR NR (green), HR SAMOSA (red) and HR NR (purple) per day, for out of bounds (top) and default value (bottom) over the entire mission lifetime (left) and 2024 only (right).

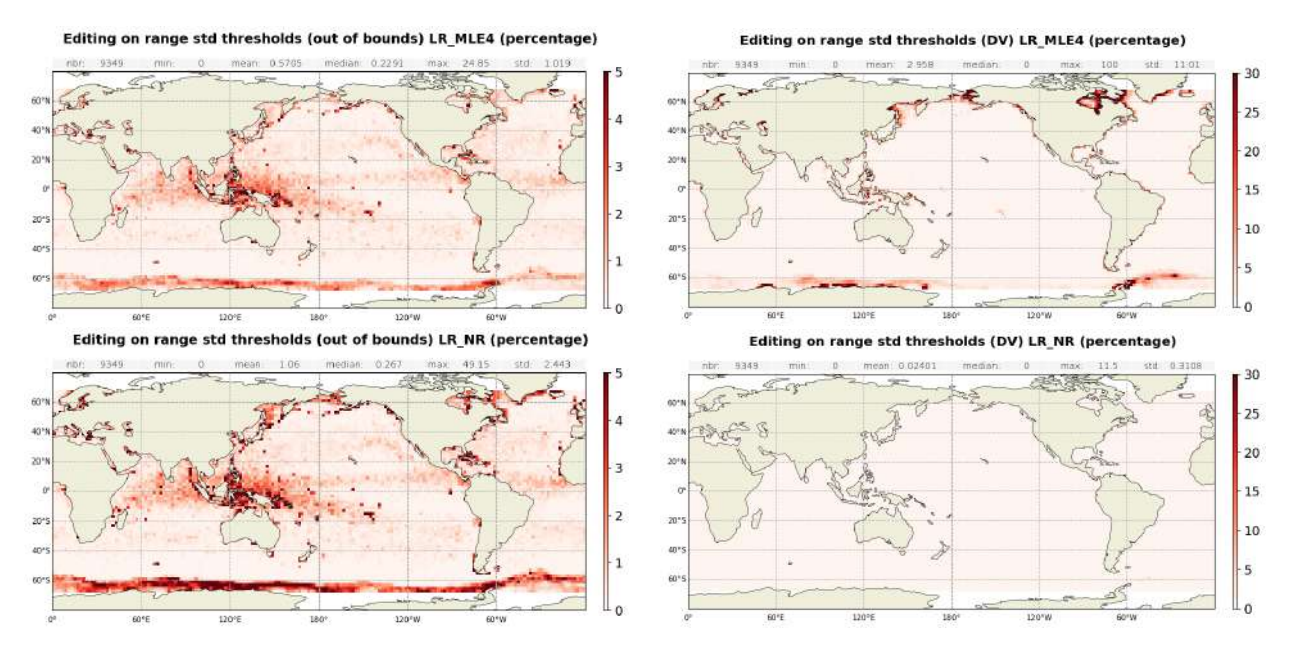


Figure 18: Maps of average percentage of data edited on range std threshold for both LR MLE4 (top) and LR NR (bottom), for out of bounds (left) and default value (right), computed on year 2024.

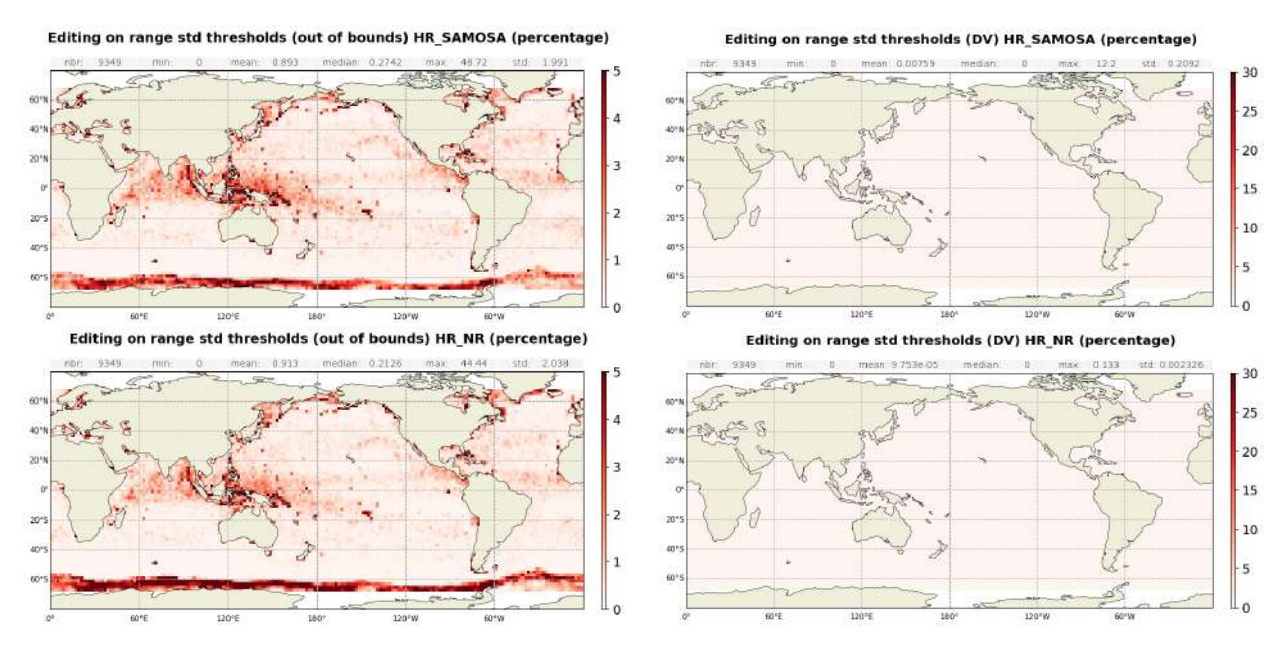


Figure 19: Maps of average percentage of data edited on range std threshold for both HR SAMOSA (top) and HR NR (bottom), for out of bounds (left) and default value (right), computed on year 2024.

Figure 20 presents the percentage of data edited based on sigma0 standard deviation criterion. It is about 4.03% for LR MLE4, 2.56 % for LR NR, 0.79% for HR SAMOSA and 1.09 % for HR NR. Most of the out of bound sigma0 standard deviation are located in regions with disturbed sea state or heavy rain, primarily around Indonesia (figure 21).

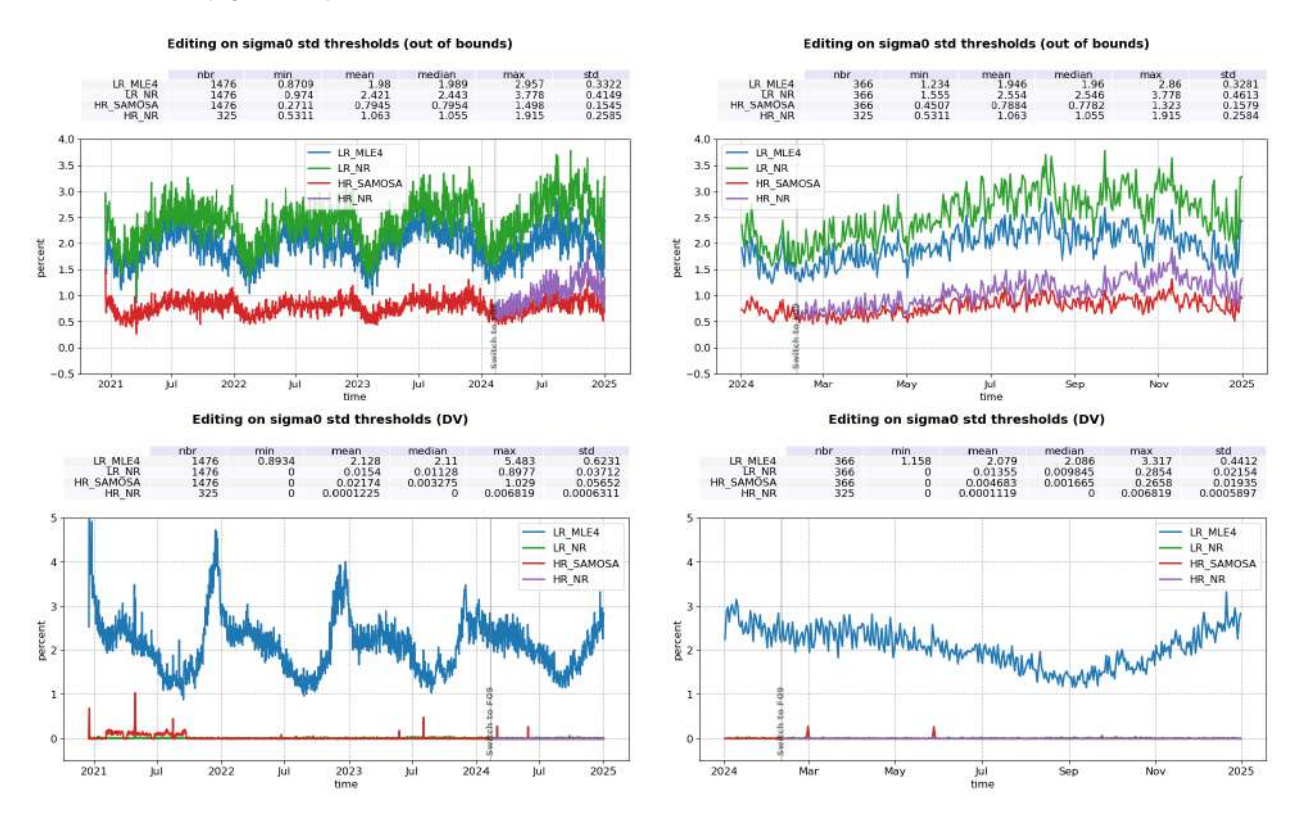


Figure 20: Percentage of data edited on sigma0 std threshold for LR MLE4 (blue), LR NR (green), HR SAMOSA (red) and HR NR (purple) per day, for out of bounds (top) and default value (bottom) over the entire mission lifetime (left) and 2024 only (right).

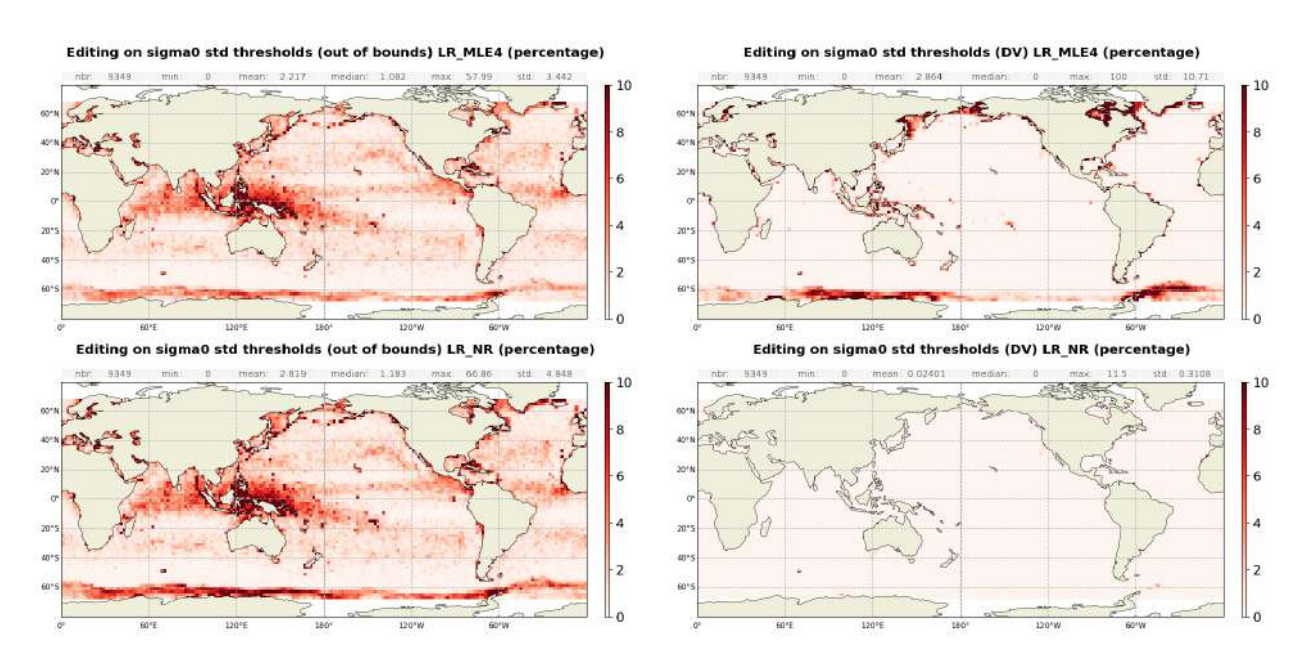


Figure 21: Maps of average percentage of data edited on sigma0 std threshold for both LR MLE4 (top) and LR NR (bottom), for out of bounds (left) and default value (right), computed on year 2024.

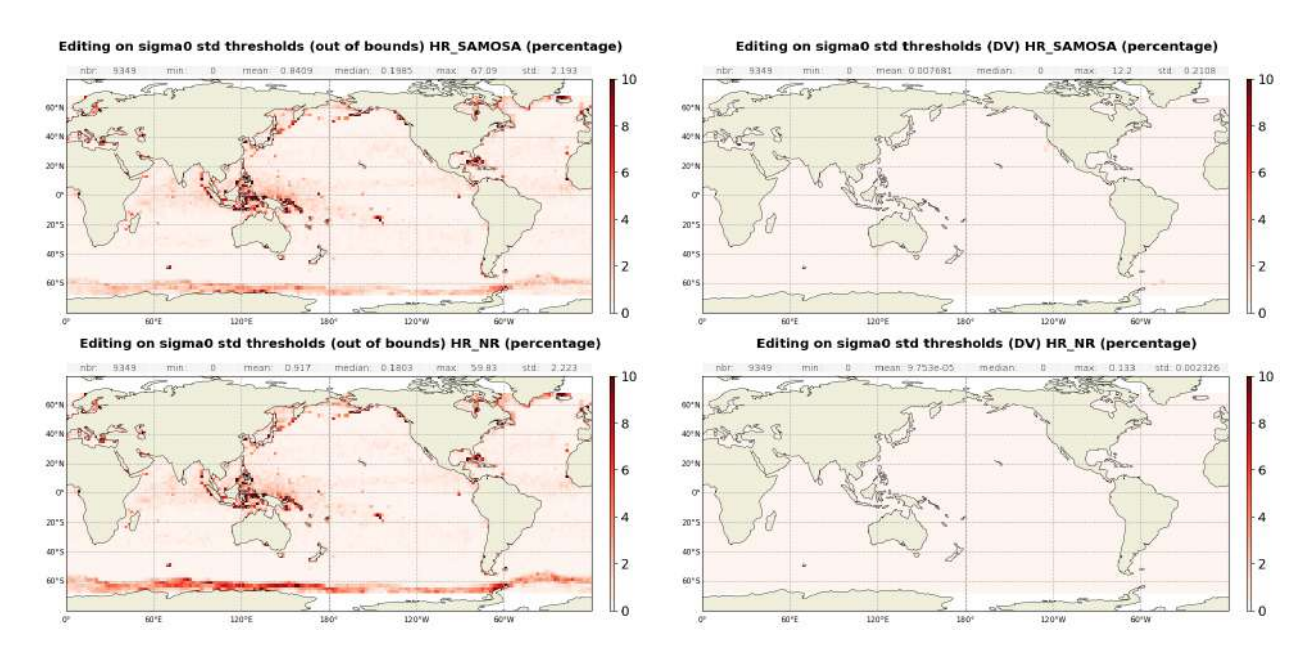


Figure 22: Maps of average percentage of data edited on sigma0 std threshold for both HR SAMOSA (top) and HR NR (bottom), for out of bounds (left) and default value (right), computed on year 2024.

#### **Backscatter coefficient**

The percentage of edited measurements due to backscatter coefficient criterion is represented on top of figure 23. It is about 2.14% for LR MLE4, 0.12 % for LR NR, 0.17% for HR SAMOSA and 0.21 % for HR NR. For LR MLE4, most of these edited measurements are at DV and located in coastal areas, ice margins and wet zones (see figures 24 and 25).

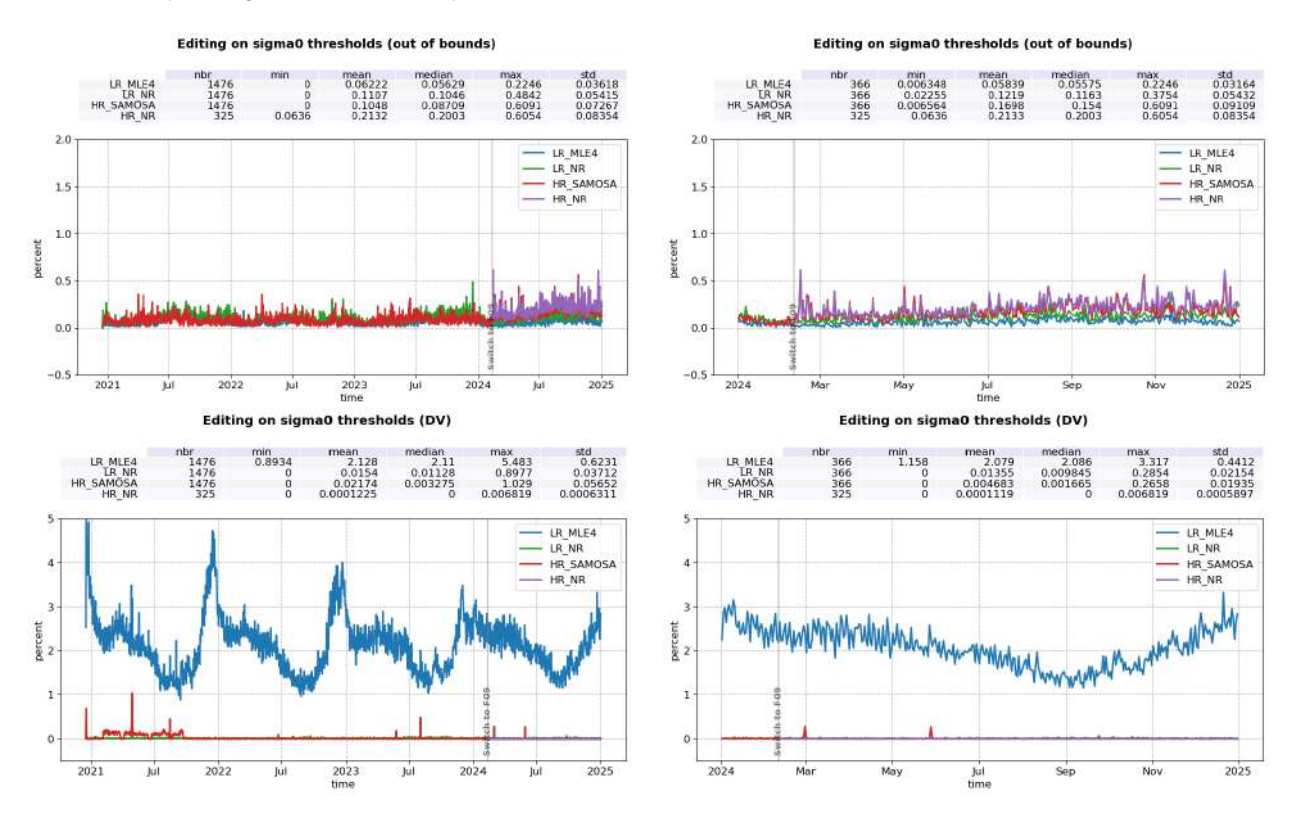


Figure 23: Percentage of data edited on sigma0 threshold for LR MLE4 (blue), LR NR (green), HR SAMOSA (red) and HR NR (purple) per day, for out of bounds (top) and default value (bottom) over the entire mission lifetime (left) and 2024 only (right).

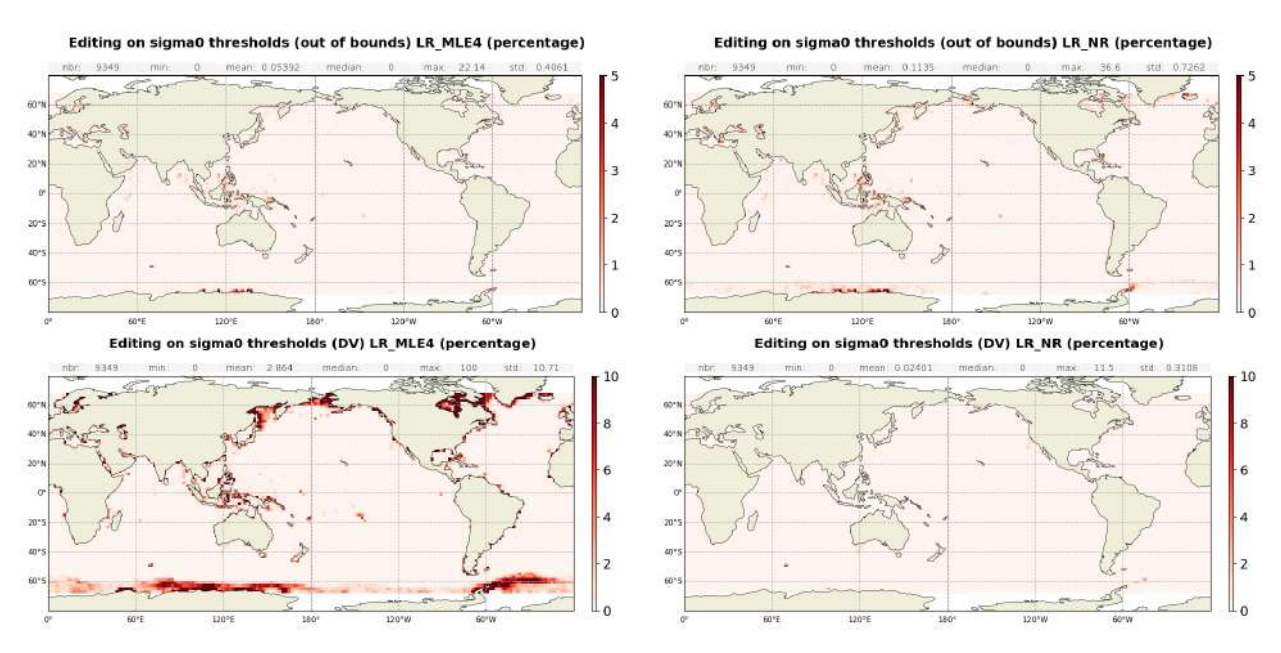


Figure 24: Maps of average percentage of data edited on sigma0 threshold for both LR MLE4 (left) and LR NR (right), for out of bounds (top) and default value (bottom), computed on year 2024.

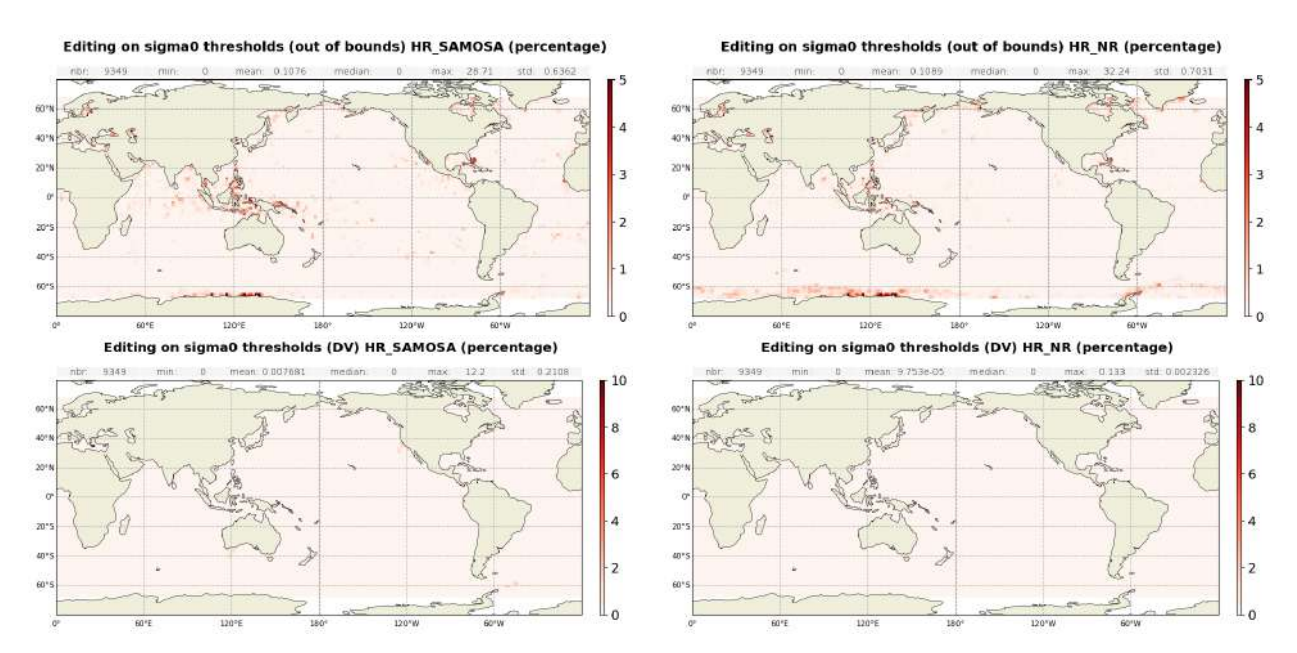


Figure 25: Maps of average percentage of data edited on sigma0 threshold for both HR SAMOSA (left) and HR NR (right), for out of bounds (top) and default value (bottom), computed on year 2024.

#### Significant wave height

The percentage of edited measurements due to significant wave heights criterion is represented on figure 26, and is about 2.51% for LR MLE4, 0.28 % for LR NR, 0.11% for HR SAMOSA and 0.56 % for HR NR. In LR MLE4, they are mostly due to default value data, and are located in circumpolar areas, while out of bounds values are located in coast regions, in the Mediterranean Sea and around Indonesia (figure 27). In HR NR, a higher percentage of measurements is edited in low SWH areas (figure 28) than in SAMOSA. This is due to the fact that in NR, SWH values can be negative, unlike in SAMOSA retracking, and negative SWH are edited in our process (see table 4).

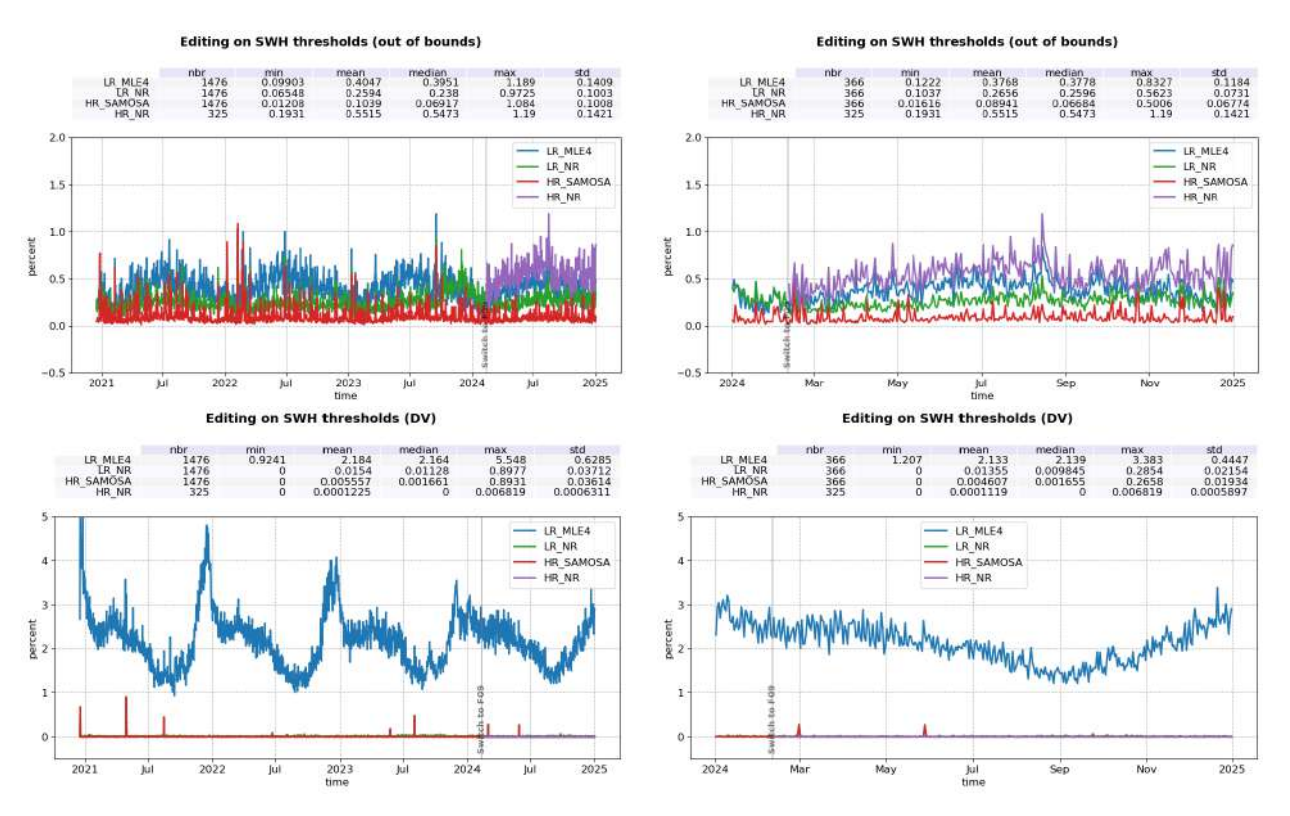


Figure 26: Percentage of data edited on SWH threshold for LR MLE4 (blue), LR NR (green), HR SAMOSA (red) and HR NR (purple) per day, for out of bounds (top) and default value (bottom) over the entire mission lifetime (left) and 2024 only (right).

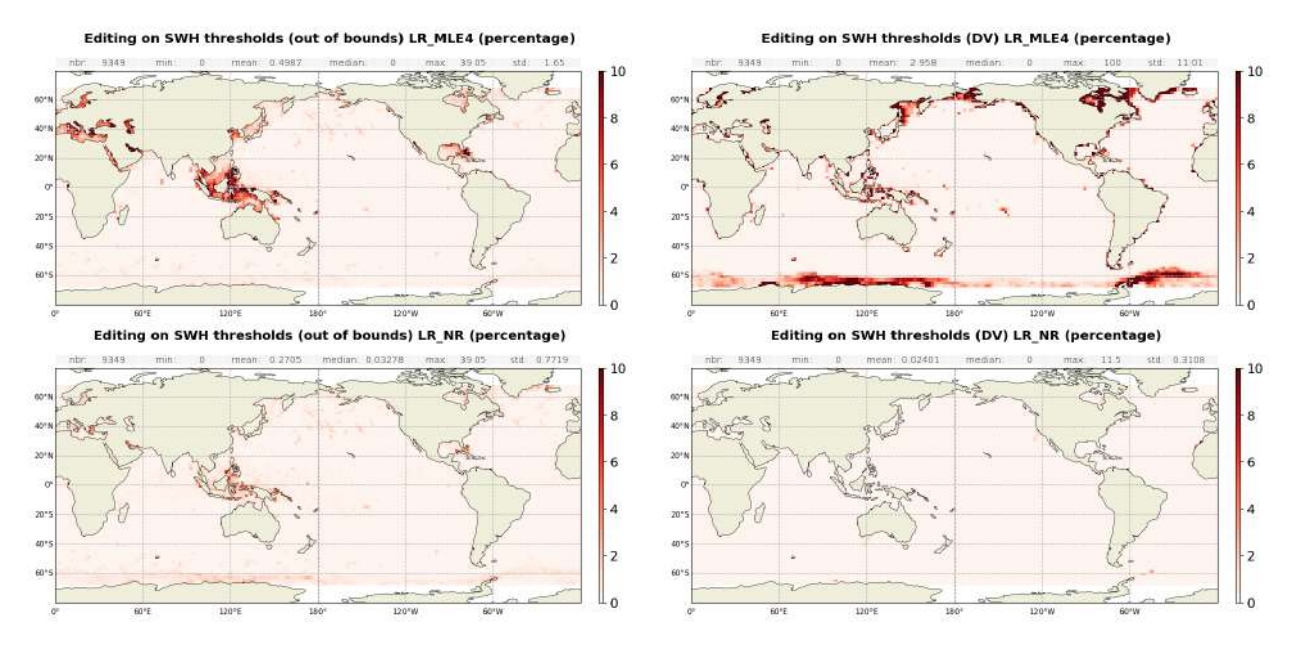


Figure 27: Maps of average percentage of data edited on SWH threshold for both LR MLE4 (top) and LR NR (bottom), for out of bounds (left) and default value (right), computed on year 2024.

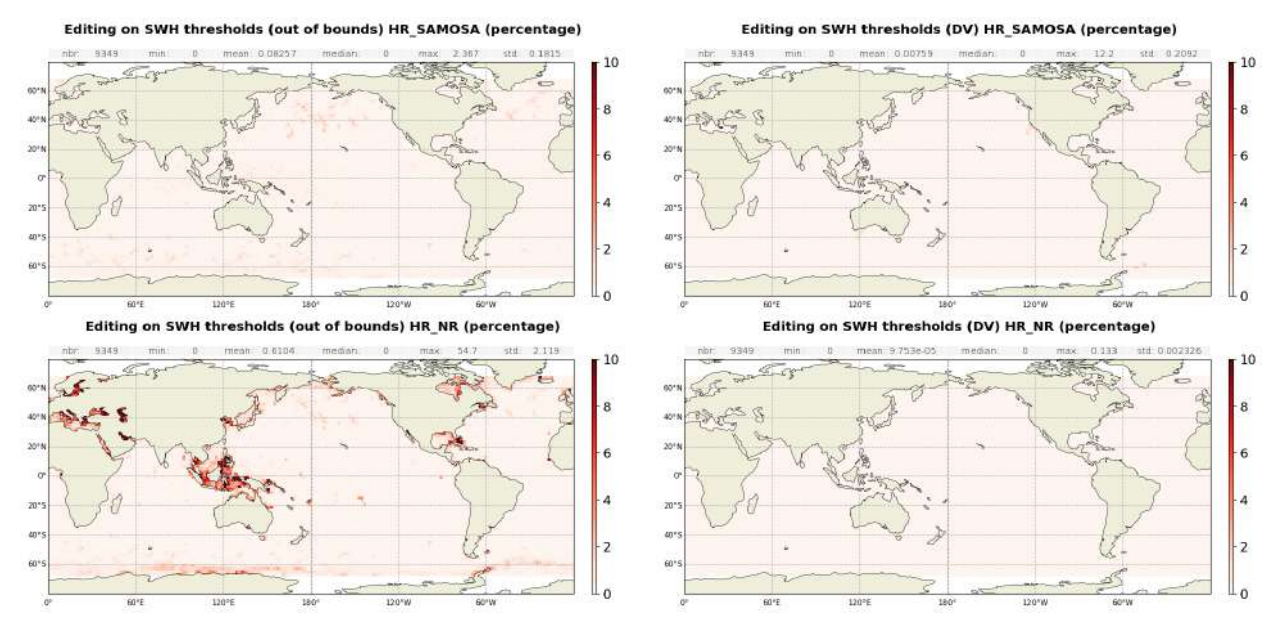


Figure 28: Maps of average percentage of data edited on SWH threshold for both HR SAMOSA (top) and HR NR (bottom), for out of bounds (left) and default value (right), computed on year 2024.

### Wind speed

The percentage of edited measurements due to altimeter wind speed criterion is represented on figure 29. It is about 2.29% for LR MLE4, 0.91 % for LR NR, 1.28 % for HR SAMOSA and 0.94 % for HR NR. Measurements are exclusively edited because of default values.

Wind speed is also edited when it includes negative values. Nevertheless, sea state bias is available even for negative wind speed values. Therefore, the percentage of edited altimeter wind speed data is higher than the percentage of edited sea state bias data (Table 4). Maps on figure 30 showing percentage of measurements edited by altimeter wind speed criterion is correlated with maps 27, 28 (SWH) and 24 and 25 (sigma0).

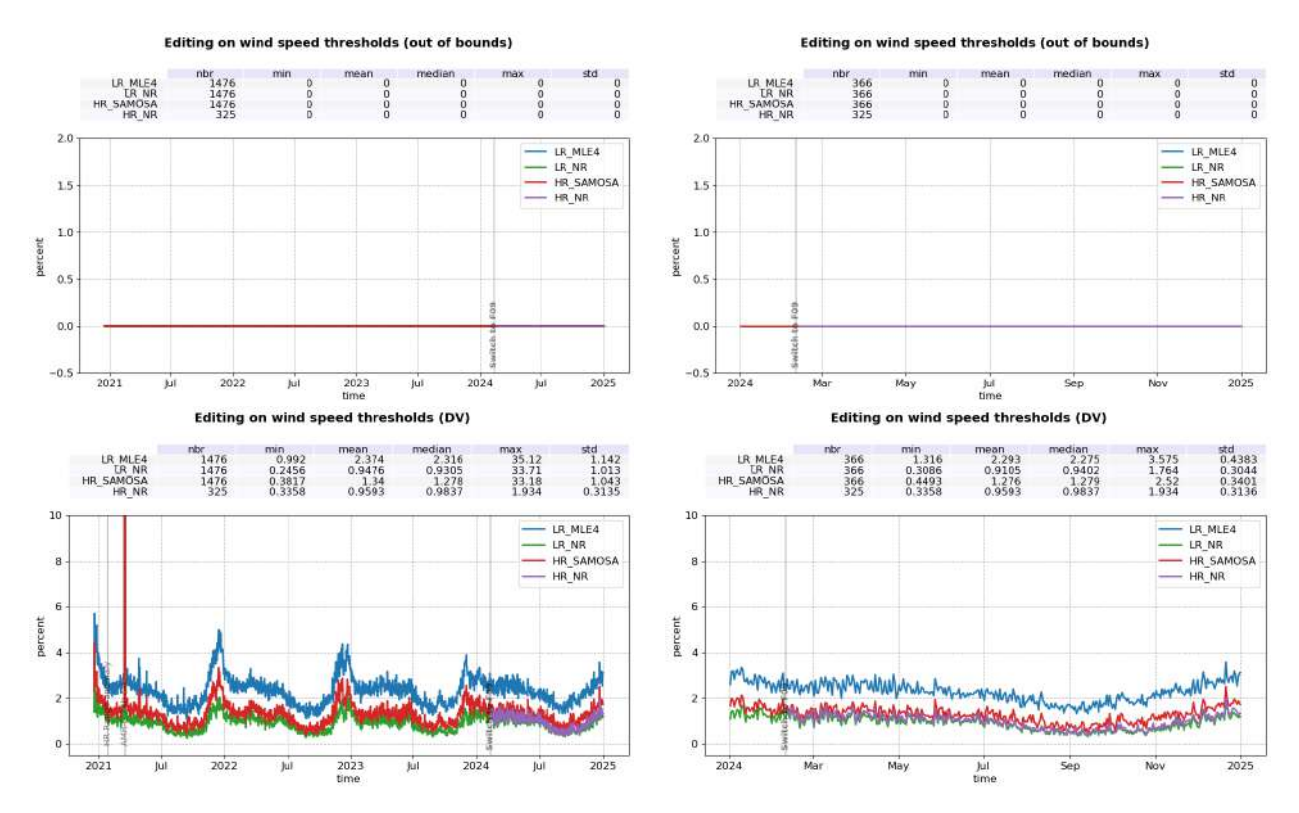


Figure 29: Percentage of data edited on wind speed threshold for LR MLE4 (blue), LR NR (green), HR SAMOSA (red) and HR NR (purple) per day, for out of bounds (top) and default value (bottom) over the entire mission lifetime (left) and 2024 only (right).

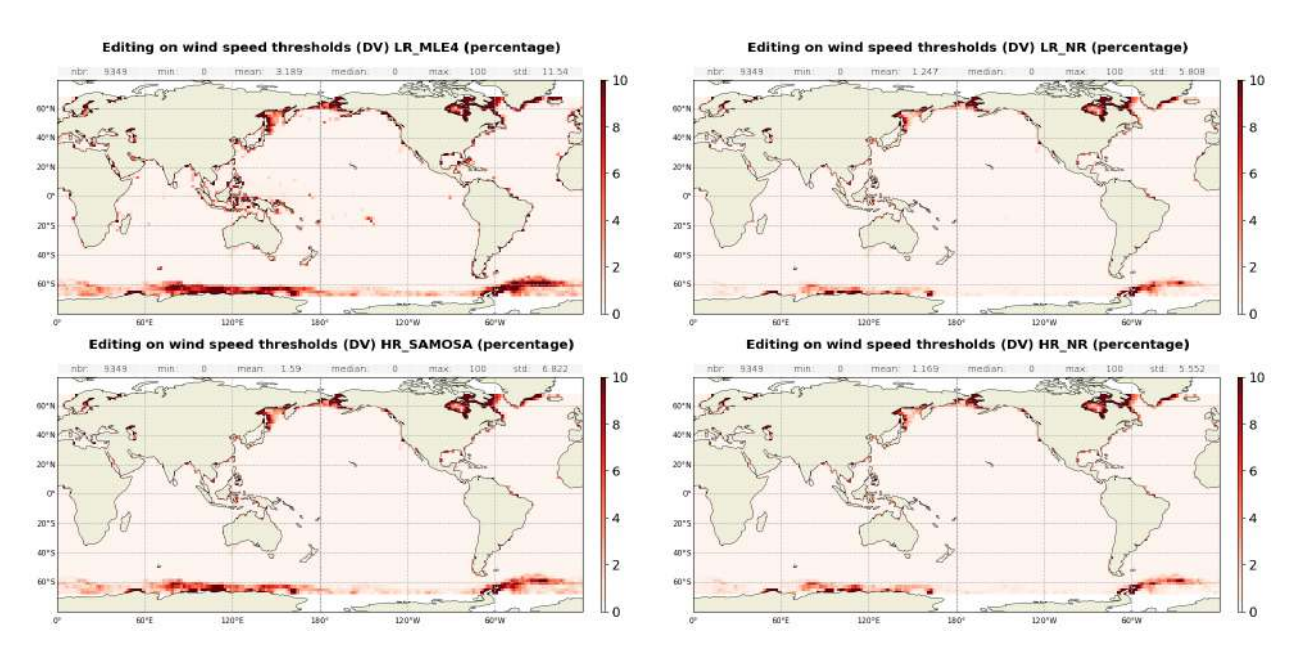


Figure 30: Maps of average percentage of data edited on wind speed threshold for LR MLE4 (top left), LR NR (right top), HR SAMOSA (bottom left) and HR NR (bottom right), for default value, computed on year 2024.

#### Sea state bias

Regarding the sea state bias criterion, the percentage of edited measurements is about 2.13% in LR MLE4, 0.01 % in LR NR and less than 0.01 % for HR retrackings. These are exclusively due to default value data (figure 31). The difference can also be observed on wind-speed and significant wave height threshold criteria (which are both used for SSB computation).

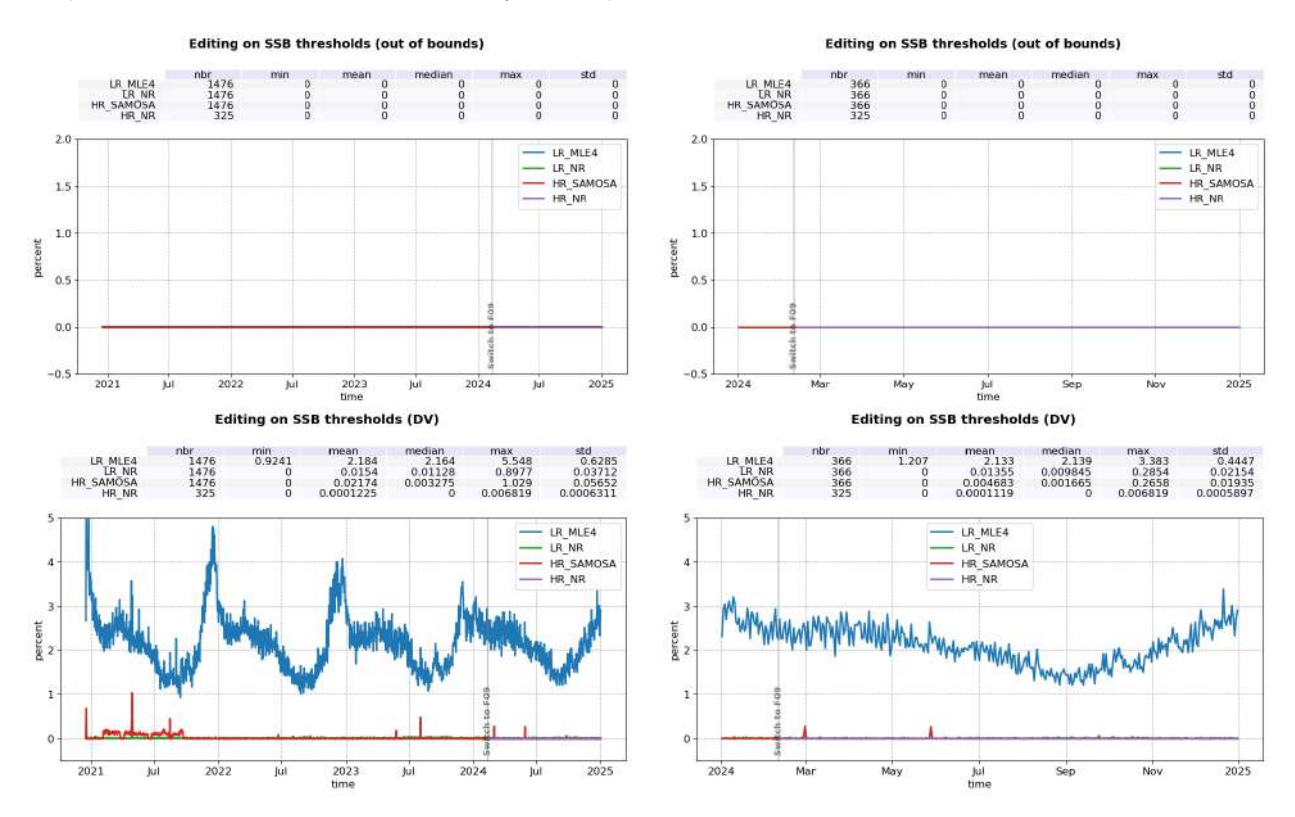


Figure 31: Percentage of data edited on SSB threshold for LR MLE4 (blue), LR NR (green), HR SAMOSA (red) and HR NR (purple) per day, for out of bounds (top) and default value (bottom) over the entire mission lifetime (left) and 2024 only (right).

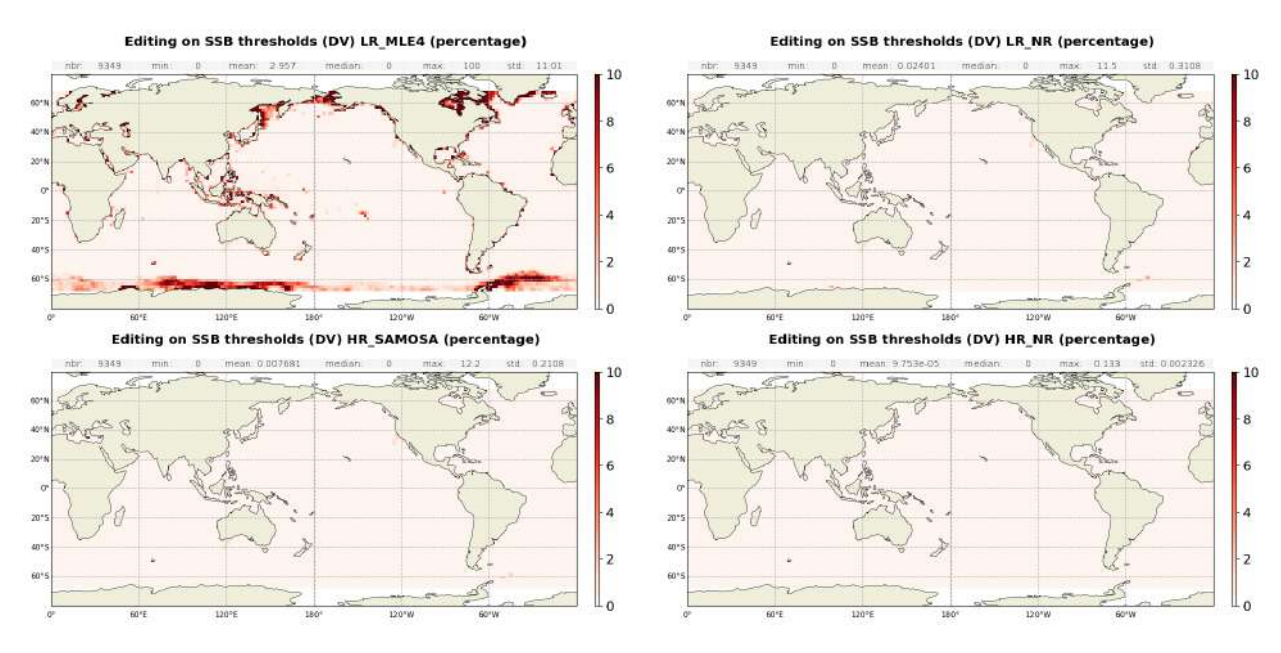


Figure 32: Maps of average percentage of data edited on SSB threshold for both LR MLE4 (top left), LR NR (top right), HR SAMOSA (bottom left) and HR NR (bottom right) for default value, computed on year 2024.

#### Filtered ionospheric correction

The mean percentage of edited data by threshold criterion on filtered ionospheric correction is 2.89 % for LR MLE4, 2.61 % for LR NR, 2.91 % for HR SAMOSA and 2.54 % for HR NR.

Note that the ionospheric correction is only computed in LR (C-band being only available in LR) and LR MLE4 and NR ionospheric corrections are used in HR products for SAMOSA and NR respectively. The small differences visible between LR and HR monitorings in figure 33 are due to the difference in data availability between the modes.

The maps on figure 34 show that measurements edited by filtered dual frequency ionosphere correction are mostly found near coasts and at ice frontiers.

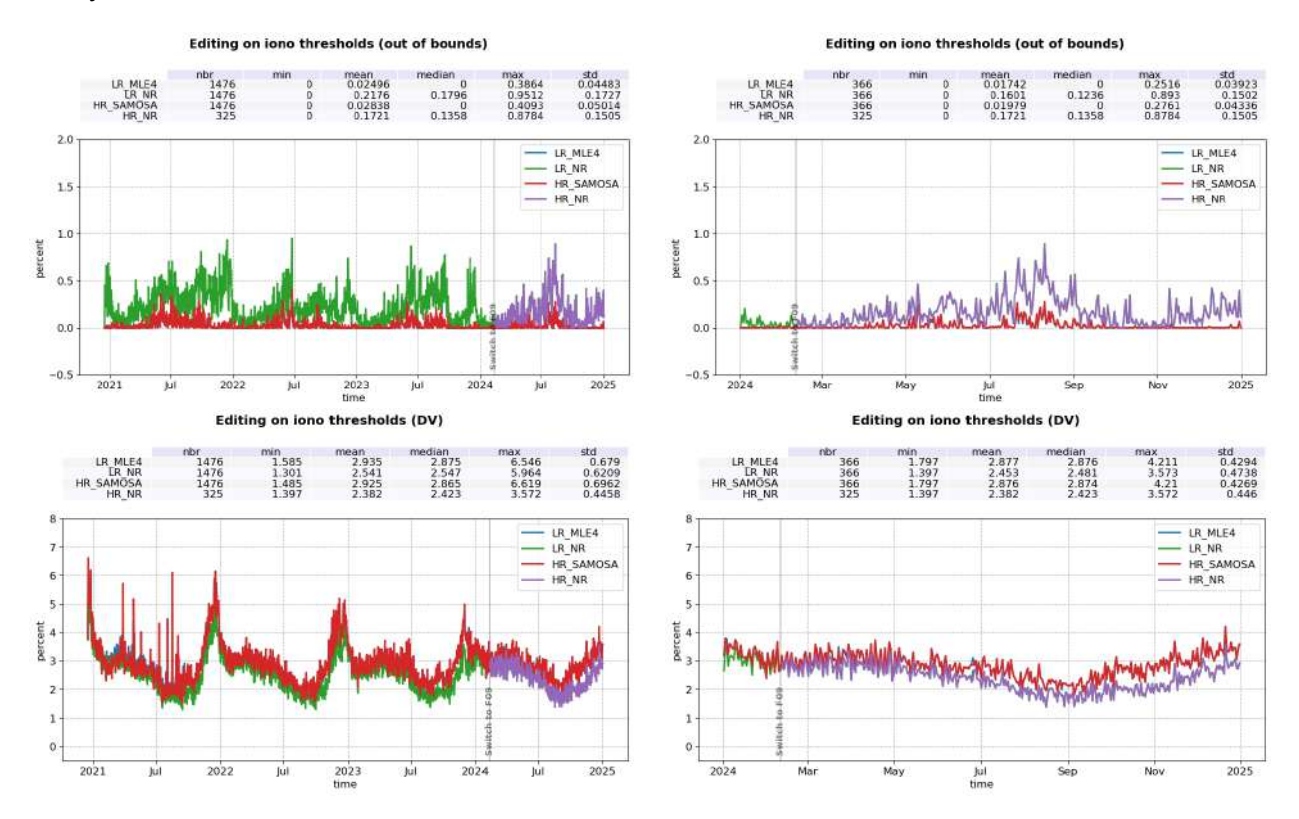


Figure 33: Percentage of data edited on filtered ionospheric correction threshold for LR MLE4 (blue), LR NR (green), HR SAMOSA (red) and HR NR (purple) per day, for out of bounds (top) and default value (bottom) over the entire mission lifetime (left) and 2024 only (right).

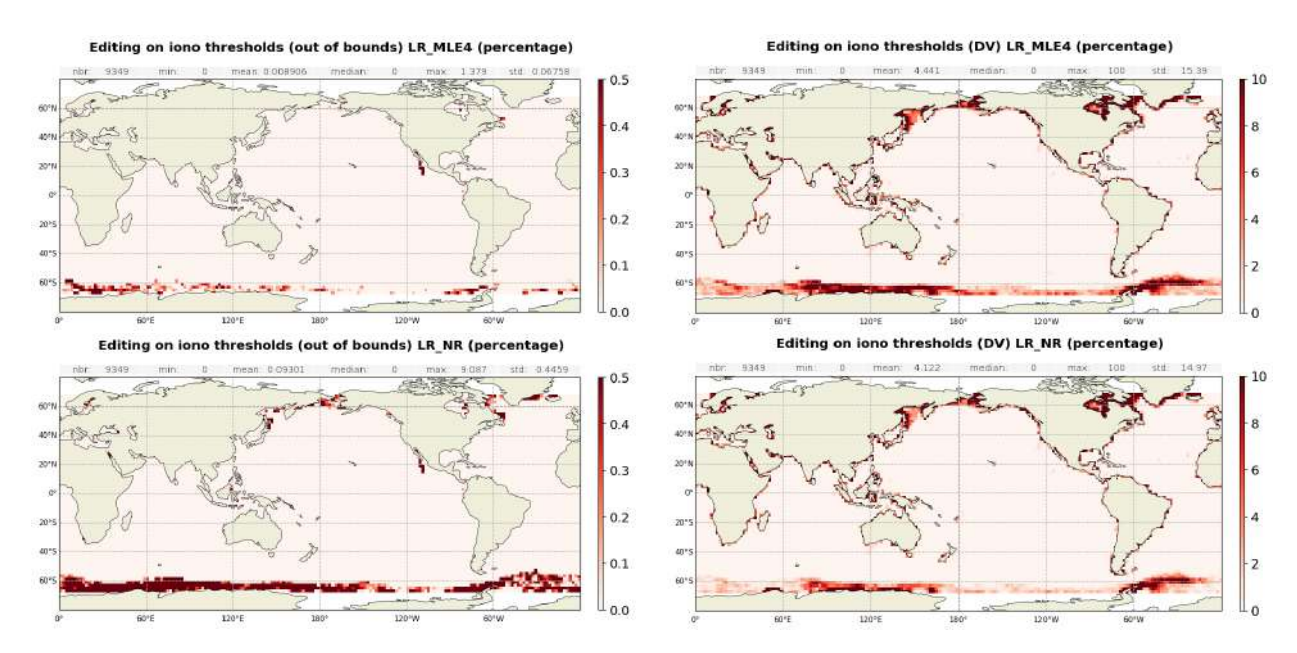


Figure 34: Maps of average percentage of data edited on LR filtered ionospheric correction threshold for both LR MLE4 (top) and LR NR (bottom), for out of bounds (left) and default value (right), computed on year 2024.

#### Square off nadir angle

The percentage of edited data on the square off nadir angle criterion (in LR data) is 0.83 % in MLE4 and 1.49 % in NR, as shown in figure 35. Maps on figure 36 show that edited measurements are mostly found in coastal regions and regions with disturbed waveforms.

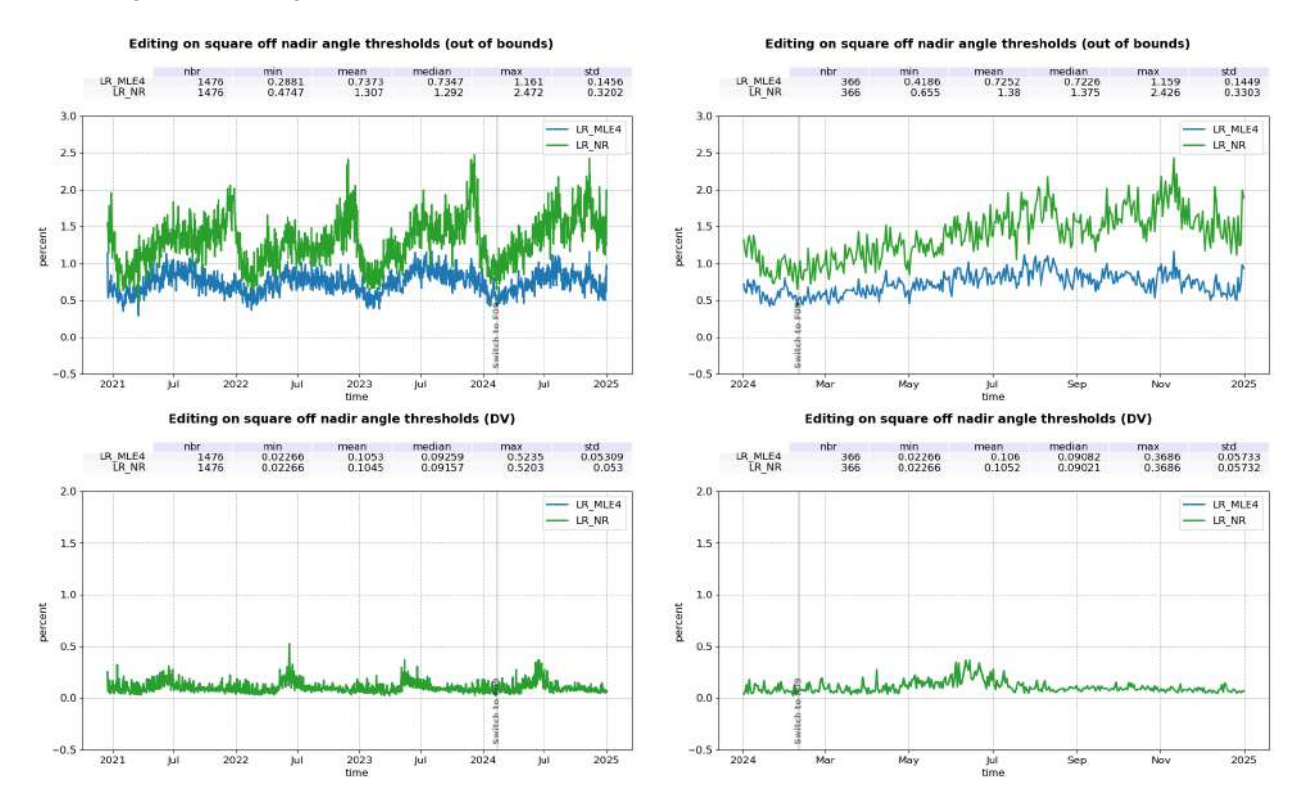


Figure 35: Percentage of data edited on square off nadir angle threshold for both LR MLE4 (blue) and LR NR (green) per day, for out of bounds (top) and default value (bottom) over the entire mission lifetime (left) and 2024 only (right).

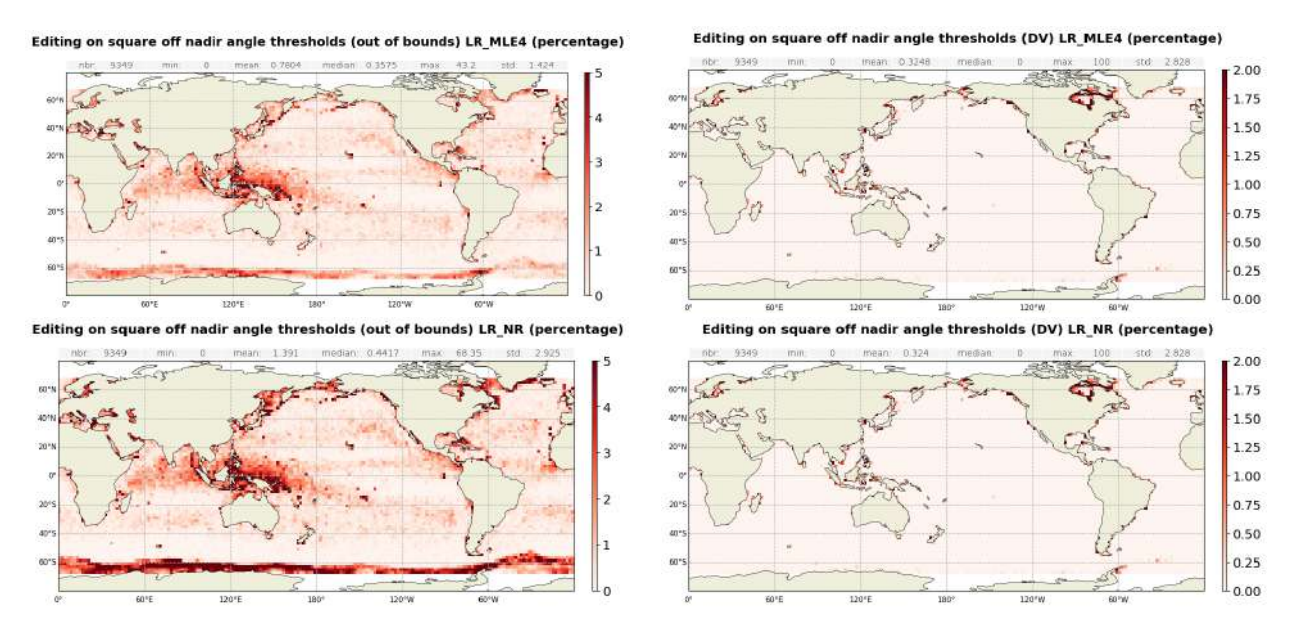


Figure 36: Maps of average percentage of data edited on square off nadir angle threshold for both LR MLE4 (top) and LR NR (bottom), for out of bounds (left) and default value (right), computed on year 2024.

#### **Dry tropospheric correction**

The editing criterion on the dry tropospheric correction allowed to detect an anomaly in this model processing. As shown on figure 37, the dry tropospheric correction is not defined on the Greenwich meridian. Investigations showed that it is also the case for the model wet tropospheric correction and the inverse barometer (not shown). This anomaly is related to interpolation issue of pressure files. It affects LR and HR products up to PB F09. This anomaly is no longer present in G01 released in 2025. All F08 data on this line are therefore always edited.

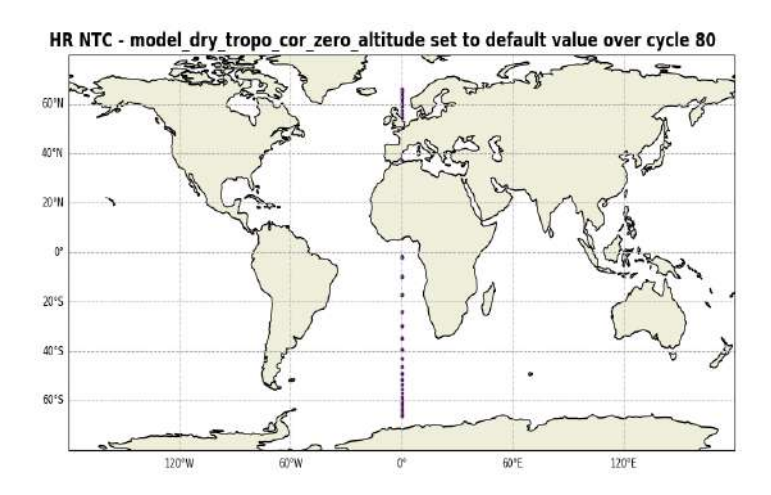


Figure 37: Map of model dry tropospheric correction set to default value. Computed for 1 cycle of HR NTC data.

### Ocean tide equilibrium

A very small fraction of measurements, both in LR (MLE4 and NR) and HR, are edited based on the equilibrium ocean tide model being at default value. This impacts about 0.01% of data in all modes (figure 38).

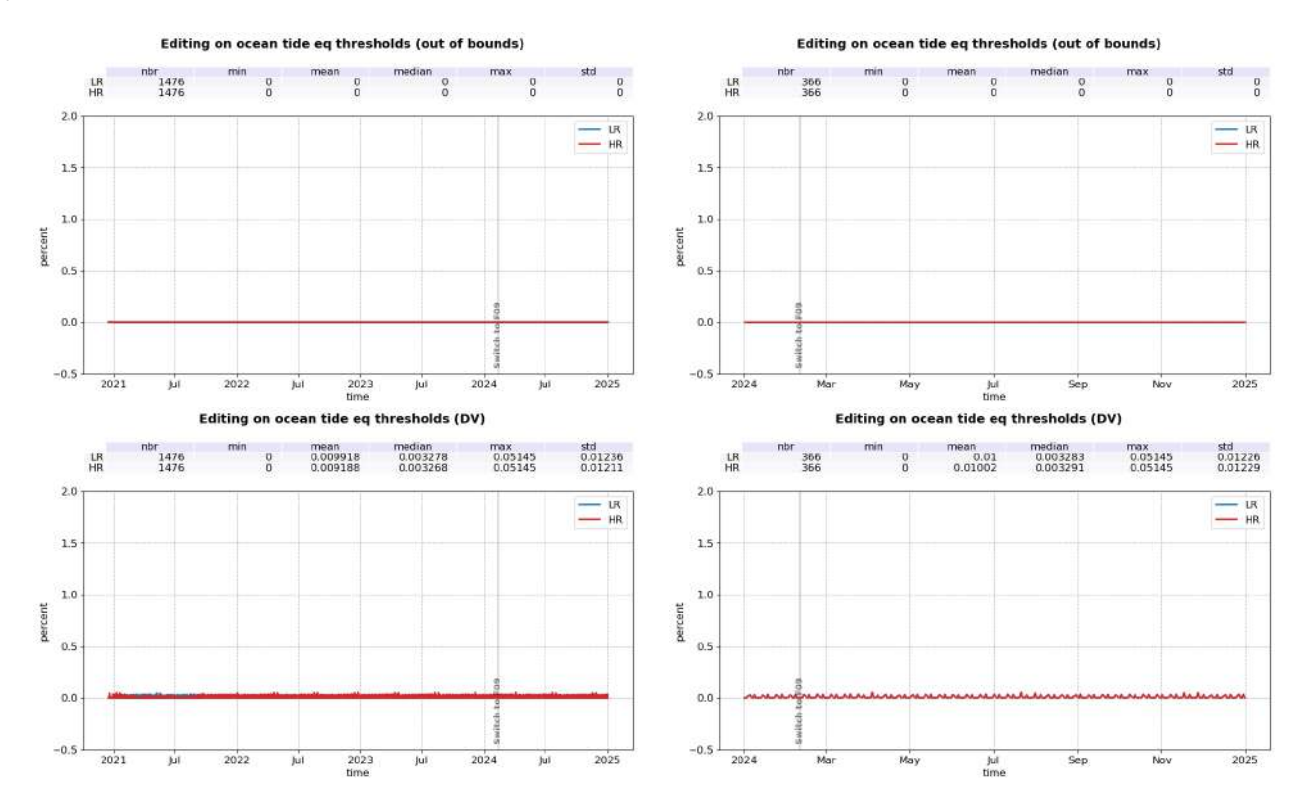


Figure 38: Percentage of data edited on equilibrium tide threshold for LR (blue) and HR (red) per day, for out of bounds (top) and default value (bottom) over the entire mission lifetime (left) and 2024 only (right).

#### Ocean tide

The percentage of edited measurements due to ocean tide is about 0.04% for all processings (figure 39). The ocean tide correction is a model output, there should therefore be no edited measurement. Indeed, there are no measurements edited in open ocean areas (figure 40). These measurements are exclusively at default values.

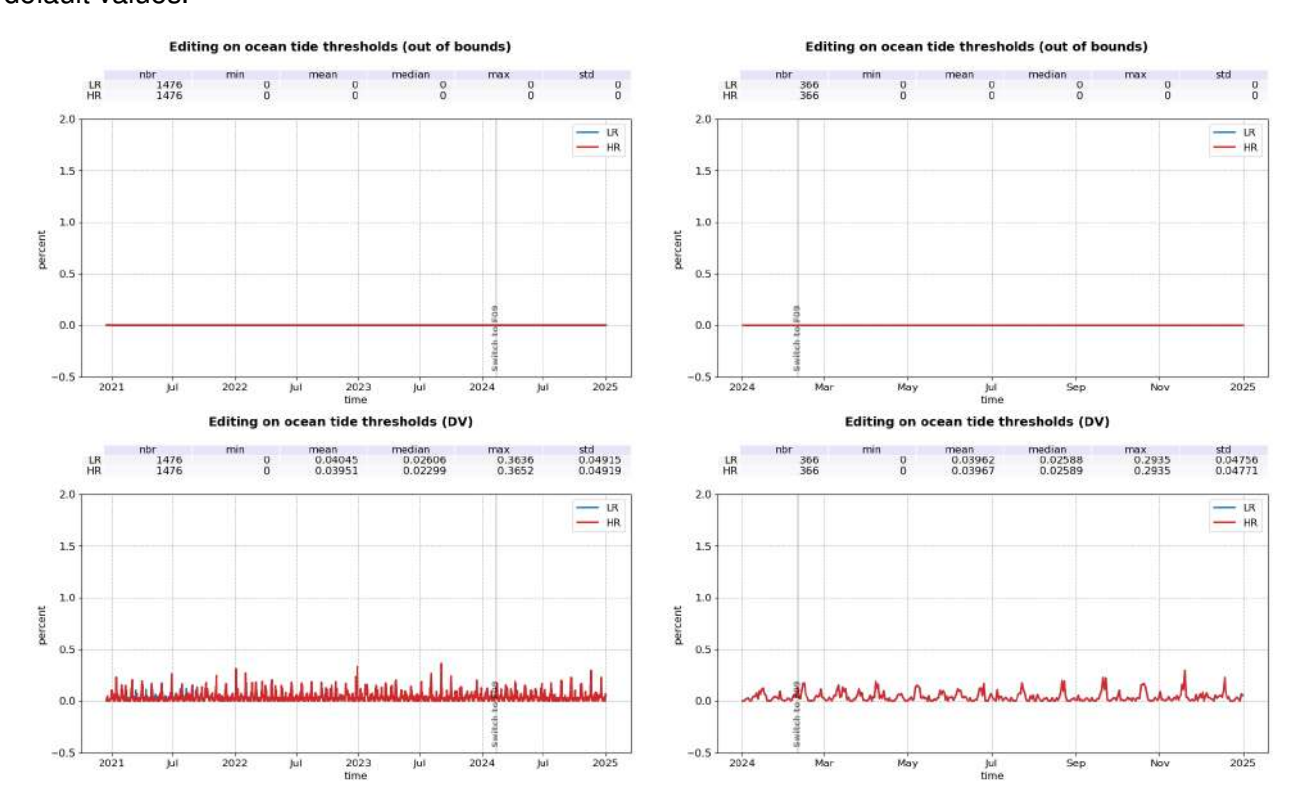


Figure 39: Percentage of data edited on ocean tide threshold for LR (blue) and HR (red) per day, for out of bounds (top) and default value (bottom) over the entire mission lifetime (left) and 2024 only (right).

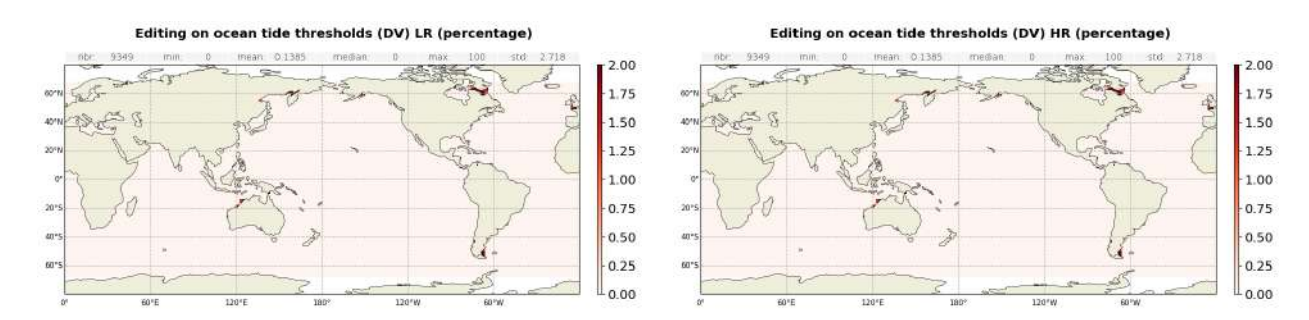


Figure 40: Maps of average percentage of data edited on ocean tide threshold for LR (left) and HR (right), for default value, computed on year 2024.

#### Wet tropospheric correction

The percentage of edited measurements due to radiometer wet troposphere correction criterion is represented in figure 41. It is 0.11 % in both LR and HR modes. As expected, edited data are located in the ITCZ (see figure 42).

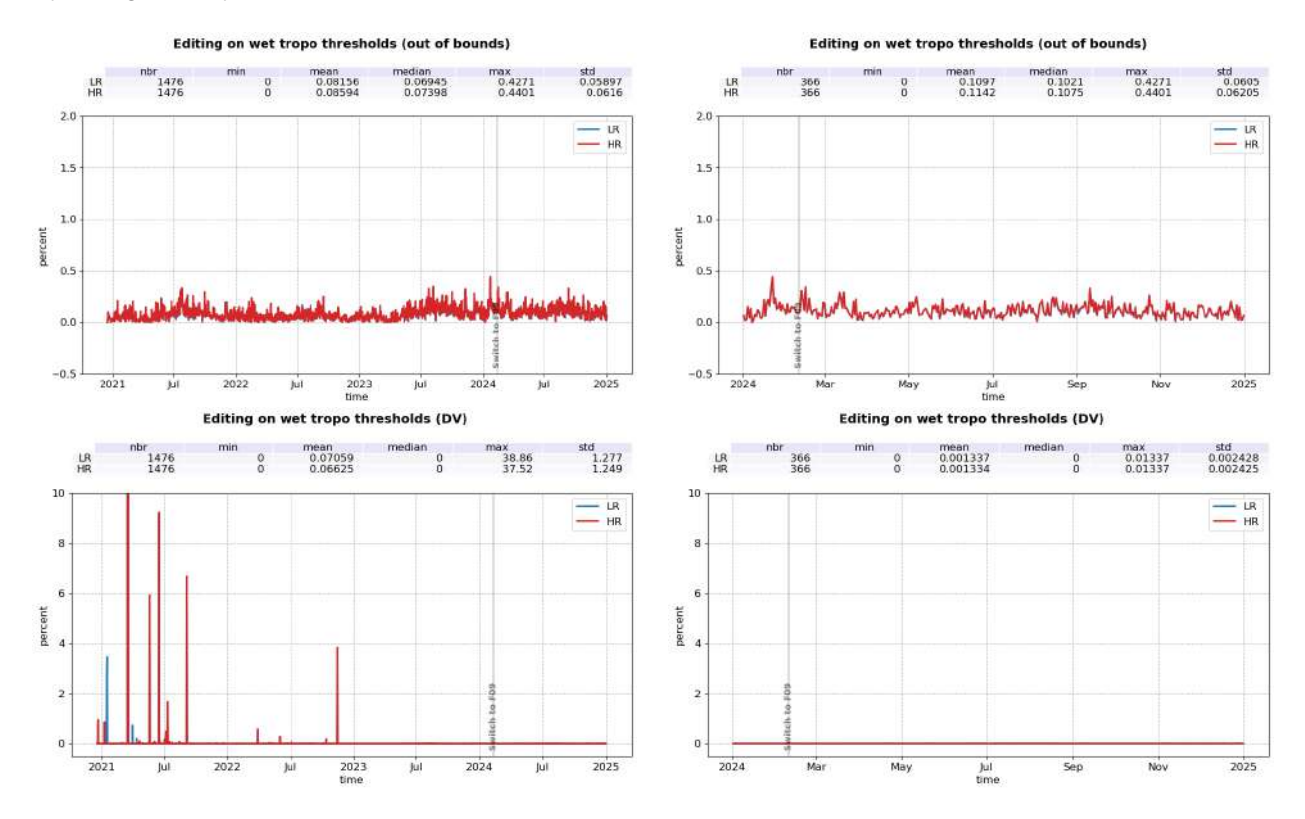


Figure 41: Percentage of data edited on wet tropospheric correction threshold for LR (blue) and HR (red) per day, for out of bounds (top) and default value (bottom) over the entire mission lifetime (left) and 2024 only (right).

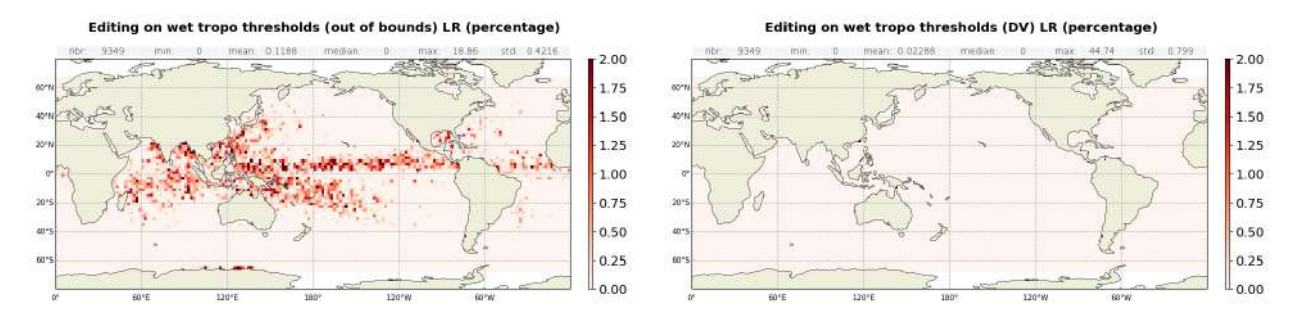


Figure 42: Maps of average percentage of data edited on radiometer wet tropospheric correction threshold, for out of bounds (left) and default value (right), computed on year 2024.

#### Sea surface height

Uncorrected sea surface height represents the difference between the orbit and the altimeter range in Ku-band. Figure 43 summarizes the editing resulting from the sea surface height threshold criterion. It removes in average 2.43% of data for LR MLE4, 1.83 % for LR NR and less than 0.01% of data for HR. In LR, the editing is exclusively due to range measurements at default values near coasts, in wet zones, as well as regions with low significant wave heights or over sea ice (figure 44).

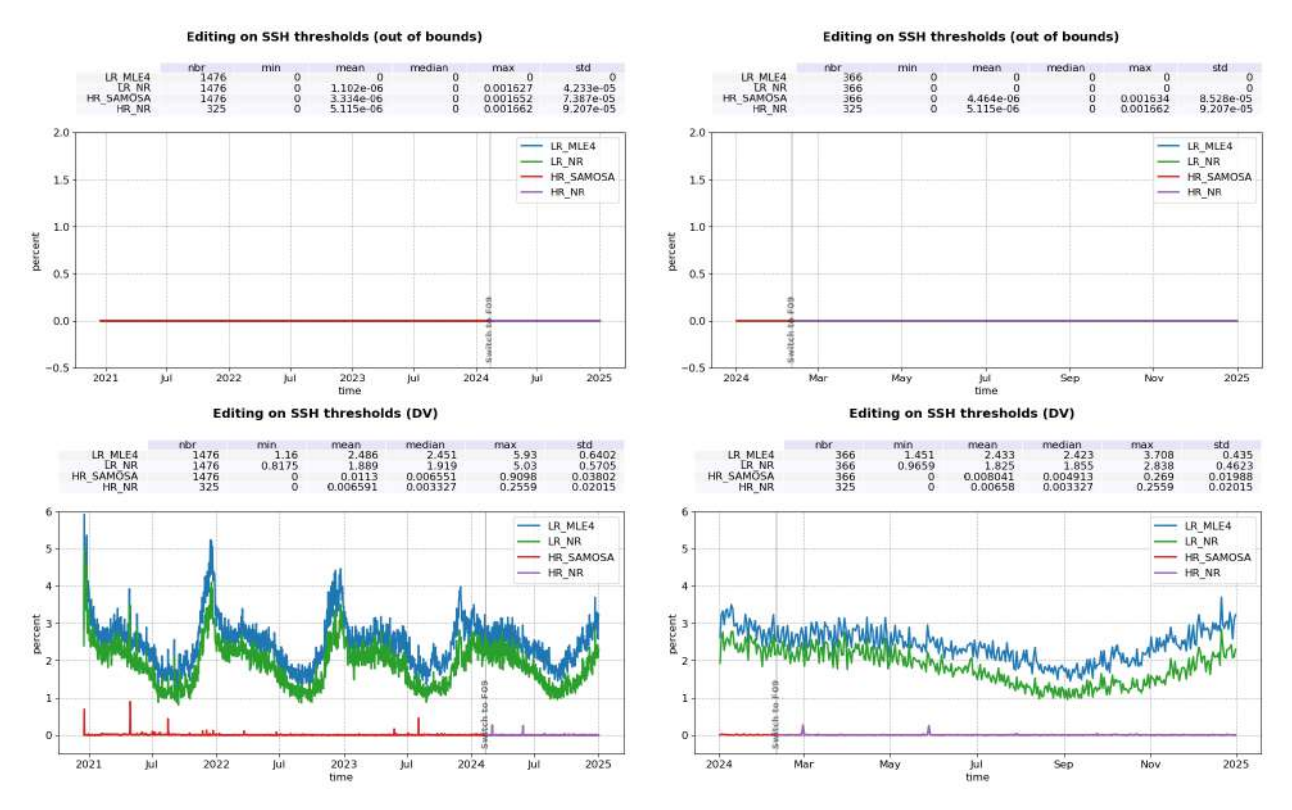


Figure 43: Percentage of data edited on SSH threshold for LR MLE4 (blue), LR NR (green), HR SAMOSA (red) and HR NR (purple) per day, for out of bounds (top) and default value (bottom) over the entire mission lifetime (left) and 2024 only (right).

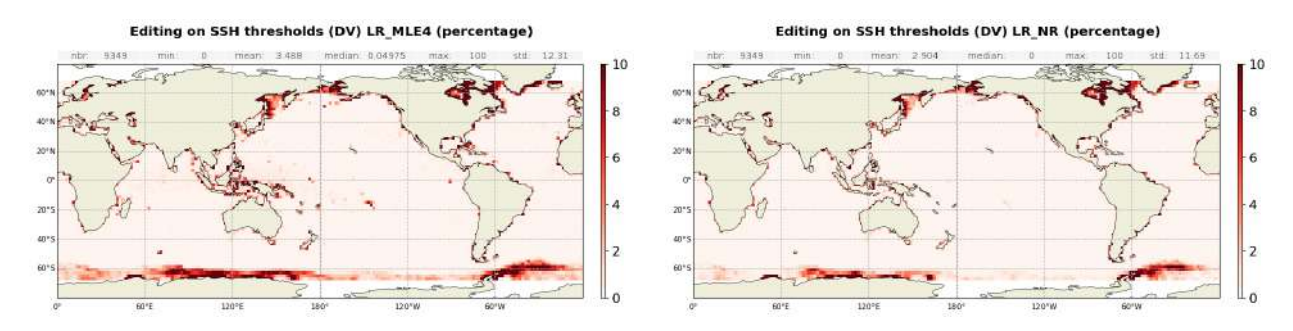


Figure 44: Maps of average percentage of data edited on SSH threshold for LR MLE4 (left), LR NR (right), for default value, computed on year 2024.

#### Sea level anomaly

The percentages of edited data by threshold criterion on SSHA are 3.45% in LR MLE4, 2.78 % in LR NR, 3.06 % in HR SAMOSA and 2.53 % in HR NR (figure 45) over 2024. Edited measurements are almost entirely due to the SSHA being at default value, mostly due to ionospheric correction and, for LR MLE4, SSB. Due to its reducing level, the Caspian sea is now almost entirely edited on the SLA criterion.

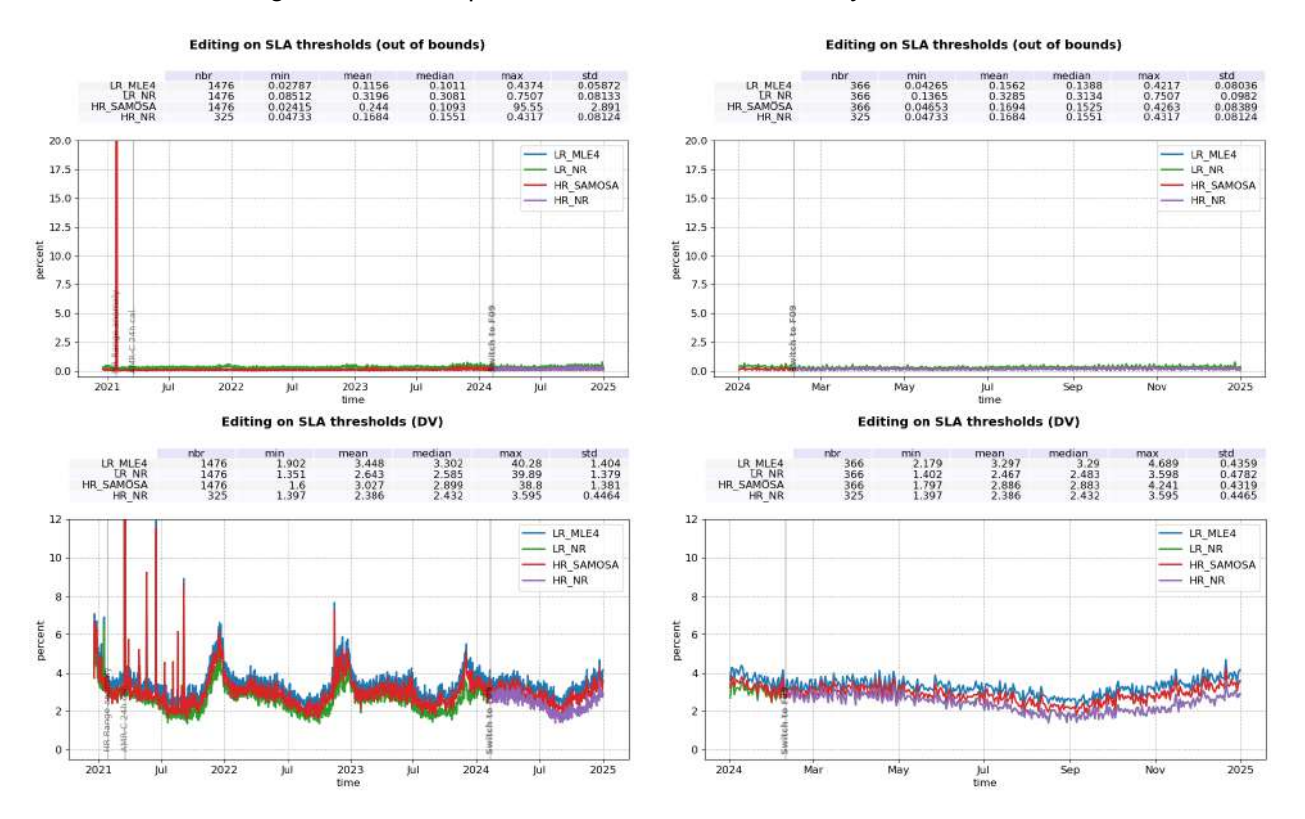


Figure 45: Percentage of data edited on SLA threshold for LR MLE4 (blue), LR NR (green), HR SAMOSA (red) and HR NR (purple) per day, for out of bounds (top) and default value (bottom) over the entire mission lifetime (left) and 2024 only (right).

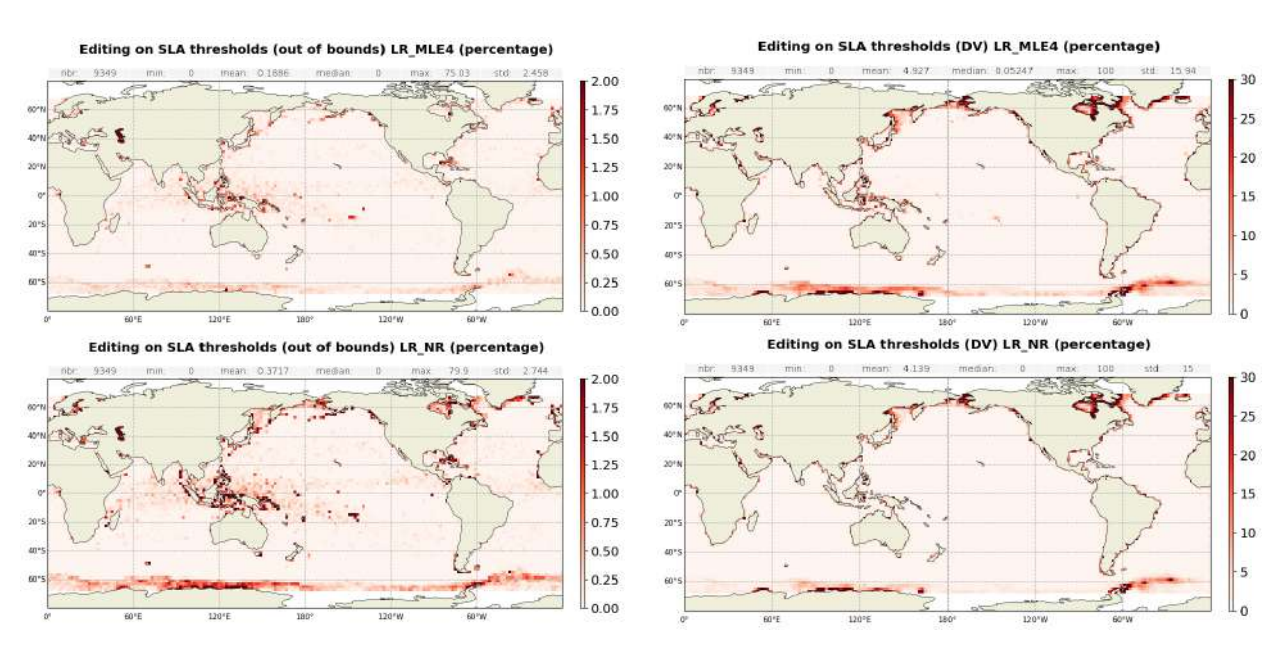


Figure 46: Maps of average percentage of data edited on SLA threshold for both LR MLE4 (top) and LR NR (bottom), for out of bounds (left) and default value (right), computed on year 2024.

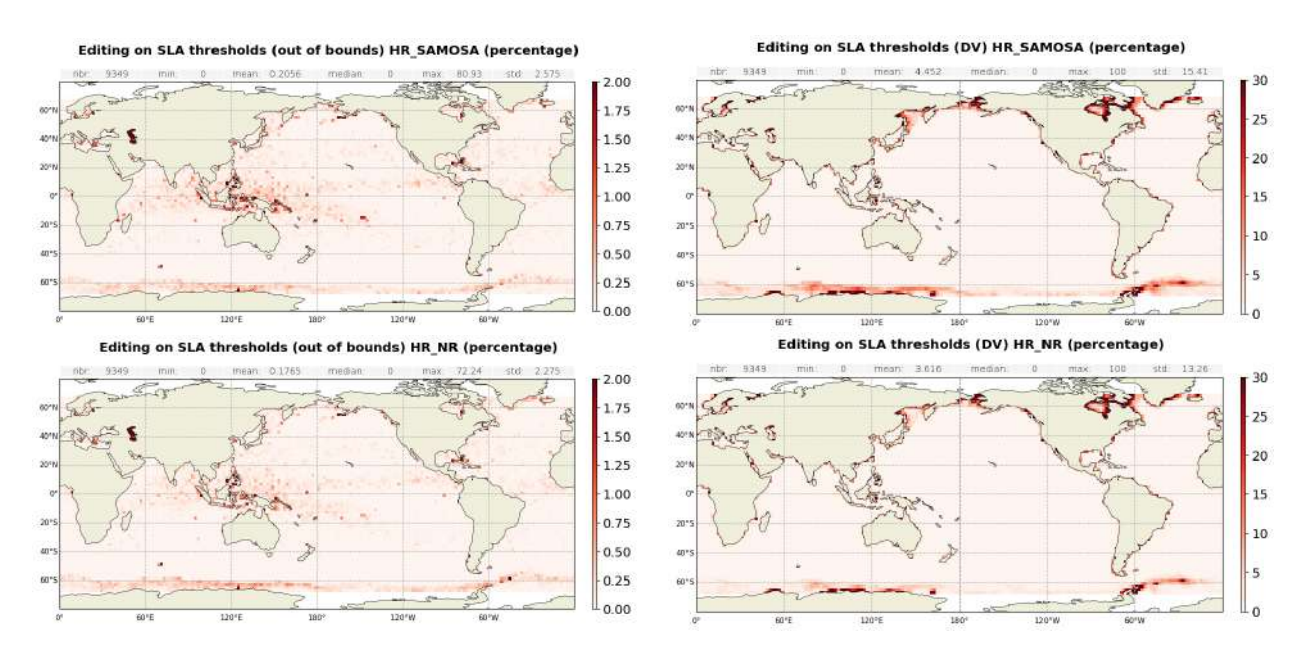


Figure 47: Maps of average percentage of data edited on SLA threshold for both HR SAMOSA (top) and HR NR (bottom), for out of bounds (left) and default value (right), computed on year 2024.

# 4.2.4. Along-track SSHA consistency

Once the thresholds editing is applied, the consistency of the along-track sea surface height anomaly is checked. The statistics of the SSHA by pass are computed, with a selection over open ocean and in areas with low oceanic variability. A pair of thresholds on mean and standard deviation are set as editing criteria. The details are listed in table 5.

No pass has been edited on this criterion over the full mission lifetime.

Parameters	Set 1	Set 2
Selection		
Bathymetry	<-1000m	<-1000m
Coastal distance	>100km	>100km
Oceanic variability	<0.3m	<0.1m
Min number of measure- ments	3	200
Thresholds		
Mean (absolute value)	0.3m	0.15m
STD	0.4m	0.2m

Table 5: Table of parameters used for the editing on the SSHA pass statistics. These parameters are identical in HR and LR.

# 5 Monitoring of altimeter and radiometer parameters

Means and standard deviations of Sentinel-6 MF main parameters have both been monitored over 2024. The goal of this chapter is to summarize these monitorings, along with Jason-3 daily monitoring for comparison.

Only the main results are included in this chapter.

## 5.1. 20 Hz range measurements

The monitoring of the number and standard deviation of 20 Hz elementary range measurements used to derive 1 Hz data is presented here. These two parameters are computed during the altimeter ground processing. Before performing a regression to derive the 1 Hz range from 20 Hz data, a MQE (mean quadratic error) criterion is used to select valid 20 Hz measurements. This first step of selection consists in verifying that the 20 Hz waveforms can be approximated by a Brown echo model (Brown, 1977 [8], Thibaut et al. 2002 [9]).

Then, through an iterative regression process, elementary ranges too far from the regression line are discarded until convergence is reached. Details on this process are available in the Sentinel-6 MF L2 Product Generation Specification [18]. Thus, monitoring the number of 20 Hz range measurements and the standard deviation computed among them is likely to reveal changes at instrumental level.

#### 5.1.1. 20 Hz range measurements number

Figure 48 presents the average number of 20 Hz elementary range measurements used to derive 1 Hz ranges in Ku and C-band. In Ku-band, more elementary measurements are used in average in LR mode (19.6 for both MLE4 and NR) than in HR (18.5), with LR C-band in between (19.1).

These values are stable over time and are in line with Jason-3 for LR data.

A slight latitude dependency can be seen in Ku-band for Sentinel-6 MF (figure 49), with lower values at high latitude. This is expected because the Sentinel-6 MF PRF varies with altitude, the number of averaged 20Hz measurements is slightly lower at high latitudes. The behavior is different on Jason-3 (bottom panel), more dependent of sea state conditions. For the C band (figure 50), values are lower near the coast and at high latitudes. This is expected as C band has a larger footprint than Ku band, and is more sensitive to coastline and ice presence.

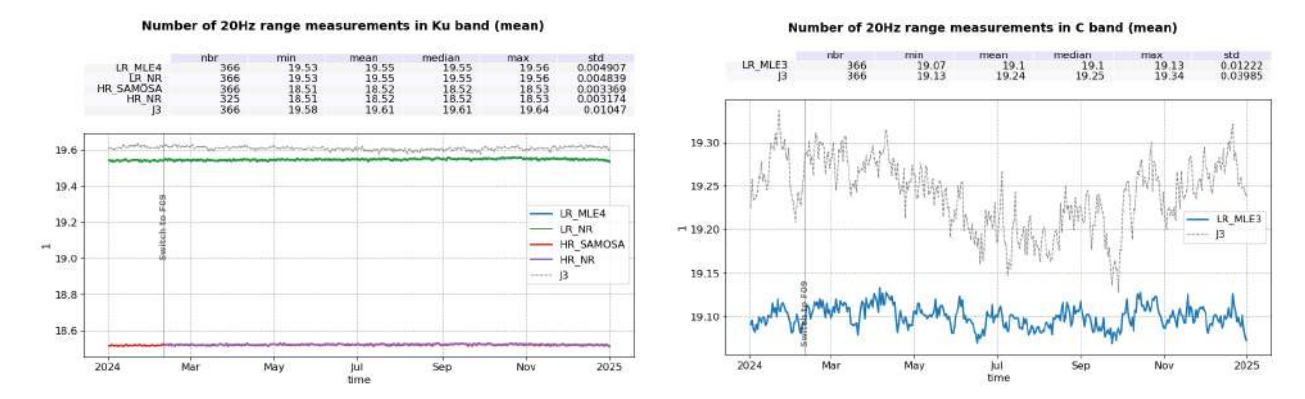


Figure 48: Mean number of 20Hz range measurements for LR MLE4 (blue), LR NR (green), HR SAMOSA (red) and HR NR (purple) per day, in Ku-band (left) and C-band (right, LR MLE3 only).

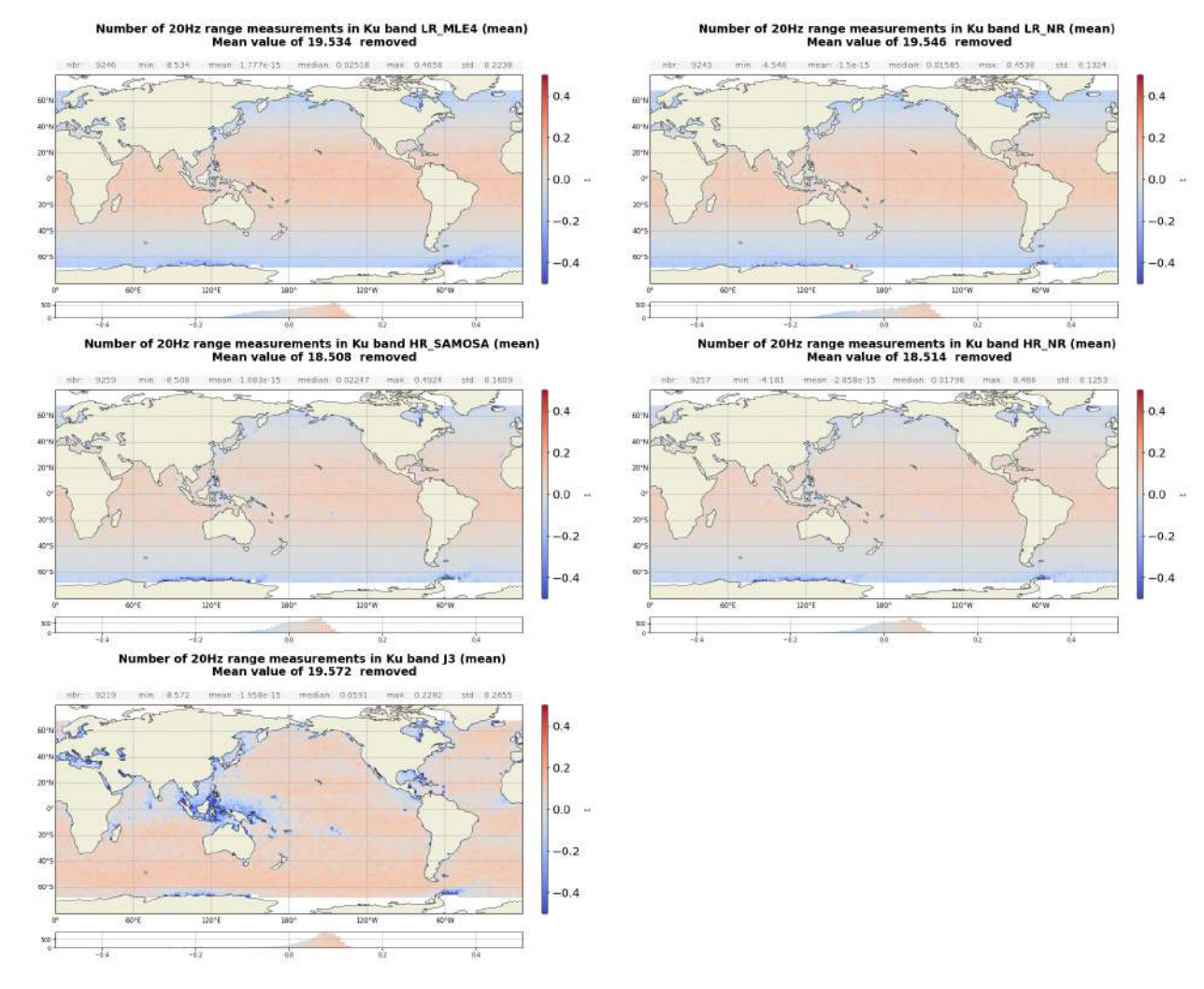


Figure 49: Centred maps of mean number of 20Hz range measurements. Top: maps for Sentinel-6 MF LR Ku band (left: MLE4, right: NR), middle: maps for Sentinel-6 MF HR (left: SAMOSA, right: NR), bottom: map for Jason-3 Ku band. Computed on year 2024.

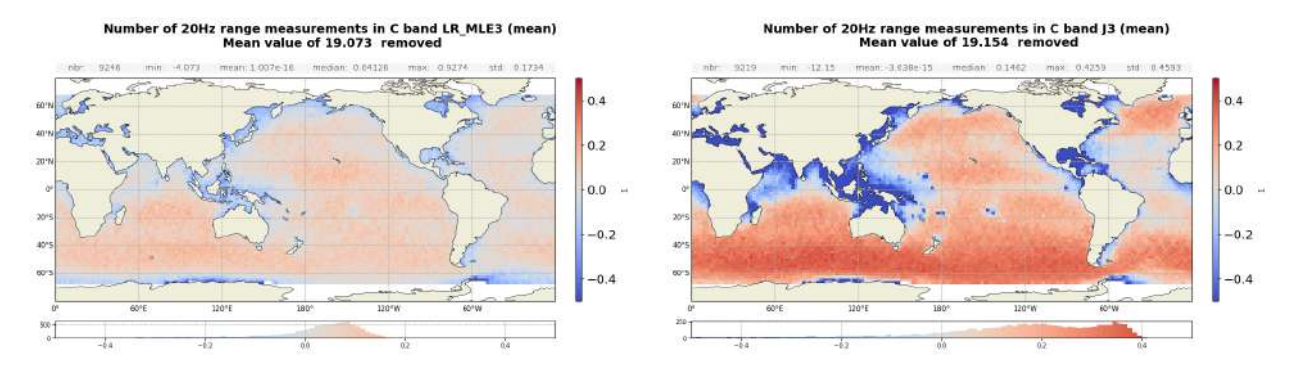


Figure 50: Centred maps of mean number of 20Hz range measurements in C band for Sentinel-6 MF (left) and Jason-3 (right).

### 5.1.2. 20 Hz range measurements standard deviation

Figure 51 presents the standard deviation of the 20 Hz elementary range measurements used to derive 1Hz ranges in Ku and C band (left and right panels respectively) per day. In Ku-band, Sentinel-6 MF LR range standard deviation is similar between MLE4 and NR, and lower than Jason-3 by 1 cm in average. It shows the improvement brought by Sentinel-6 MF in terms of noise.

Sentinel-6 MF HR range noise is even lower than LR, by 2.7 cm for both SAMOSA and NR, thanks to the HR processing.

Due to the reduced number of pulses, C-band range standard deviation is the highest (0.26 m).

Standard deviation of measurements is correlated to significant wave height (figure 52).

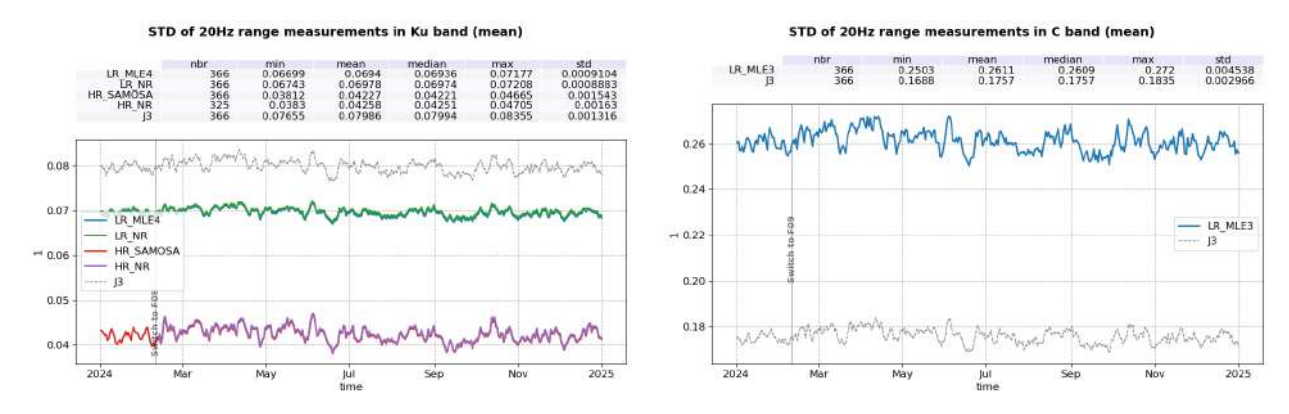


Figure 51: Mean STD of 20Hz range measurements for LR MLE4 (blue), LR NR (green), HR SAMOSA (red) and HR NR (purple) per day, in Ku-band (left) and C-band (right, LR MLE3 only, in blue).

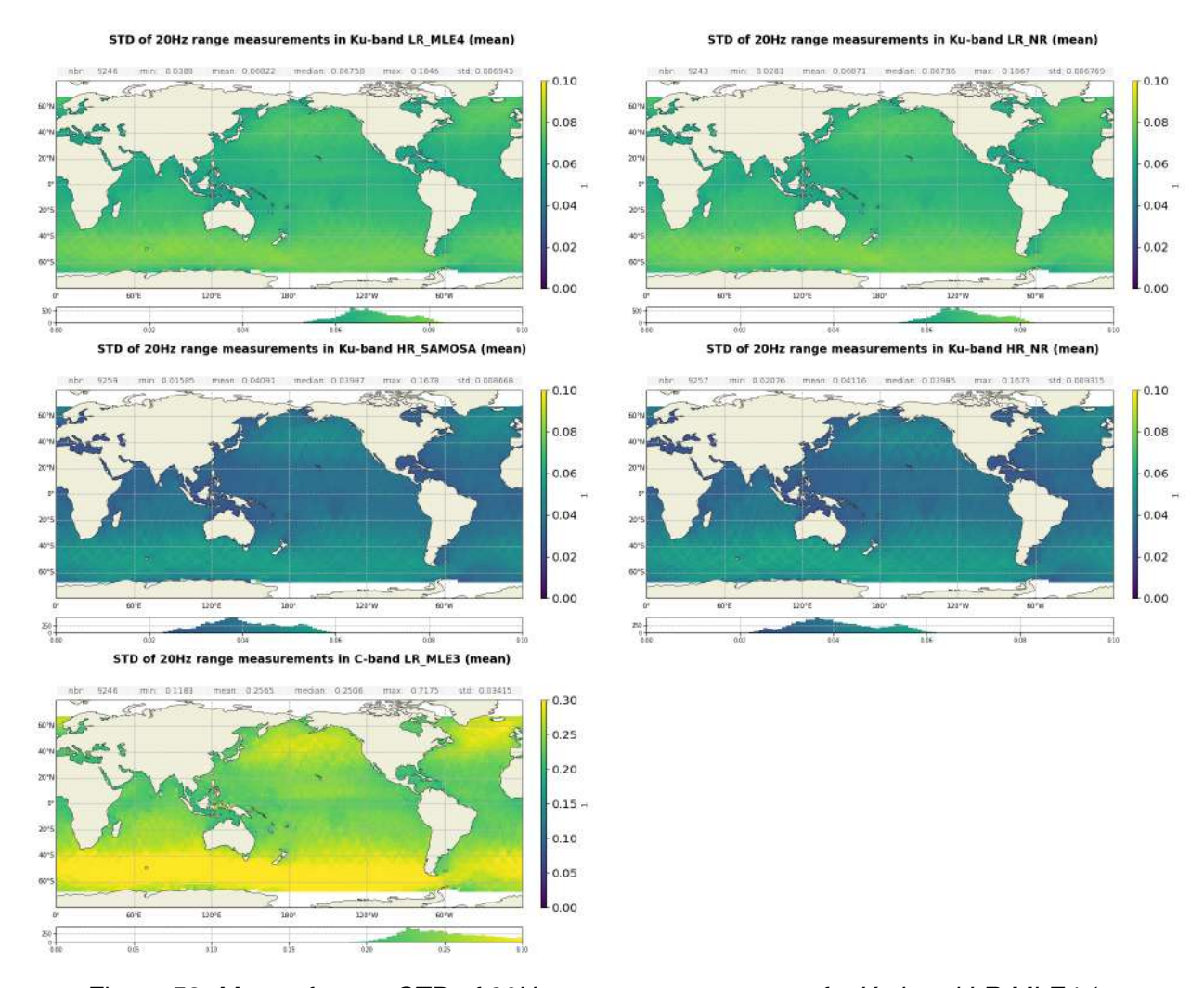


Figure 52: Maps of mean STD of 20Hz range measurements for Ku-band LR MLE4 (top left), LR NR (top right), HR SAMOSA (middle left), HR NR (middle right) and C band (bottom). Computed on year 2024.

# 5.2. Off nadir angle from waveform

This section analyses the square of the off-nadir angle derived from MLE4 and NR waveform retrackers from LR dataset.

The off-nadir angle is derived from the slope of the trailing edge of the waveform during the altimeter processing: it can either be caused by real platform mispointing or by backscattering properties of the surface. The square of the off-nadir angle, averaged on a daily basis (taking into account valid measurements only), has been plotted for Sentinel-6 MF and Jason-3 on figure 53. Mispointing from NR retracking is reduced from 0.008 deg<sup>2</sup> in MLE4 to 0.003 deg<sup>2</sup>. Note that the PB G01 deployed April 2025 aligns MLE4 mispointing to NR thanks to the update of MLE4 instrumental Look-Up Tables.

The corresponding maps for 2024, presented on figure 54, shows higher square off nadir angle in coastal areas and around Indonesia. Figure 55 shows the dependency between the waveform mispointing and the SWH. Mispointing is higher at low SWH (above 0.04 and 0.03 deg<sup>2</sup> at 0 m for NR and MLE4 respectively), however there is no correlation above 2m SWH for either MLE4 and NR.

The standard deviation of the square off nadir angle (right panel) is also much higher at low SWH.

The mispointing distributions are presented in Figure 56 for Sentinel-6 MF and Jason-3. Sentinal-6 MF distribution are centred around 0.008 and 0.003 deg<sup>2</sup> for MLE4 and NR respectively, while Jason-3's is centred on 0. All three time series are stable in time.

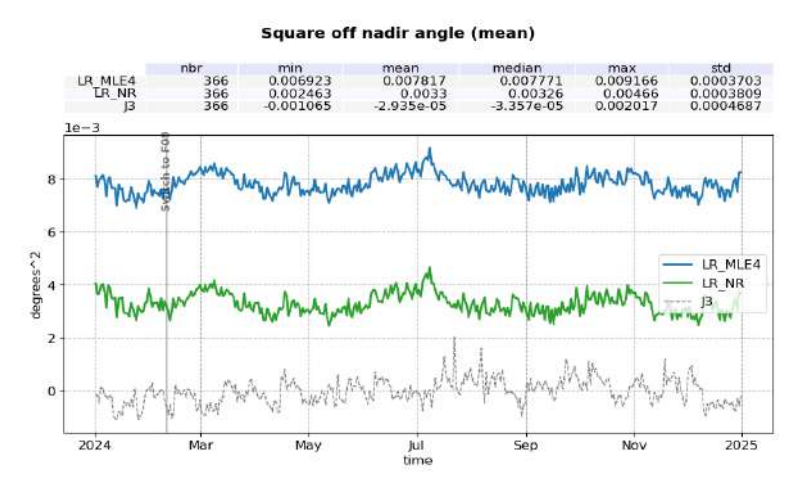


Figure 53: Mean square off nadir angle per day for LR MLE4 (blue) and LR NR (green).

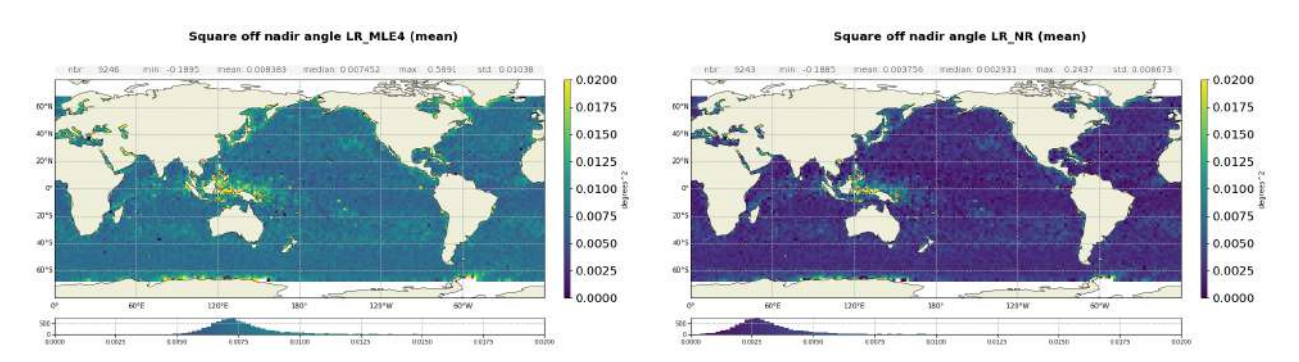


Figure 54: Map of mean square off nadir angle for LR MLE4 (left) and LR NR (right).

Computed on year 2024.

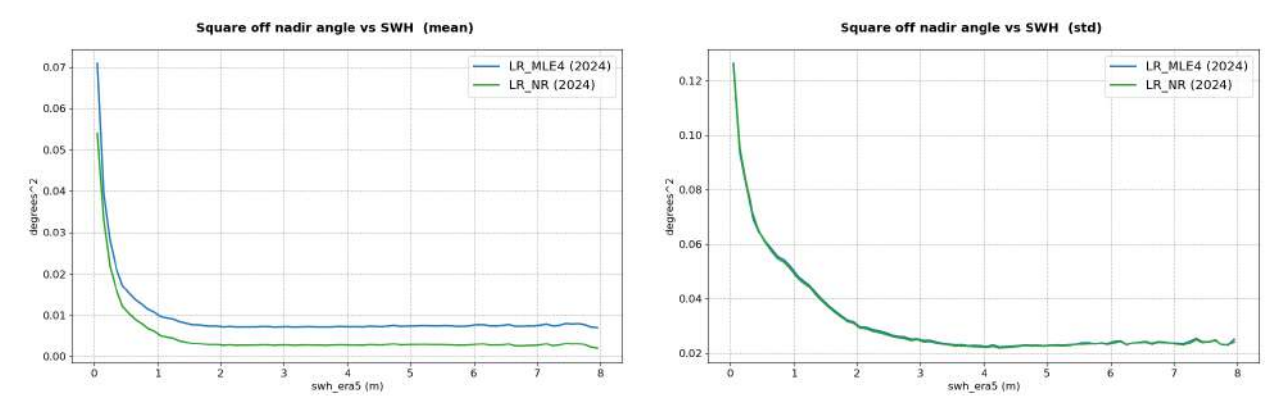


Figure 55: Square off nadir angle wrt SWH for MLE4 (blue) and NR (green).

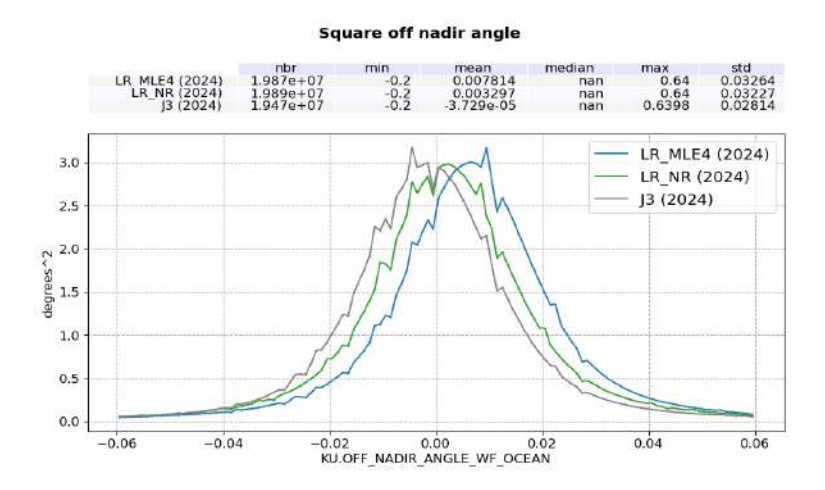


Figure 56: Histogram of square off nadir angle for Sentinel-6 MF MLE4 (blue), NR (green) and Jason-3 (black).

The mean differences between Sentinel-6 MF HR and LR ranges are centred around 1.9 cm for HR SAMOSA - LR MLE4 (figure 57 in black) and less than 1 mm for HR NR - LR NR (in grey), a jump of about +2 mm is visible at the PB F09 update due to the implementation of the range walk correction on HR SAMOSA.

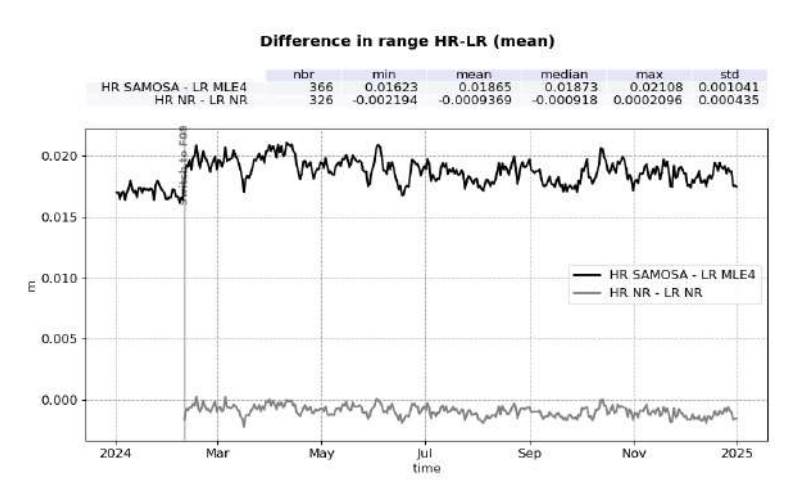


Figure 57: HR SAMOSA - LR MLE4 (black) and HR NR - LR NR (grey) differences in range per day.

The biases between HR and LR ranges are strongly correlated to SWH, as shown in figure 58. Between HR SAMOSA and LR MLE4, the range bias increases by 4.3 cm between 1 and 7 m wave. This correlation is mostly explained by the impact of the different value of wave skewness coefficient used in the LR retrackings (skewness 0.1) and in the HR SAMOSA retracking side (no skewness). This is why the correlation is reduced to about +2 cm between 1 and 7 m SWH in the bias between HR NR, which has a skewness set to 0.1 as well, and LR NR. The residual dependency between LR NR and HR NR is under investigation and probably partly due to pulse-to-pulse correlation effect on LR data. An update of the alpha-p LUT function for HR SAMOSA to account for the skewness would improve consistency with other retrackers.

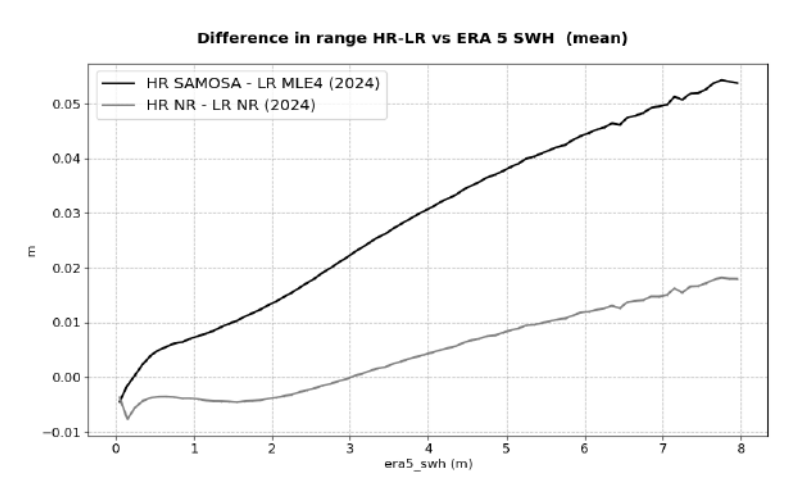


Figure 58: HR SAMOSA - LR MLE4 (black) and HR NR - LR NR (grey) range differences as a function of ERA5 model SWH.

Along track wind has a known effect on HR data and more particularly on HR range [12]. To highlight this impact, two gridded maps of HR (SAMOSA and NR respectively) versus LR (MLE4 and NR respectively) range differences are drawn on figures 59 and 60 respectively, one for ascending tracks and the other one for descending tracks. Next, the difference between these two maps is computed (ascending minus

descending). Such process allows to remove all systematic error on the bias (such as waves) and to only highlight HR variations with respect to LR that depend on track direction. In both cases, bottom left panels clearly show an anti-correlation to meridional wind patterns (bottom right), ranging between -1 and 1 cm.

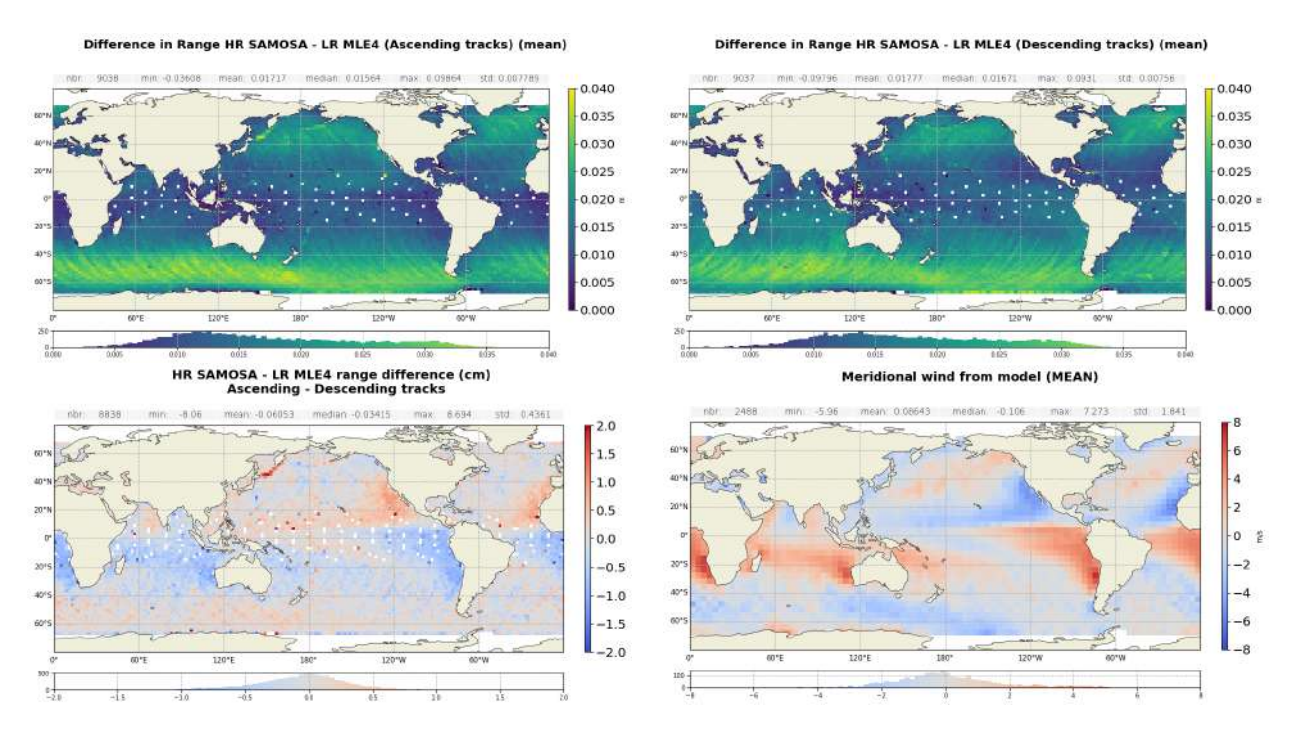


Figure 59: Maps of HR SAMOSA - LR MLE4 difference in range, for ascending tracks (top left) and descending tracks (top right). Bottom left: difference of the two maps above. Bottom right: along-track wind from model. Computed on year 2024.

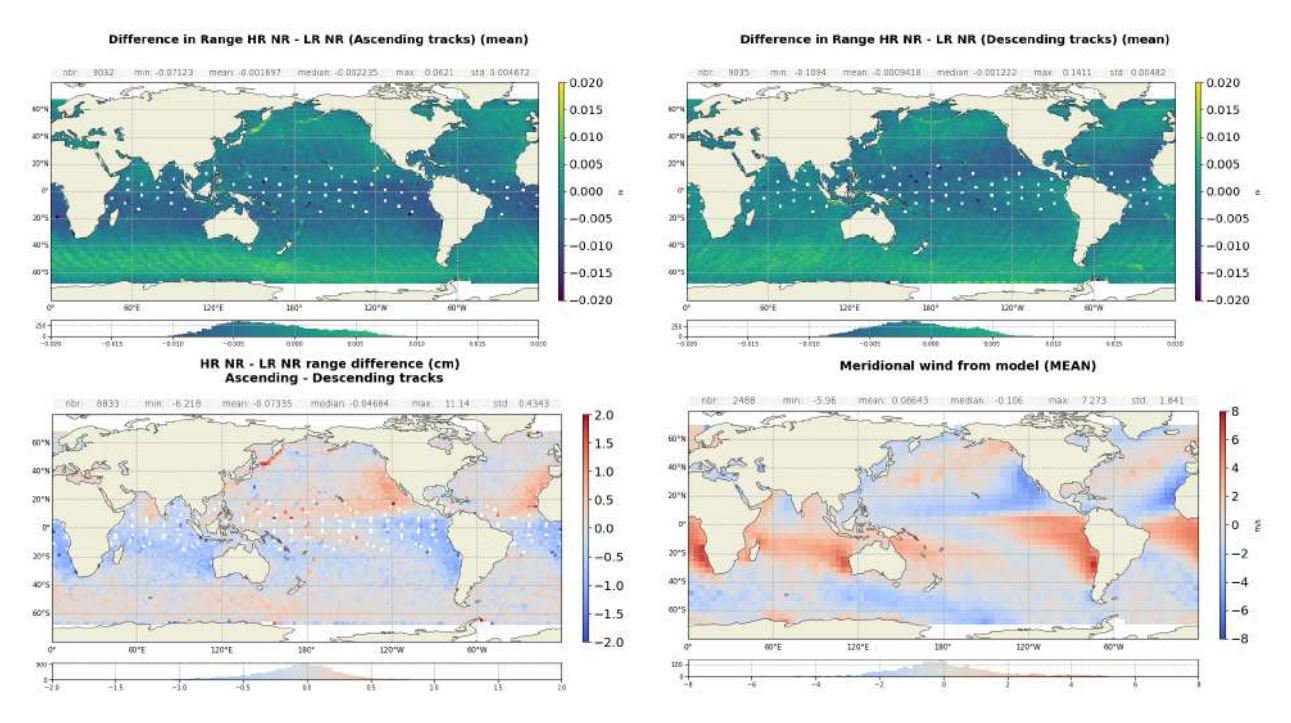


Figure 60: Maps of HR NR - LR NR difference in range, for ascending tracks (top left) and descending tracks (top right). Bottom left: difference of the two maps above. Bottom right: along-track wind from model. Computed on year 2024.

The daily monitoring of LR NR - LR MLE4 range difference is presented on figure 62. The time series is stable. A -2 mm jump is observed at the date of the PB F09 deployment. It is related with a constant bias introduced to correct the LR NR retracker. Note that the time series is still too short to quantify the impact of the NR on the long-term stability with respect to MLE4. The standard deviation monitoring (right panel) presents a yearly variation with higher values from June to September and lower values from December to May, and can be linked with seasonal SWH variations (cf below).

The distributions of range biases are presented on figure 61. LR bias is of 3.9 mm while HR bias is less stable due to skewness difference and centred around -1.65 cm.

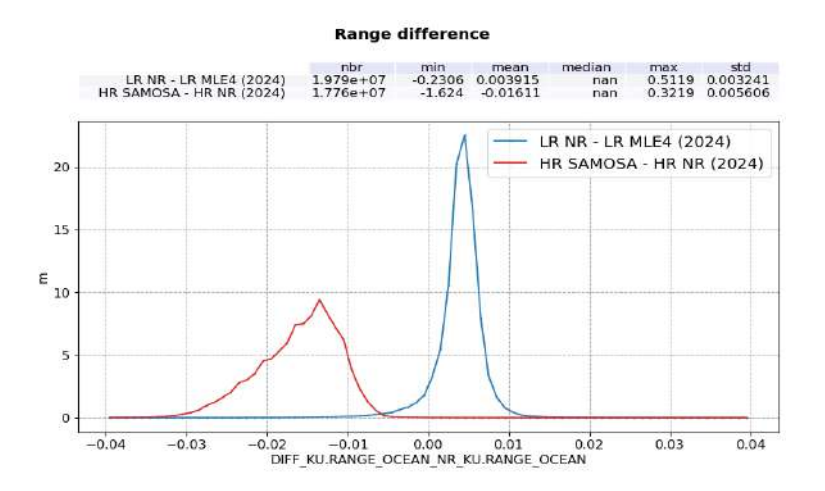


Figure 61: Histogram of HR SAMOSA - LR MLE4 (blue) and HR NR - LR NR (red) differences in range.



Figure 62: Time monitoring of Sentinel-6 MF LR NR - LR MLE4 (blue) and HR NR - HR SAMOSA (red) range difference per cycle, for the mean (left) and the standard deviation (right).

On figure 63 are presented the maps of the LR NR - LR MLE4 and HR NR - HR SAMOSA range differences (top panels) and their dependencies to ERA 5 model SWH (bottom panel). The differences are correlated to SWH, with about +7mm increase between 1 and 7m SWH in LR. This bias increase is caused by a non-optimal calibration of the MLE4 LUT, which has been revised with the PB G01 in 2025. In HR, the bias is of -1.7 cm between 1 and 7m SWH, and caused by the skewness difference between SAMOSA and NR, as explained before.

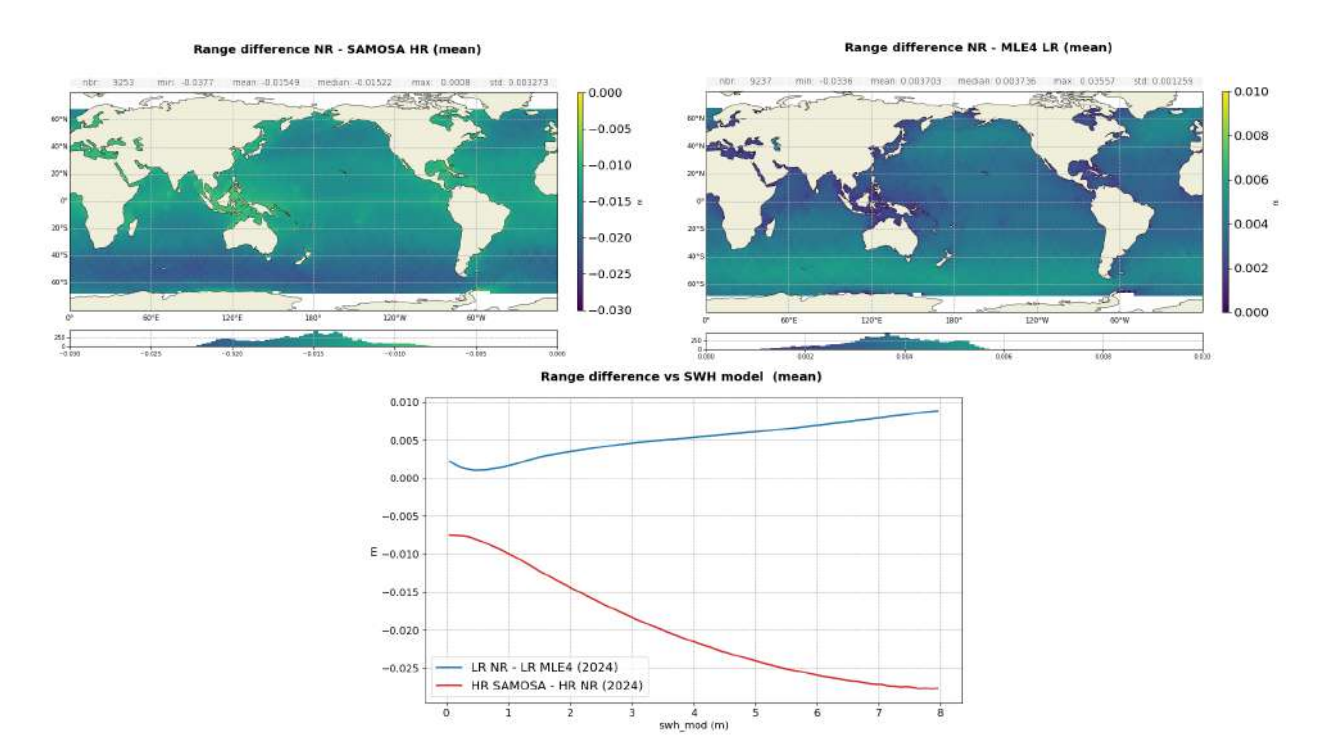


Figure 63: HR-LR differences for Ku-band range for HR NR - HR SAMOSA (top left) and LR NR - LR MLE4 (top right). Bottom: difference with respect to ERA5 SWH.

# 5.4. Significant wave height

The mean geographical distribution of SWH over 2024 for each retracking solution (either LR or HR) is depicted in figure 64 for Ku- and C-band . All solutions show a similar geographical pattern.

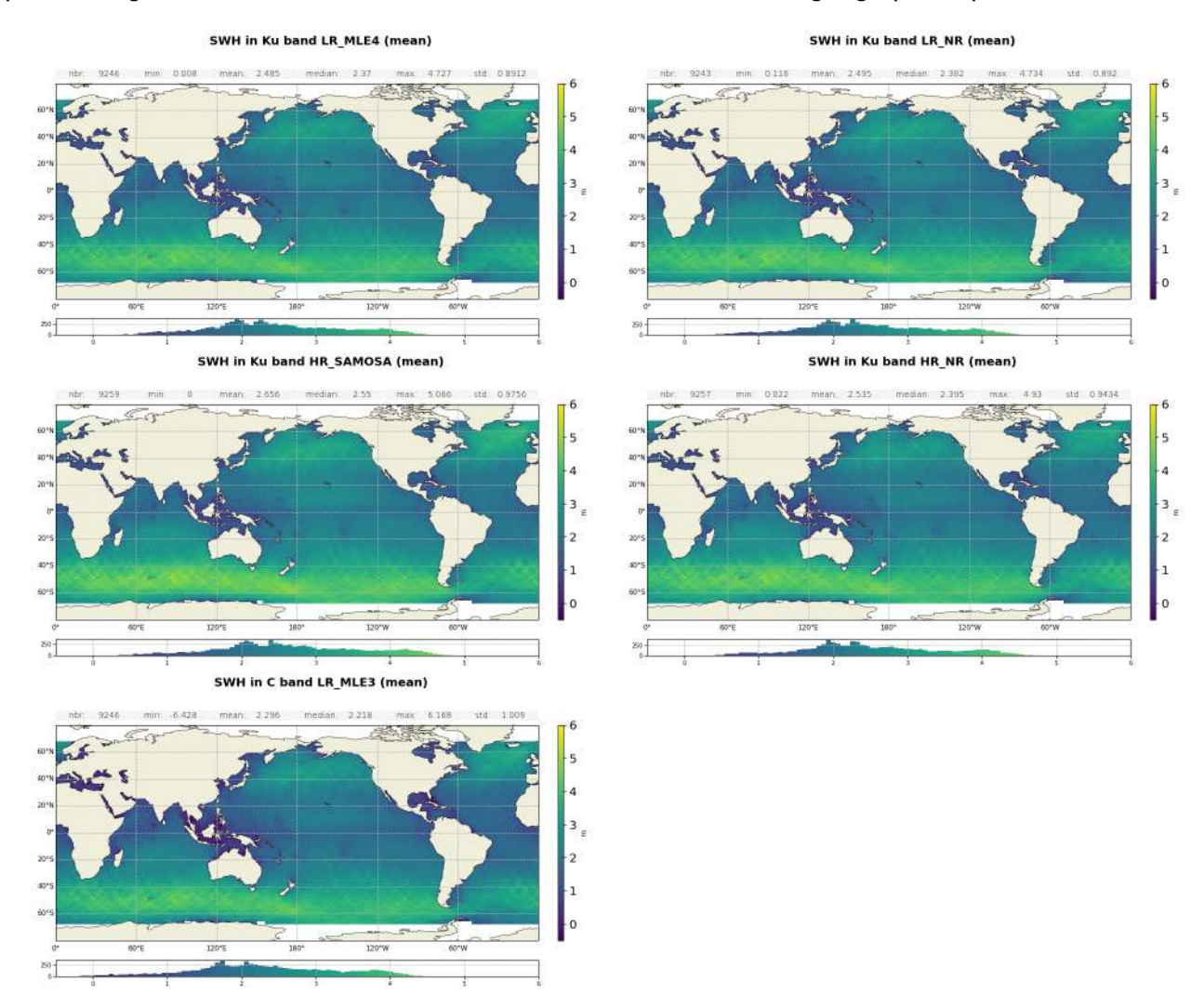


Figure 64: Maps of mean SWH for Ku band LR MLE4 (top left), LR NR (top right), HR SAMOSA (middle left), HR NR (middle right) and C band (bottom). Computed in the year 2024.

The mean Ku band SWH value is centred around 2.67 m for LR MLE4, 2.68 m for LR NR, 2.85 m for HR SAMOSA and 2.71m for HR NR. Sentinel-6 MF LR Ku band SWH are in line with Jason-3, centred around 2.66 m, except at very low wave heights, where Sentinel-6 MF performs better, due to its improved handling of low wave heights in the Level 2 processing. For C-band, the average SWH is 2.49 m for Sentinel-6 MF and 2.68 m for Jason-3, due to LUT differences. These values are stable over time, as shown on figure 65.

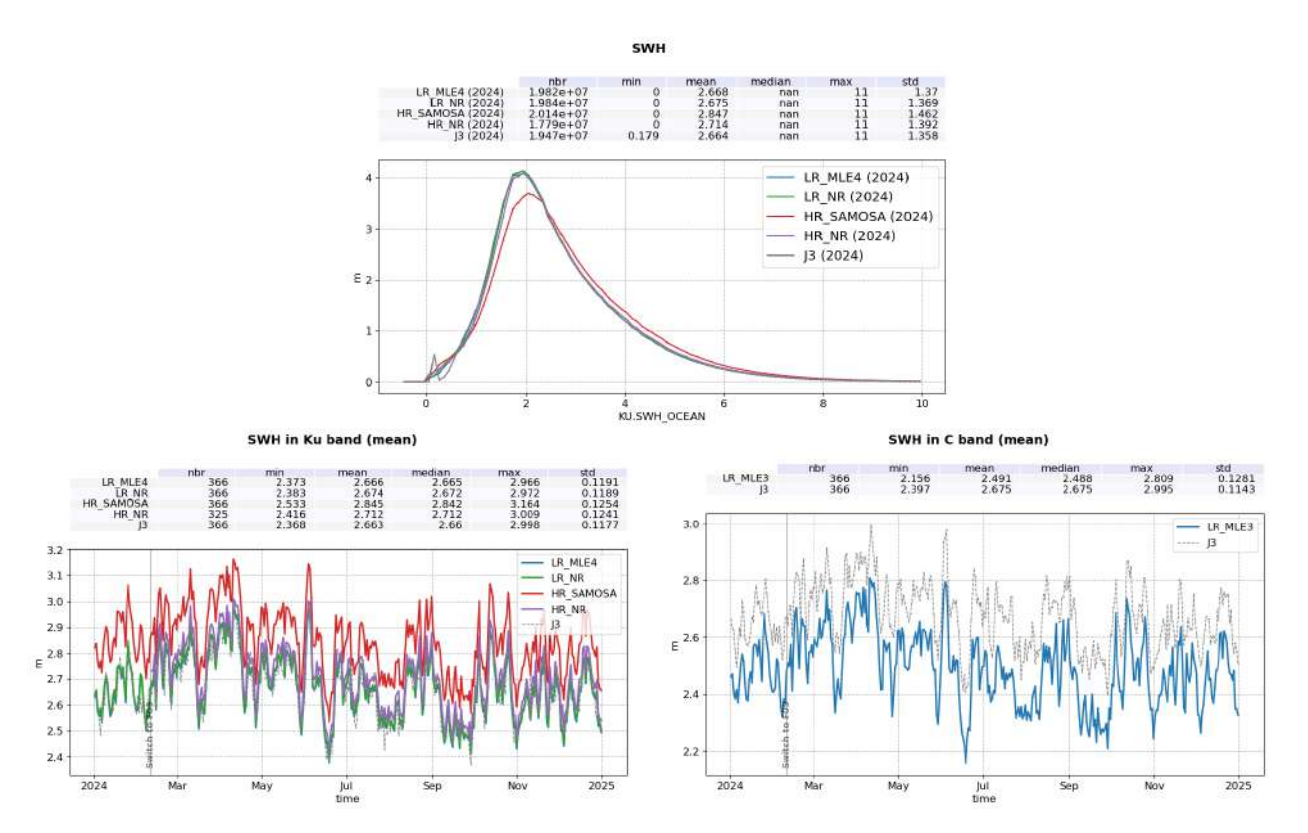


Figure 65: Top: Histogram of Ku-band SWH for Sentinel-6 MF LR MLE4 (blue), LR NR (green), HR SAMOSA (red), HR NR (purple) and Jason-3 (black). Bottom: daily monitoring of SWH mean in Ku-band (left) and C-band (right).

Sentinel-6 MF SAMOSA HR SWH results are not aligned with Sentinel-6 MF LR nor with Jason-3 due to not yet corrected impact of ocean vertical velocity on SAMOSA data [14]. It results in a bias with respect to LR MLE4 SWH of 20.4 cm in average (figure 66 left panel), which strongly depends on SWH values (figure 66 bottom panel). It ranges from about 5 to 40 cm between 1 and 7 m SWH. A small jump is visible on the HR SAMOSA and LR MLE4 at the switch to PB F09 (about -2.5 cm). This is due to the implementation of the range walk correction in the HR processing, impacting both the range and SWH retrievals. The long-term effect of the range walk correction will be assessed in the future full mission reprocessing planned for 2025.

HR NR, on the other hand, is corrected from vertical wave motion thanks to a LUT implemented in PB F09 (see section 3.4.). As a result, its difference with LR NR is essentially flat between 1 and 7 m SWH. There is a small 5 cm residual bias still under investigation. The impact of the VWM correction applied on HR NR is also visible in the HR SAMOSA - HR NR difference (figure 68), with a -35 cm correlation to SWH between 1 and 7 m. In PB F09, the VWM correction is available at 1 Hz in the Level-2 products. It enables to clearly see the impact of this VWM correction on the data, as shown on figure 67 representing the difference between LR NR and HR NR SWH, with and without VWM correction. This figure clearly show the strong improvement brought by the VWM correction with the reduction of the bias with respect to LR and the suppression of its correlation to SWH. Computing the VWM correction using Sentinel-6 MF parameters instead of MFWAM model might further reduce residual biases.

Note that in PB G01, the VWM correction is also applied to SAMOSA SWH.

On 2024/12/03 from 00:00 to 15:00 (cycle 149, passes 226 to 242), missing MFWAM model data resulted in missing HR NR vertical wave motion correction and consequently degraded HR NR SWH, SSB and SSHA. This translates into an upper peak in the monitoring.

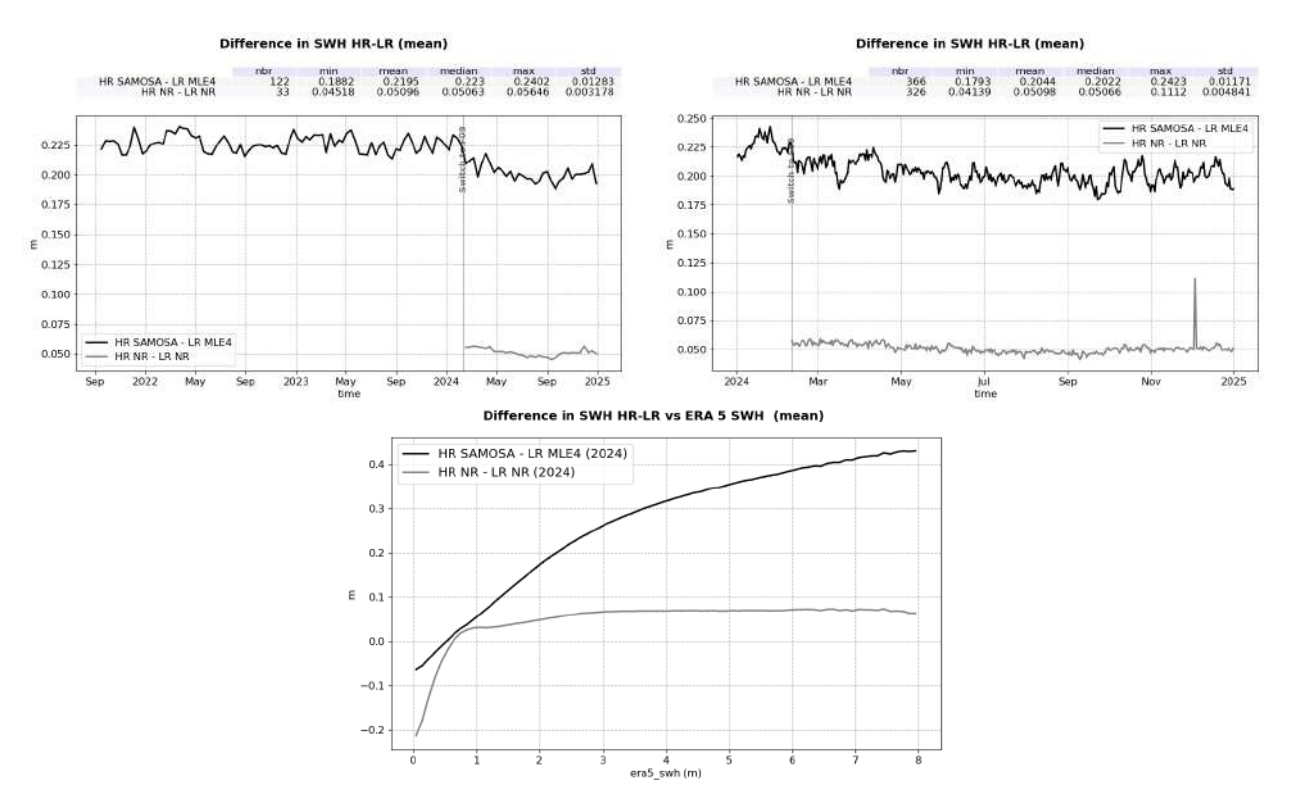


Figure 66: HR-LR differences for Ku-band SWH for SAMOSA - MLE4 (black) and NR (grey). Top left: mean per cycle over side B, top right: mean per day over 2024. Bottom: difference with respect to ERA5 SWH.

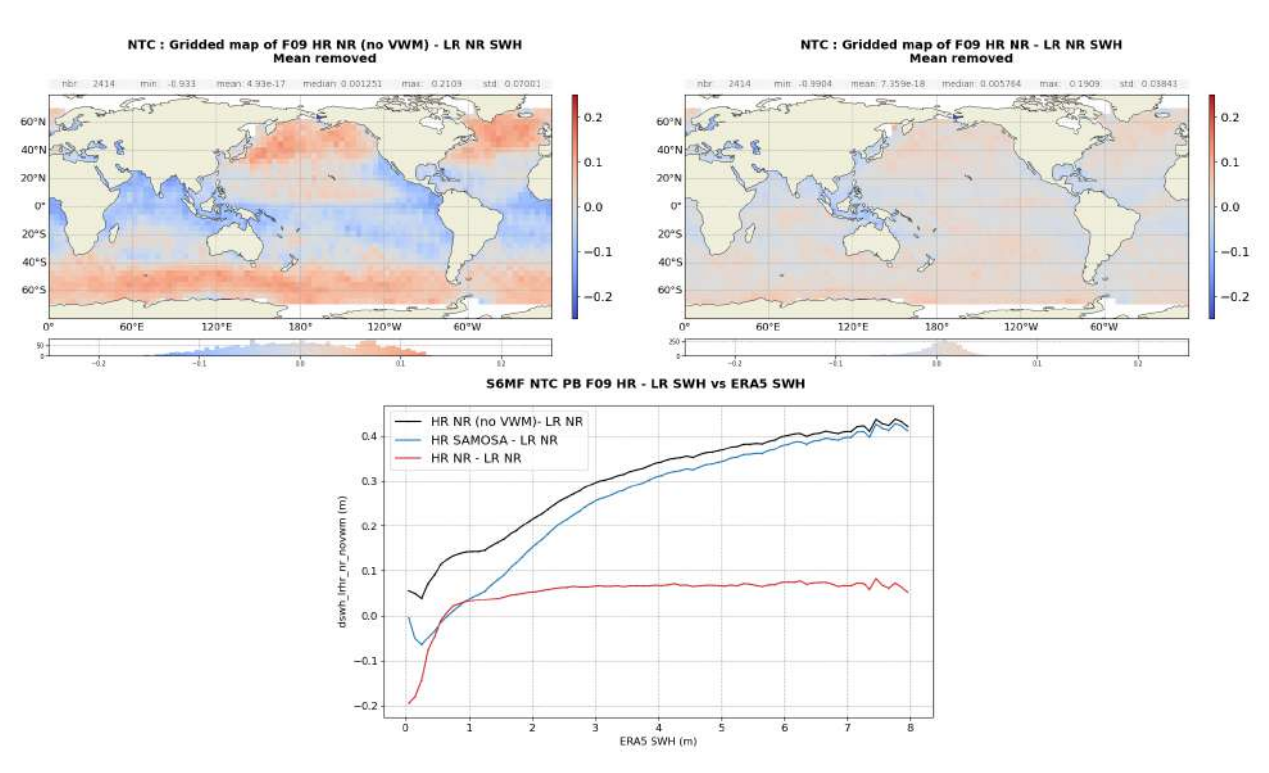


Figure 67: HR-LR NR Ku-band SWH difference. Top left: map for HR NR without VWM correction. Top right: map for HR NR with VWM correction. Bottom: corresponding curves with respect to ERA5 SWH in black and red respectively and for HR SAMOSA in blue. Computed over 1 month of F09 data.

LR NR - LR MLE4 differences do not show any correlation to SWH, only a 1.2 cm global bias due to LR MLE4 that is strongly reduced with the MLE4 LUT update in PB G01 in April 2025. Looking at the corresponding long-term monitoring (blue curve on figure 68 top left panel), a small jump of about 1 cm is visible on the 2023-10-05. It is linked to the deployment of the PB F08 patch version, correcting an anomaly on LR NR SWH (see section 3.4. for more details). The upward peak on December 2024 corresponds to degraded HR NR SWH due to missing MFWAM model data on the 2024/12/03.

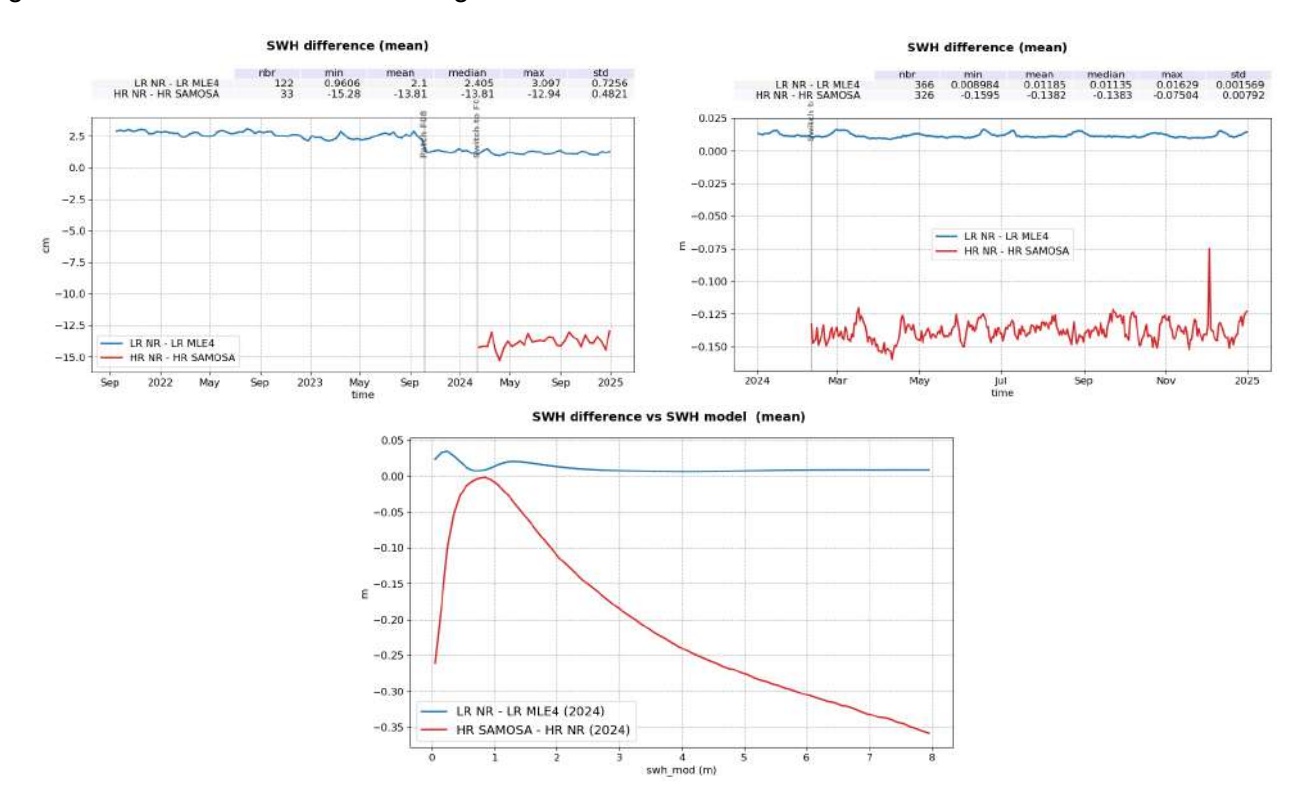


Figure 68: Ku-band SWH differences for LR NR - LR MLE4 (blue) and HR SAMOSA - HR NR (red). Top left: mean per cycle over side B, top right: mean per day over 2024.

Bottom: difference with respect to ERA5 SWH.

Figure 69 shows the difference between altimeter and model SWH over side B for all retrackers. In February 2024, the ERA-5 model has been updated, resulting into a jump of more than 5 cm on all curves. This jump is not linked to the PB update to F09. After this model update, the biases between altimeter and model SWH are higher but more stable.

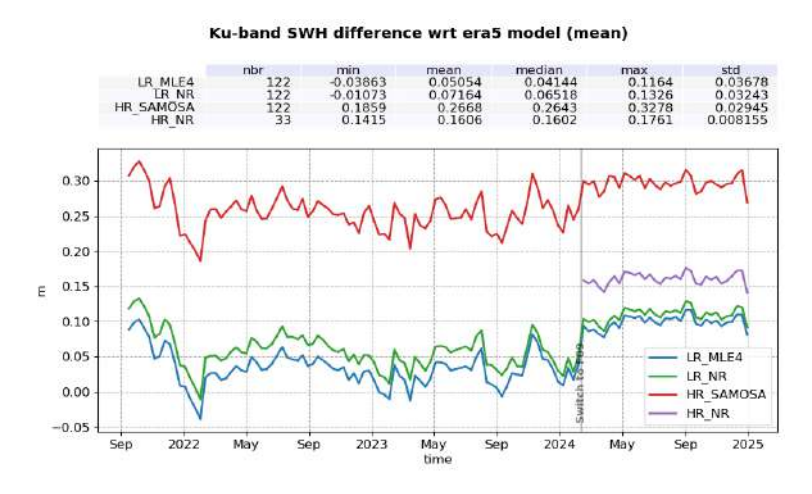


Figure 69: Cyclic mean of the altimeter minus ERA5 model SWH difference for LR MLE4 (blue), LR NR (green), HR SAMOSA (red) and HR NR (purple). Computed over side B.

### 5.5. Backscatter coefficient

The monitoring of the backscatter coefficient (sigma0) per day is presented on figure 70. With the deployment of PB F09, corrections in the backscatter coefficient calculation [5] have been implemented, causing jumps of +0.9 dB in LR MLE4, -6.1 dB in HR SAMOSA and +0.9 db in LR MLE3 in C band. With PB F09, LR backscatter coefficients are now aligned and centred around 13.2 dB. In HR, the two sigma0 are also very similar (centred around 11.9 dB for SAMOSA and 11.8 dB for NR). These values are closer to the Jason-3 value of 13.6 dB. This is true as well for the C band, with a sigma0 centred around 14.6 dB for Sentinel-6 MF and 15.3 dB for Jason-3.

No other jump or drift is visible in the data.

The geographical distributions of the Ku-band HR (SAMOSA and NR), Ku band LR (MLE4 and NR) and C-band sigma0 are presented on figure 71. No significant difference observed at first order between the different sigma0 geographical distributions.

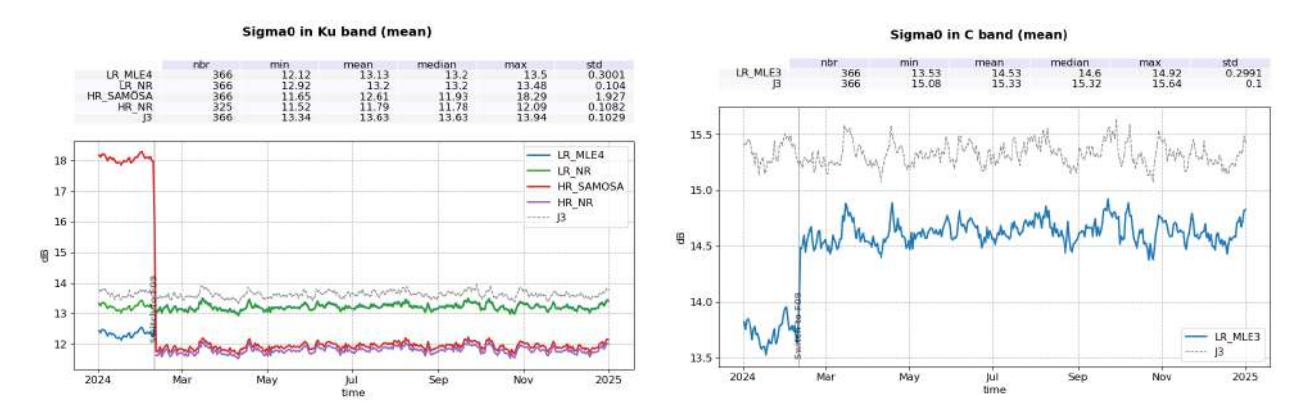


Figure 70: Daily monitoring of Sigma0 mean in Ku-band (left) for Sentinel-6 MF LR MLE4 (blue), LR NR (green), Sentinel-6 MF HR (red) and Jason-3 (black) and C-band (right).

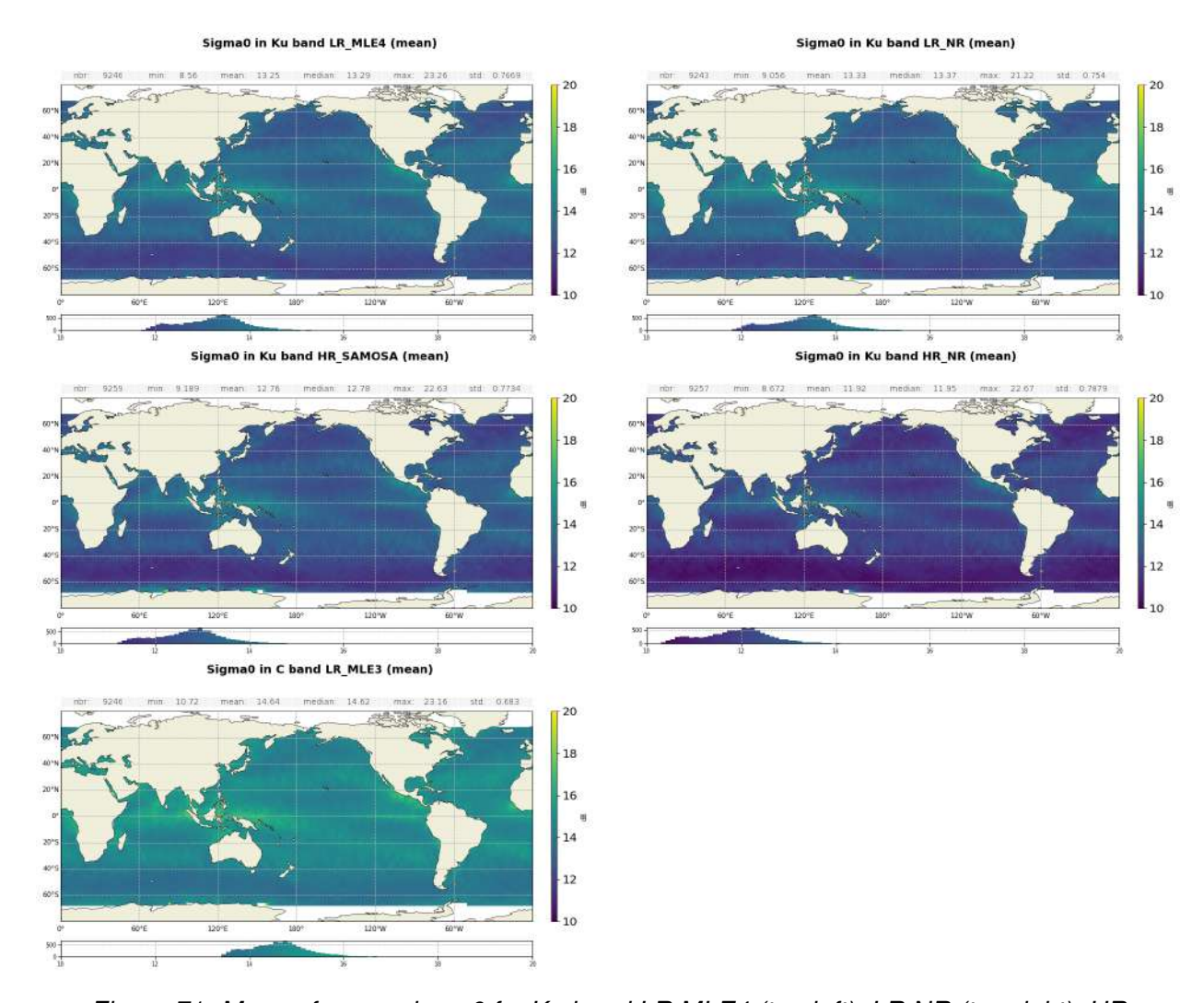


Figure 71: Maps of mean sigma0 for Ku-band LR MLE4 (top left), LR NR (top right), HR SAMOSA (middle left), HR NR (middle right) and C band (bottom). Computed on year 2024.

Figure 72 presents the sigma0 differences between NR and MLE4 in LR mode as well as NR and SAMOSA in HR mode. Other than the jump due to PB F09 update, the time series are stable.

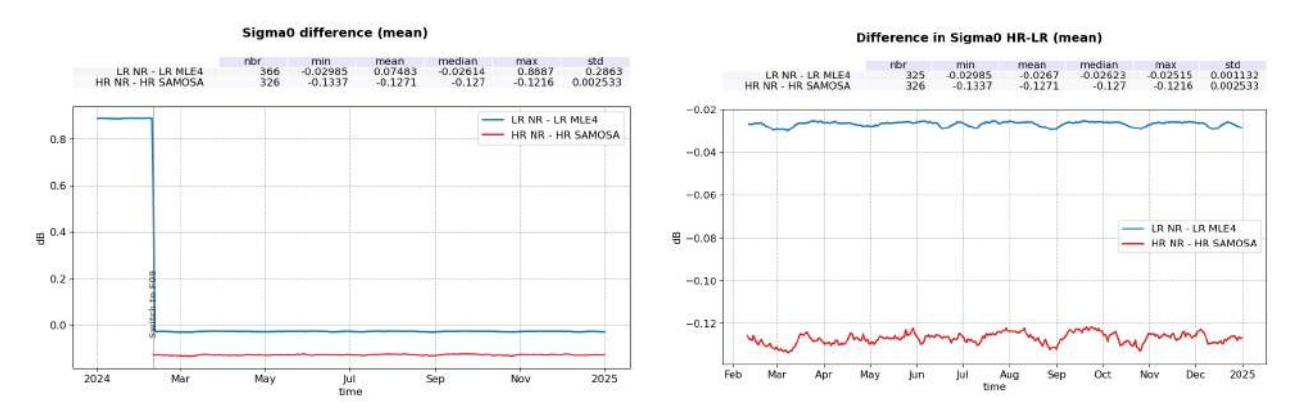


Figure 72: Monitoring of the LR NR - MLE4 (blue) and HR NR - SAMOSA (red) sigma0 differences per day, over 2024 (left) and since F09 update (right).

Figure 73 presents the HR SAMOSA - LR MLE4 (black) and HR NR - LR NR (grey) sigma0 differences, which are centred around -1.4 and -1.5 dB respectively. Besides the PB F09 jump, the time series are stable.

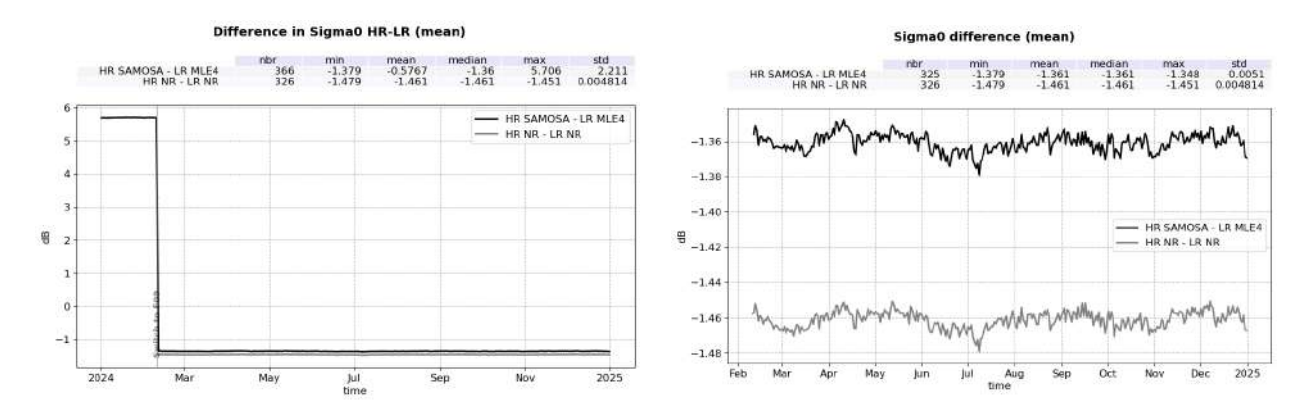


Figure 73: Daily monitoring of the HR SAMOSA - LR MLE4 (black) and HR NR - LR NR (grey) sigma0 difference, over 2024 (left) and since F09 update (right).

## 5.6. Wind speed

For Sentinel-6 MF wind speed computation, the same algorithm as for Jason-3 GDR-F is applied (Collard, 2005 [19]). Its computation takes in input Sentinel-6 MF sigma0 and SWH derived from each mode and retracker. The geographical distribution of altimeter wind speed over 2024 is presented on figure 64 for Sentinel-6 MF LR and HR, and Jason-3. All wind speeds averaged over 2024 share similar geographical patterns.

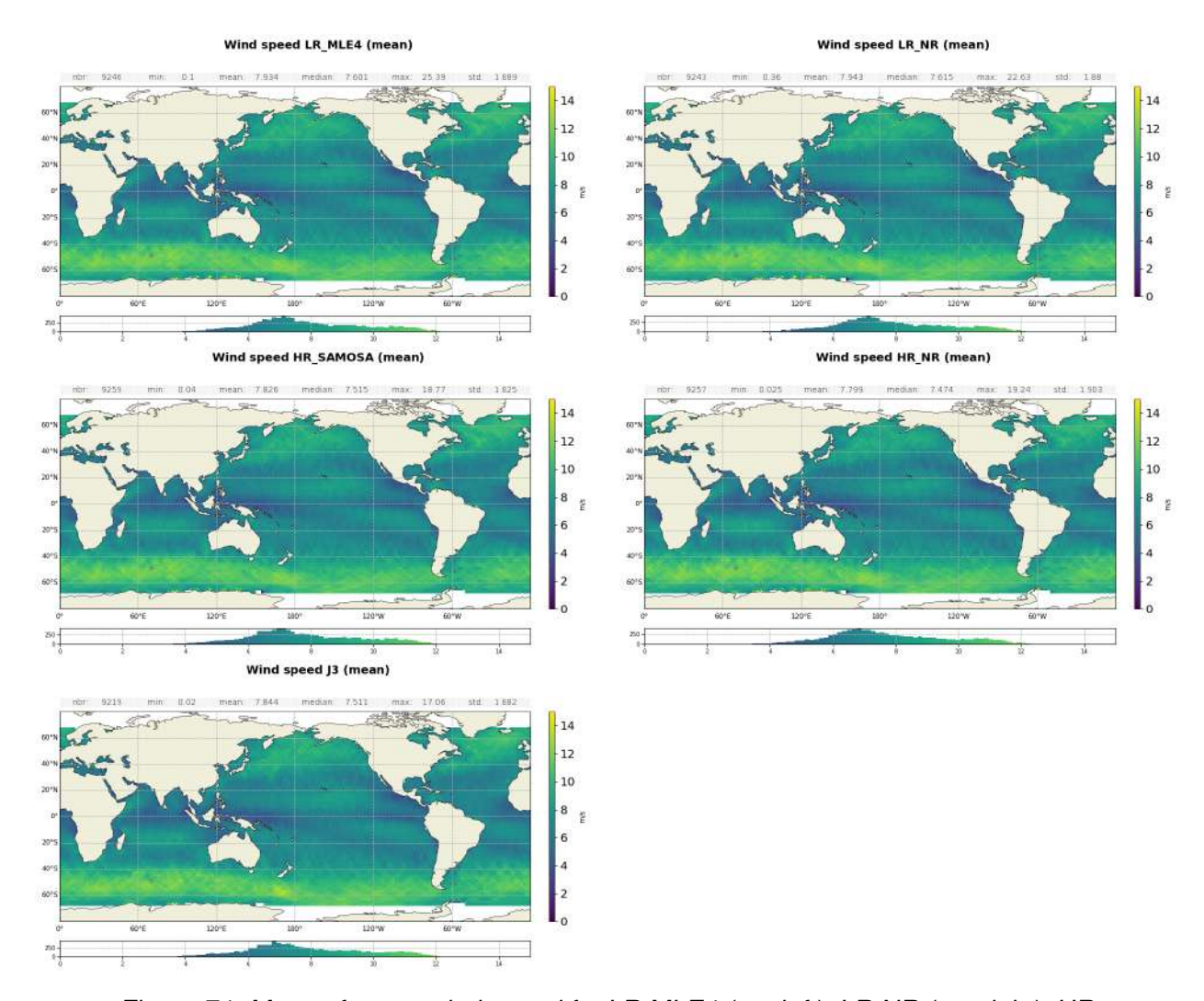


Figure 74: Maps of mean wind speed for LR MLE4 (top left), LR NR (top right), HR SAMOSA (middle left), HR NR (middle right) and Jason-3 (bottom). Computed on year 2024.

The monitoring of the wind speed per day is presented on figure 75 and the corresponding distribution on figure 76. Wind speed is of the same order between all datasets, centred around 8.2 m/s for Sentinel-6 MF LR retrackers as well as Jason-3, and 8.1 m/s for HR, with similar variations, no drift or jump.

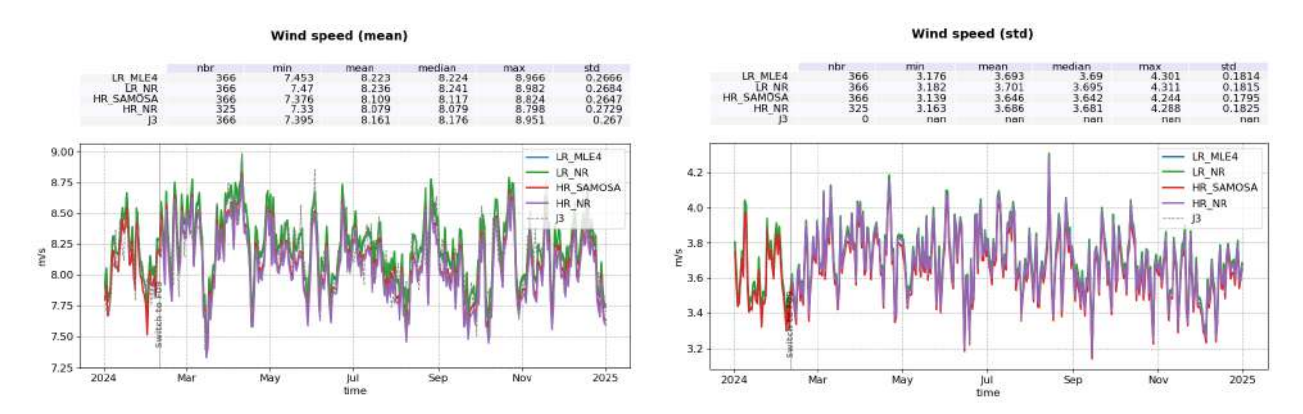


Figure 75: Mean (left) and standard deviation (right) wind speed per day for LR MLE4 (blue), LR NR (green), HR SAMOSA (red), HR NR (purple) and Jason-3 (black).

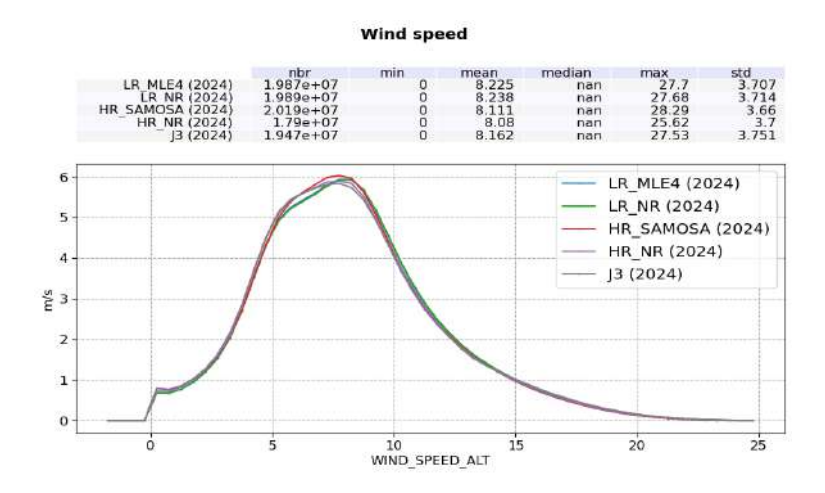


Figure 76: Histogram of wind speed for Sentinel-6 MF LR MLE4 (blue), LR NR (green), HR SAMOSA (red), HR NR (purple) and Jason-3 (black). Computed over 2024.

Figure 77 presents the wind speed differences between retrackers in LR and HR modes in blue and red respectively. In PB F09, the LR NR - LR MLE4 difference is stable. A small jump of about +2 cm/s is visible at the switch between PB F08 and F09, resulting from various corrections in the LR processing (both on NR and MLE4). However, the HR NR - HR SAMOSA differences seem to show a drift of very small amplitude, of the order of -1 cm/s over the year and stronger temporal variations. This drift is under investigation.

The corresponding maps (bottom panels) present a correlation with high Mean Sea Surface (MSS) gradients and a different bias on the Caspian Sea in LR mode. Such behavior originates from sigma0, as map of LR MLE4 versus LR NR sigma0 present the same features (as reported in [11]). The origin of this MSS gradient sensitivity difference between the two LR retrackers is yet to be understood.

HR NR versus HR SAMOSA difference is strongly correlated to SWH. The bias increases by +30 cm/s between 1 and 7 m SWH, while an increase of only +1.5 cm/s is observed between LR NR and LR MLE4 wind-speed. Such a behavior for HR can be linked to the VWM impact HR SWH. This effect is corrected for HR NR SWH but not for HR SAMOSA (see section 5.4. for more details). As SWH is an input of the wind-speed computation, VWM impact on SAMOSA SWH can translate to SAMOSA wind speed.

The monitoring of the HR SAMOSA - LR MLE4 (black) and HR NR - LR NR (grey) wind speed differences is presented on figure 78. Over 2024, differences are centred around -0.03 m/s for HR SAMOSA - LR MLE4 and -0.09 m/s for HR NR - LR NR, with a seasonal variability.

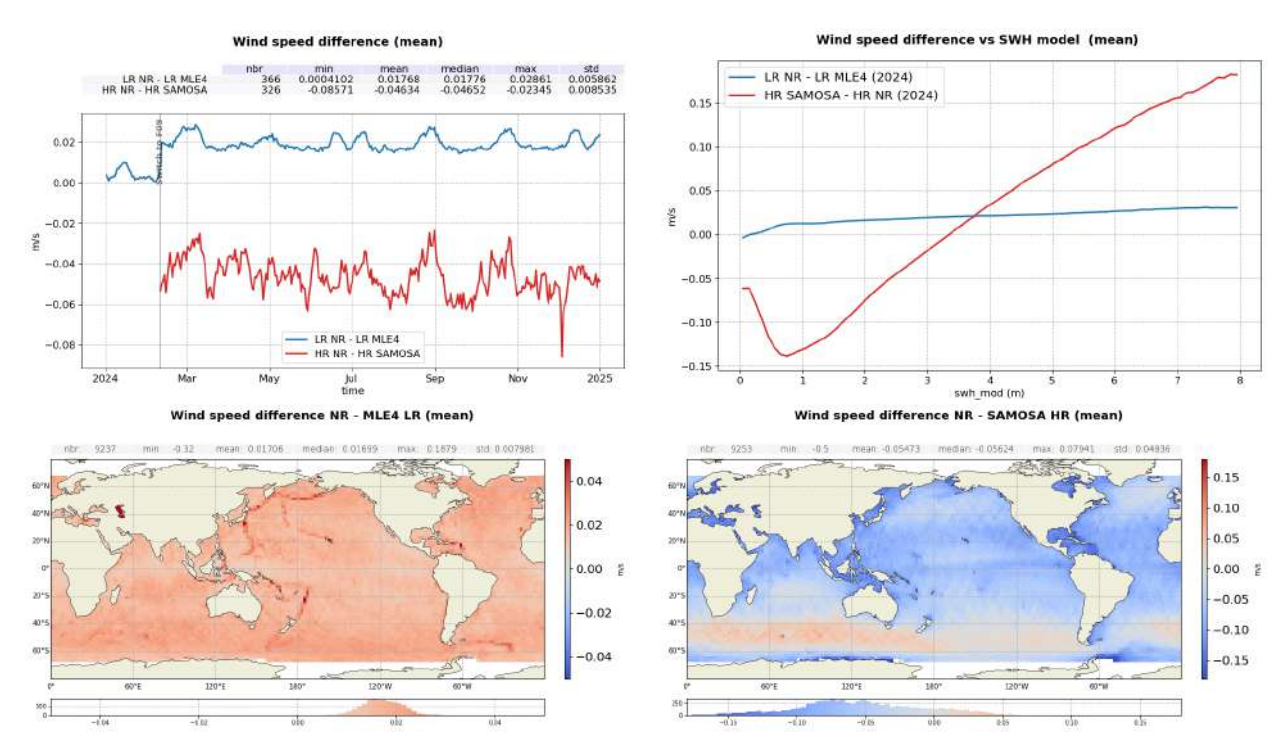


Figure 77: Monitoring per day (top left), correlation to model SWH (top right) and maps (bottom panels) of the LR NR - MLE4 and HR NR - SAMOSA wind speed differences.

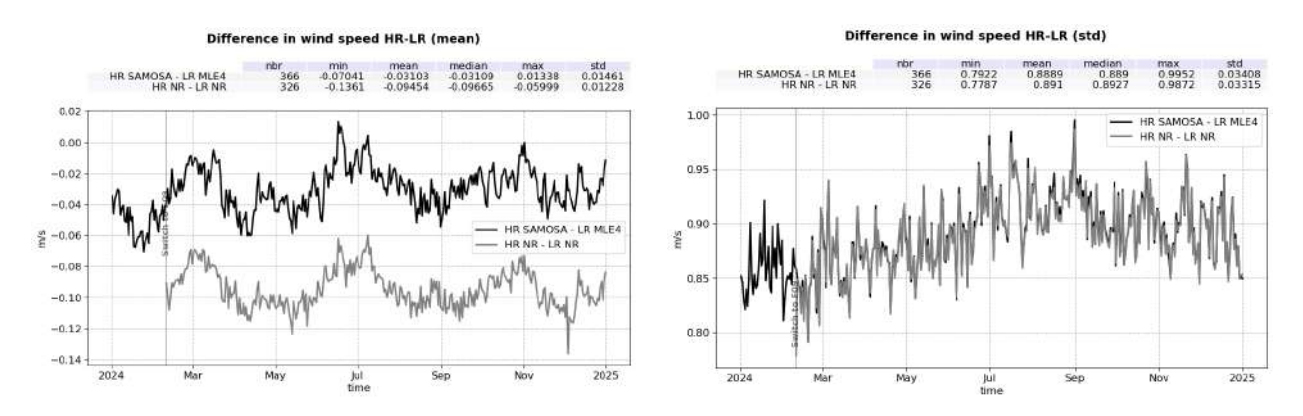


Figure 78: Mean (left) and standard deviation (right) HR SAMOSA - LR MLE4 (black) and HR NR - LR NR (grey) wind speed difference per day.

The monitoring of the difference between the altimeter-derived wind speed and the model is plotted on figure 79. The mean difference per day is higher for Sentinel-6 MF LR retrackings (28.9 cm/s and 30.7 cm/s for LR MLE4 and LR NR respectively) than for HR retrackings (24.6 cm/s and 19.9 cm/s for HR SAMOSA and HR NR respectively) and Jason-3 (24.8 cm/s).

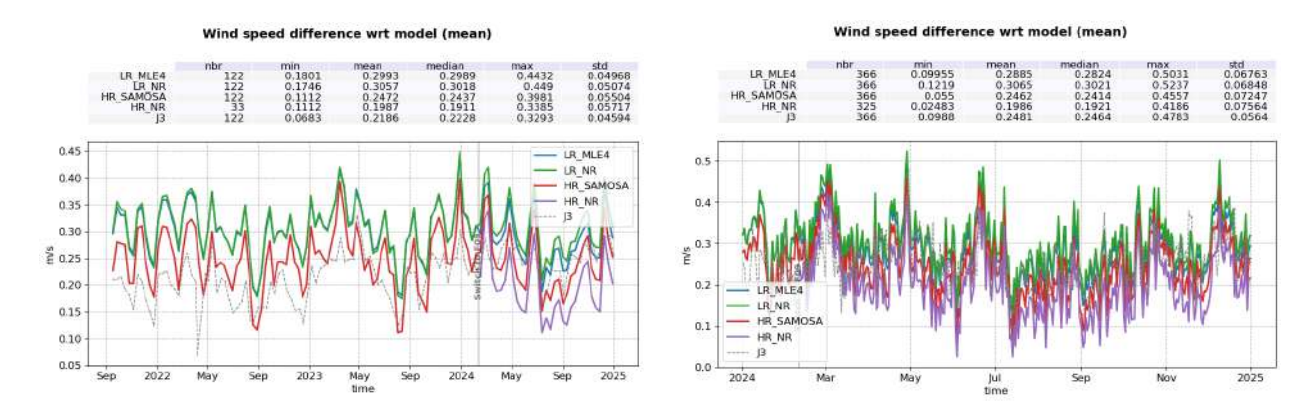


Figure 79: Mean per cycle over side B (left) and per day over 2024 only (right) wind speed difference wrt model for LR MLE4 (blue), LR NR (green), HR SAMOSA (red), HR NR (purple) and Jason-3 (grey).

## 5.7. Sea state bias

Sentinel-6 MF sea state biases (SSB) are computed using Jason-3 GDR-F SSB parametrization. Its computation takes in input Sentinel-6MF wind-speed and SWH derived from each mode and retracker. More details are available in the L2 PGS [18].

Maps of Ku-band SSB averaged over the year 2024 show the same geographical patterns between Jason-3 and Sentinel-6 MF retrackings (figure 80).

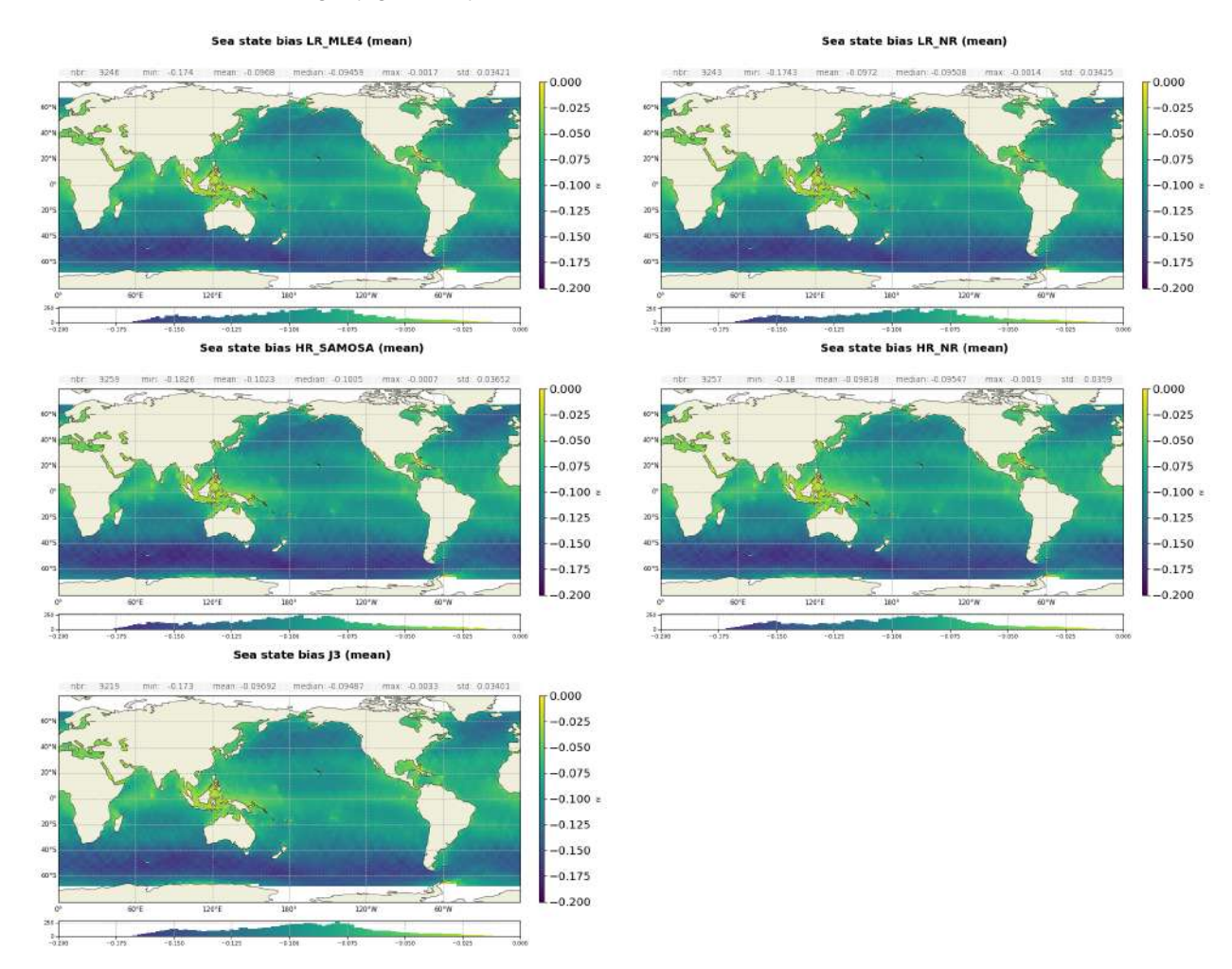


Figure 80: Maps of mean SSB for LR MLE4 (top left), LR NR (top right), HR SAMOSA (middle left), HR NR (middle right) and Jason-3 (bottom). Computed on year 2024.

Ku-band SSB are centred around -10.4 cm for Sentinel-6 MF LR MLE4 and NR, -10.9 cm for HR SAMOSA and -10.5 cm for HR NR. Sentinel-6 MF SSB is in very good agreement with Jason-3, also centred around -10.4 cm.

In C-band, the average SSB is of -9.4 cm for Sentinel-6 MF and Jason-3. These values are stable over time, as shown on figure 81.

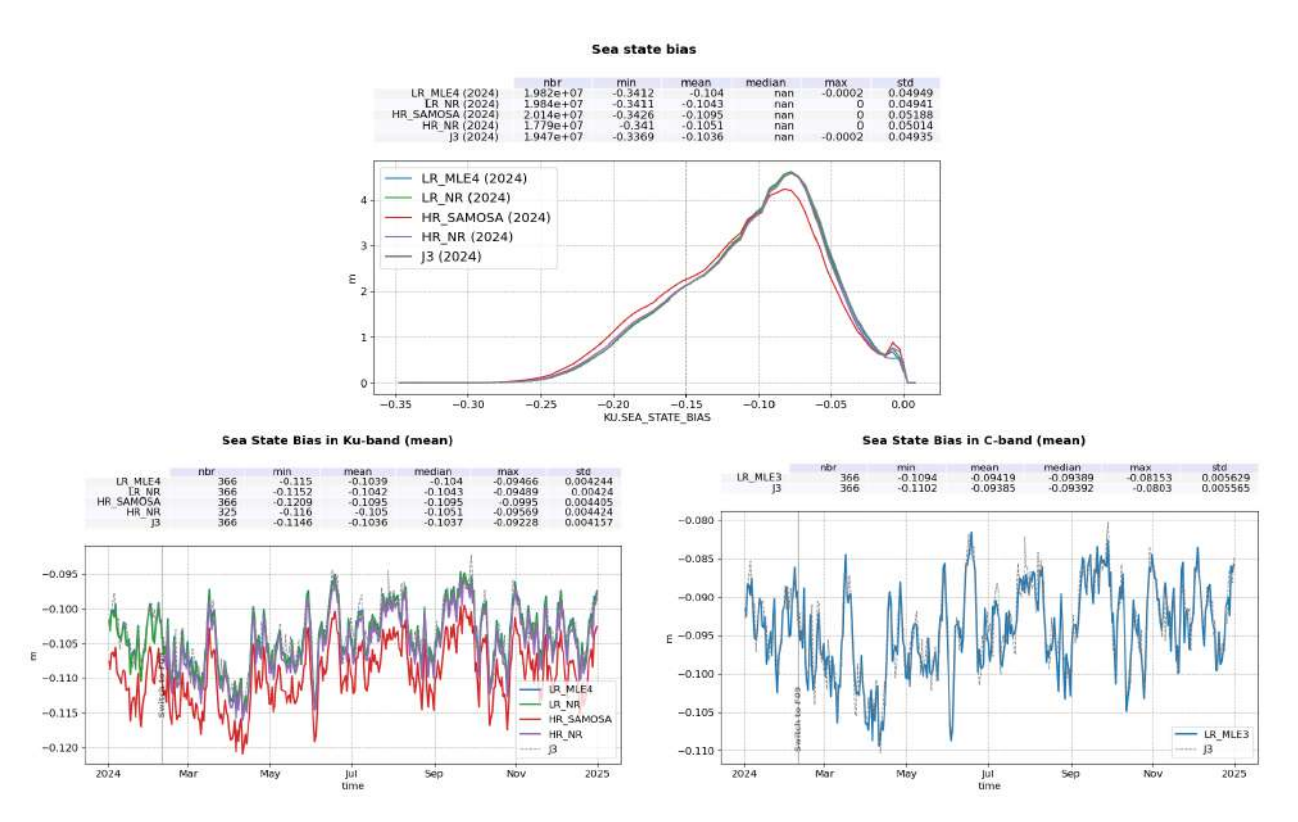


Figure 81: Top: Histogram of Ku-band SSB for Sentinel-6 MF LR MLE4 (blue), LR NR (green), HR SAMOSA (red), HR NR (purple) and Jason-3 (black), over 2024. Bottom: daily monitoring of SSB mean in Ku-band (left) and C-band (right).

Figure 82 presents the SSB differences between LR NR and LR MLE4, as well as between HR NR and HR SAMOSA. Differences are centred around -0.4 mm and 4.6 mm respectively and stable in time, but with a SWH correlation visible on the corresponding maps (bottom panels) and in the mean difference as a function of ERA 5 model SWH (top right panel), with increases of about +0.5 mm increase between 1 and 7 m SWH in LR, and +6 mm between 1 and 4 m SWH in HR.

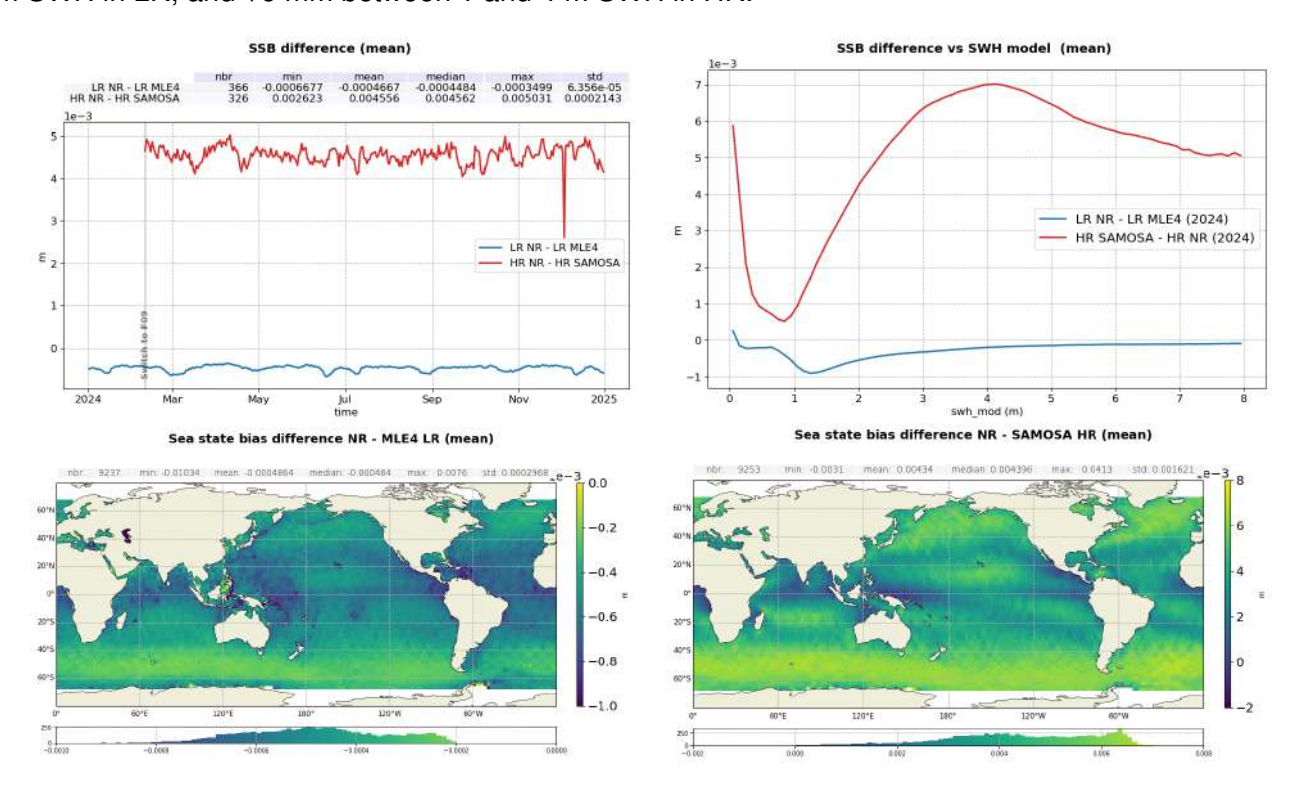


Figure 82: Monitoring per day (top left), correlation to model SWH (top right) and maps (bottom panels) of the LR NR - MLE4 and HR NR - SAMOSA SSB differences.

The monitoring of the HR - LR SSB differences is presented on figure 83. The difference is centred around -6.6 mm for HR SAMOSA - LR MLE4 and -1.5 mm for HR NR - LR NR. A small jump of about +1 mm is visible for HR SAMOSA - LR MLE4 at the PB F09 update, which is linked to the impact of the range walk application on SAMOSA. The downward peak on December 2024 corresponds to degraded HR NR SSB, due to missing MFWAM model data on the 2024/12/03.

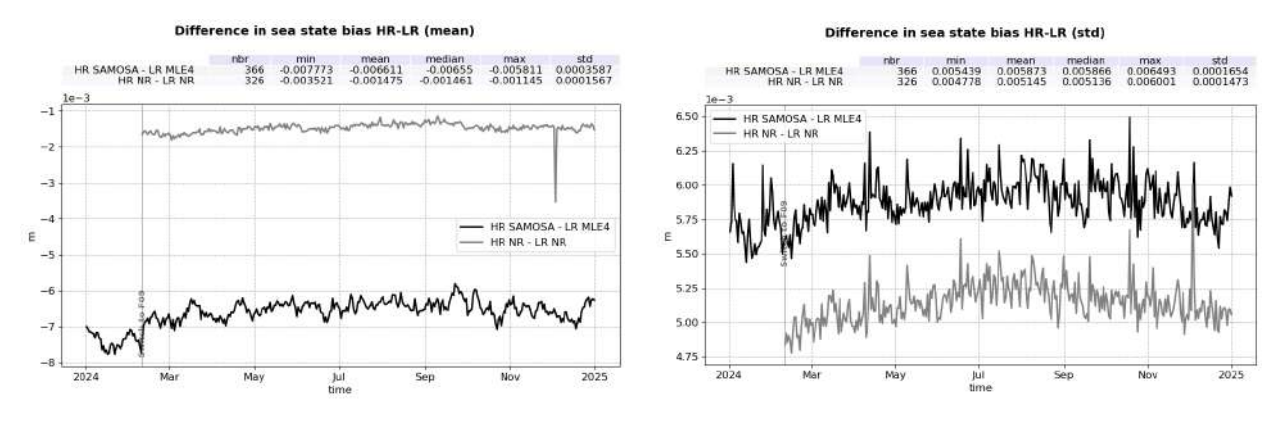


Figure 83: Mean (left) and standard deviation (right) HR-LR MLE4 SSB difference per day.

Small differences in SSB can be linked to the fact that all retrackers share the same SSB parametrization, that has been computed for Jason-3. Dedicated parametrization could improve the consistency between retrackers, especially for SAMOSA that seems to be the most impacted in terms of biases, distribution shape and correlation to SWH.

## 5.8. Ionospheric correction

Sentinel-6 MF altimeter ionosphere correction is derived from LR data, in Ku and C-band. The ionosphere correction in HR products is copied from LR products and thus identical.

The filtering process of dual-frequencies ionospheric correction is described in [16].

The monitoring of the filtered dual-band ionospheric correction is presented on figure 84, along with the corresponding distributions. There is a very good agreement between Sentinel-6 MF LR MLE4, LR NR and Jason-3 ionospheric corrections, that follow the same variations with a downward trend due to the intensification of the current solar cycle. Averages in 2024 are -6.8 and -6.7 cm for Sentinel-6 MF LR MLE4 and LR NR respectively and -6.4 cm for Jason-3, the bias being stable over time.

The geographical distribution of Sentinel-6 MF filtered ionospheric correction is presented on figure 85.

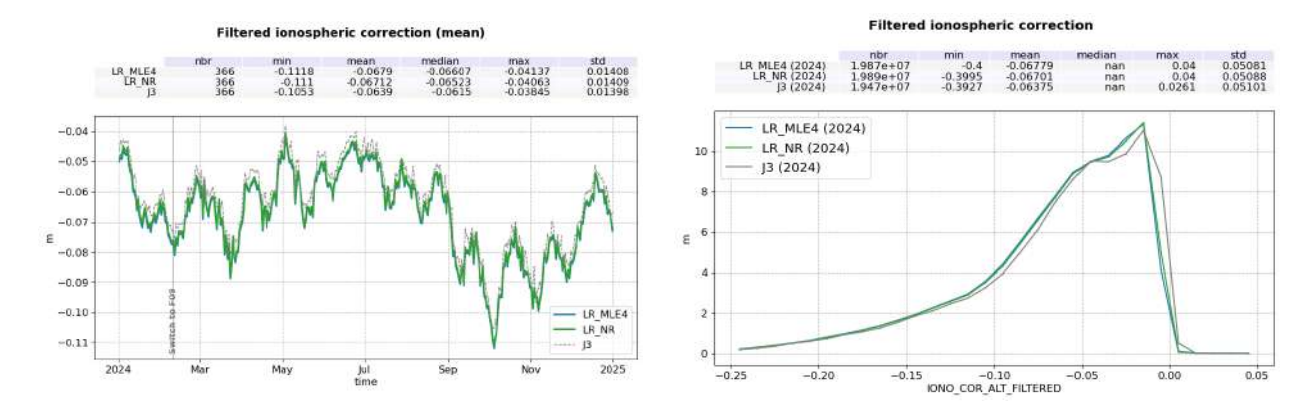


Figure 84: Monitoring of filtered ionospheric correction for Sentinel-6 MF LR MLE4 (blue), LR NR (green) and Jason-3 (black). Left: Mean per day. Right: Histogram computed 2024.

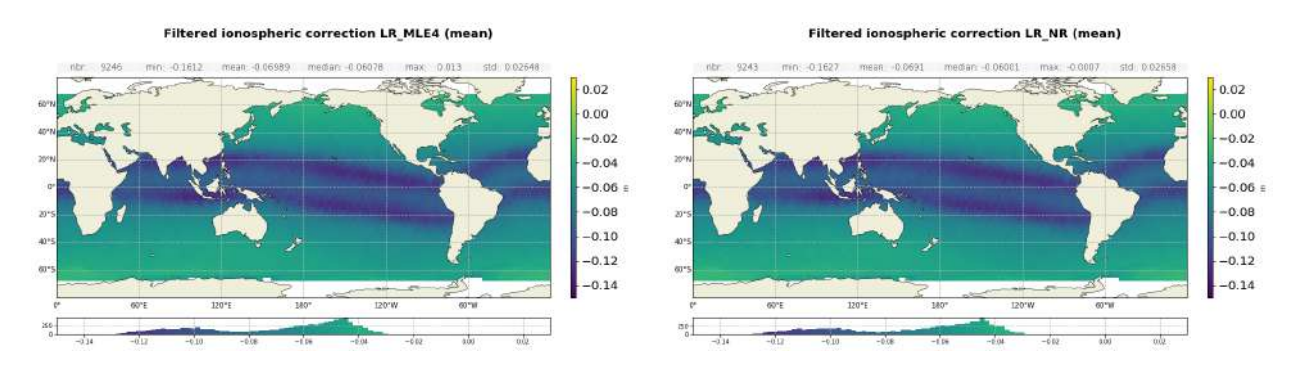


Figure 85: Maps of mean filtered ionospheric correction for Sentinel-6 MF LR MLE4 (left) and LR NR (right). Computed on year 2024.

Figure 86 presents the daily monitoring of the NR - MLE4 filtered ionospheric correction difference. A -3 mm jump is visible at the PB F09 update due to range (cf section 5.3.). In F09, the remaining bias of 0.7 mm results from the combining biases between NR and MLE4 of the range and the SSB in Ku-band.

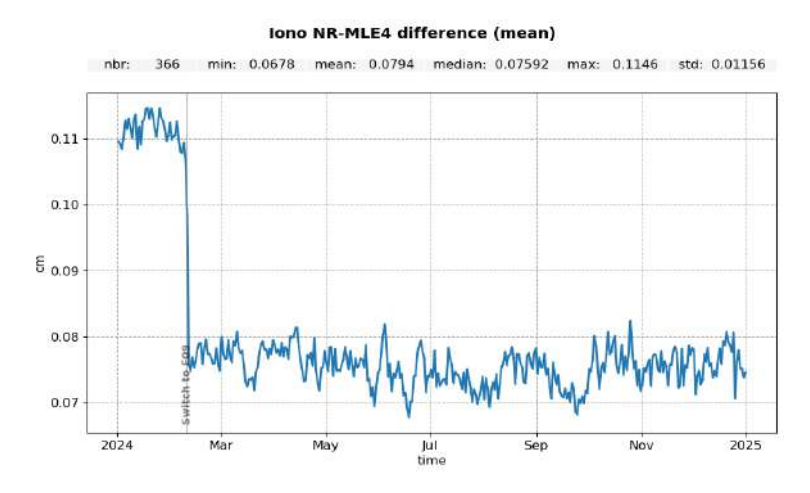


Figure 86: Time monitoring of the NR - MLE4 filtered ionospheric correction difference per day in cm.

The monitoring of the filtered minus GIM model ionospheric corrections differences are presented on figure 87. As expected, both Sentinel-6 MF MLE4 and NR curves, as well as Jason-3, follow identical variations. Sentinel-6 MF altimeter ionosphere corrections show in average a better consistency to GIM model than Jason-3. The biases with respect to GIM are centred around 1.2 cm and 1.3 cm for Sentinel-6 MF LR MLE4 and LR NR respectively, while it is of 1.6 cm for Jason-3. Spikes in the time series are due to solar storms degrading GIM ionospheric correction (2024-03-05 to 2024-03-07, 2024-05-11, 2024-10-10 to 2024-10-11, 2024-12-28 and 2024-12-30).

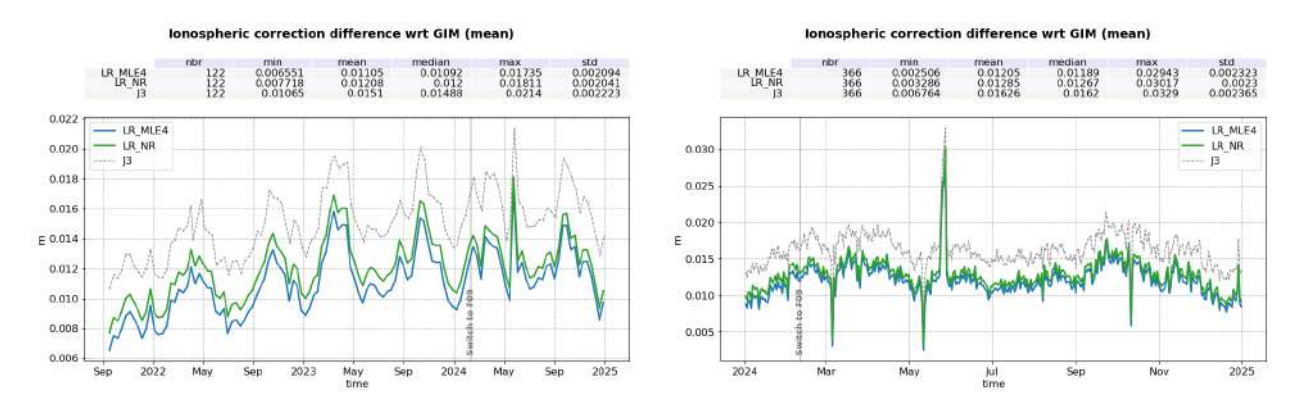


Figure 87: Mean per cycle over side B (left) and per day over 2024 only (right) filtered iono - GIM iono for Sentinel-6 MF LR MLE4 (blue). LR NR (green) and Jason-3 (black).

The maps of altimeter versus GIM difference are presented on figure 88. Sentinel-6 MF and Jason-3 present similar biases along the geomagnetic equator and their overall distribution is similar.

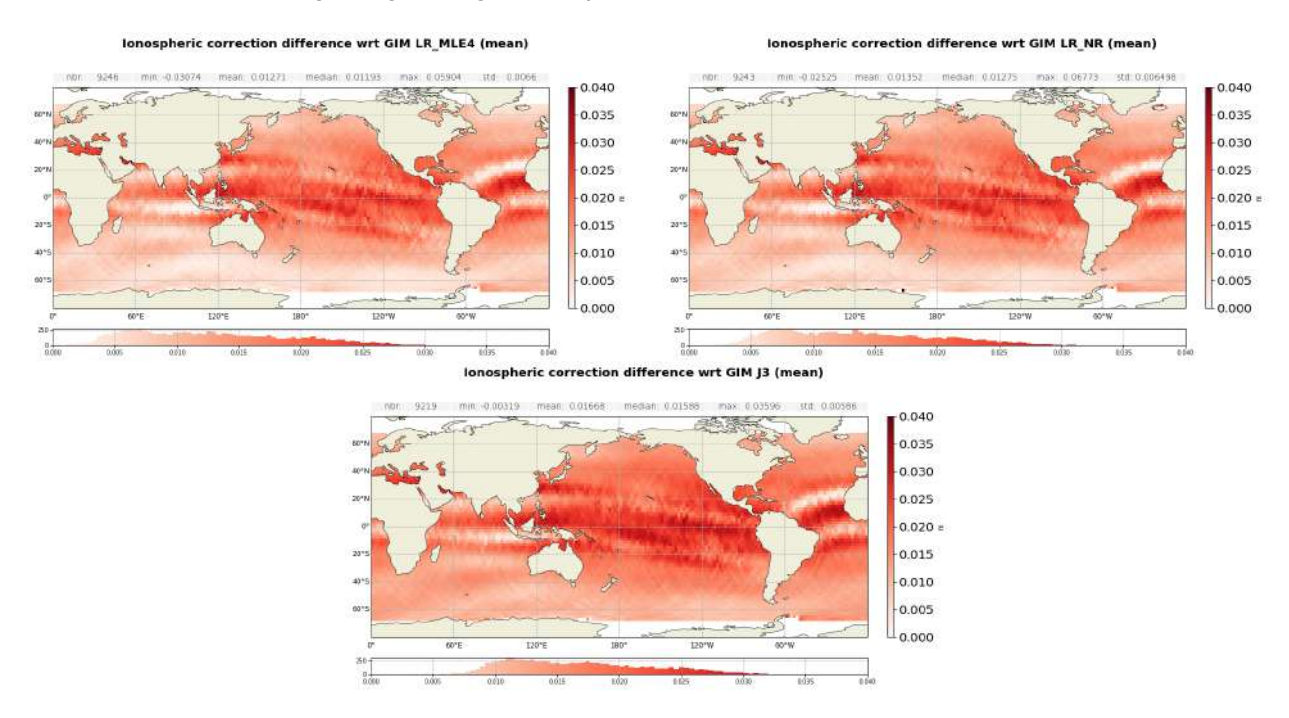


Figure 88: Maps of mean filtered ionospheric correction - GIM iono for Sentinel-6 MF LR MLE4 (left), LR NR (right) and Jason-3 (bottom). Computed on year 2024.

#### 5.9.1. Overview

In order to evaluate radiometer wet troposphere correction, liquid water content, water vapour content and atmospheric attenuation, Sentinel-6 uses a three-frequencies AMR (Advanced Microweve Radiometer) (18.7, 23.8 and 34.0 GHz), similar to the one used on Jason-3, in combination to HRMR (High Resolution Microwave Radiometer) data for more reliable measurements in coastal areas.

Note that the 23.8 GHz channel is the primary water vapour sensing channel, meaning a higher water vapour concentration leads to larger 23.8 GHz brightness temperature values. As a consequence, top right and bottom right parts of figure 89 are anti-correlated. Moreover, the 34 GHz channel and the 18.7 GHz channel, which have less sensitivity to water vapour, facilitate the removal of the contributions from cloud liquid water and excess surface emissivity of the ocean surface due to wind, which also act to increase the 23.8 GHz brightness temperature.

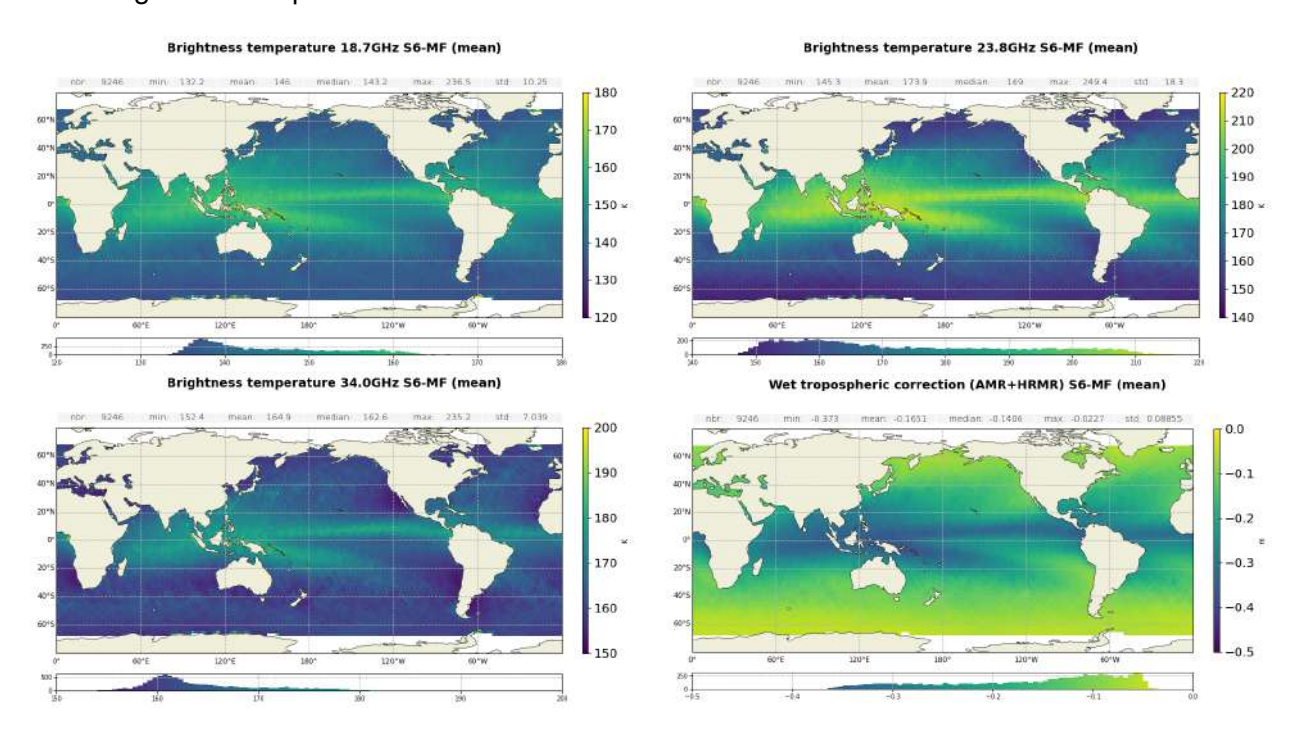


Figure 89: Maps of mean brightness temperature for channels 18.7 GHz (top left), 23.8GHz (top right), 34.0GHz(bottom left) in K and mean wet tropospheric correction (bottom right) in m. Computed on year 2023.

The distributions of the wet tropospheric corrections for Sentinel-6 MF and Jason-3 are presented on figure 90. Both distributions are similar, with Sentinel-6 MF centred around -15.6 cm and Jason-3 around -15.5 cm.

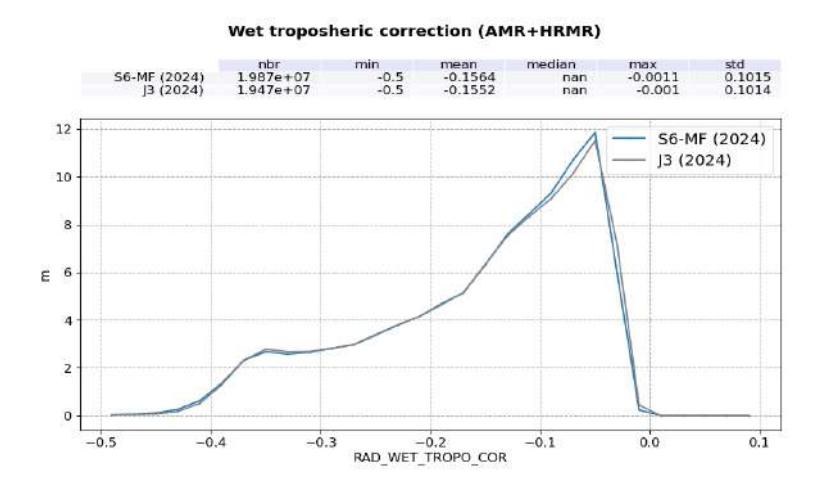


Figure 90: Histogram of wet tropospheric correction in m for Sentinel-6 MF (blue) and Jason-3 (black) computed over 2024.

### 5.9.2. Comparison with model

The wet troposphere correction computed from ECMWF model data has been used to check the Sentinel-6 MF and Jason-3 radiometer corrections. The cross-comparison between all radiometers and models available is necessary to analyse the stability of each wet troposphere correction. An overview of the wet troposphere correction importance for mean sea level is given in Obligis et al. [17].

The difference between measured and model data is computed on a daily basis and is plotted on figure 91 for Sentinel-6 MF and Jason-3 for comparisons. Over 2024, the wet tropospheric correction for Sentinel-6 MF is closer to the model than Jason-3 (0.4 mm and 2.2 mm respectively).

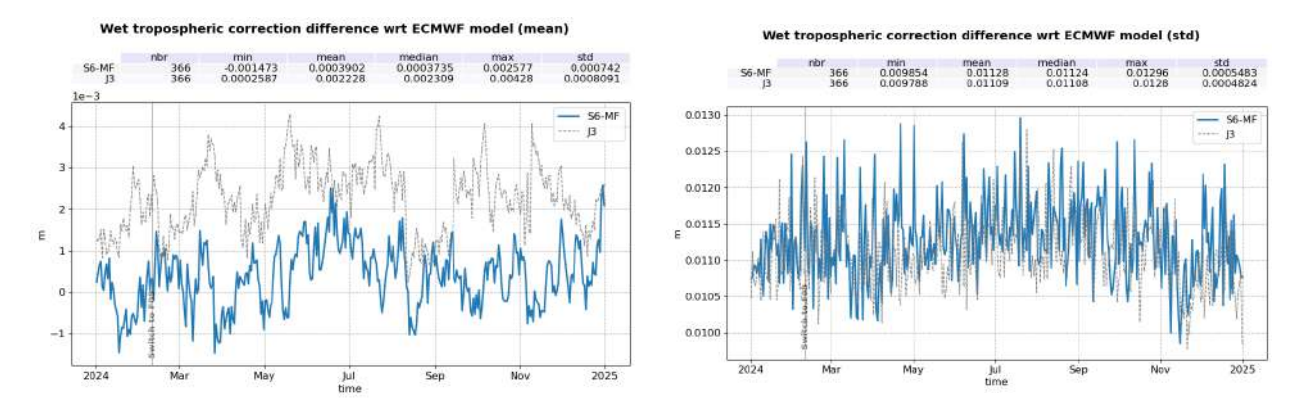


Figure 91: Mean (left) and standard deviation (right) HRMR+AMR wet troposhperic correction - ECMWF model per day for Sentinel-6 MF (blue) and Jason-3 (black).

The maps of the differences between measured and model data are presented on figure 92. They show that Sentinel-6 MF and Jason-3 present a similar overall distribution.

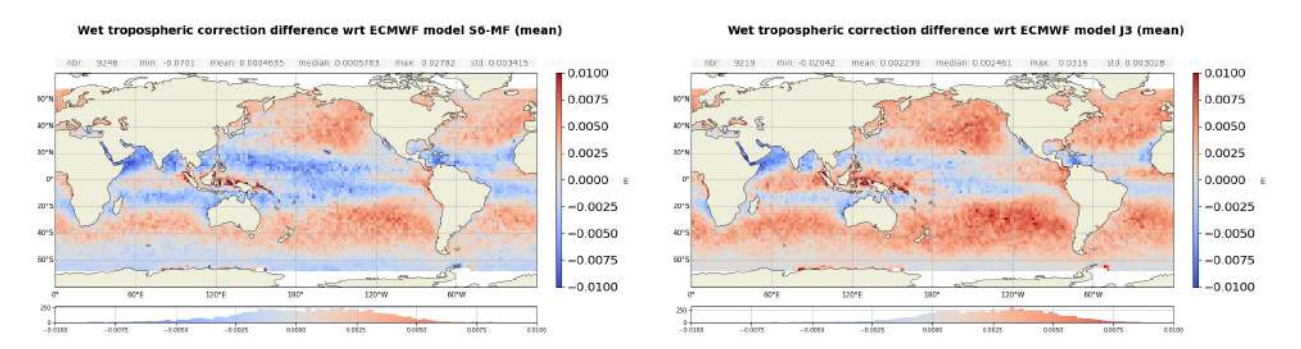


Figure 92: Maps of mean HRMR+AMR wet troposhperic correction - ECMWF model for Sentinel-6 MF (left) and Jason-3 (right).

#### 5.9.3. Comparison with AMR computed correction

HRMR radiometer is designed to support AMR radiometer with the purpose to extend microwave retrievals near the coast under cloud-free conditions. In order to estimate HRMR contribution, the wet troposphere correction computed with AMR measurement only is subtracted from the one computed with the combined HRMR+AMR measurement. The resulting daily monitoring (figure 93, left) shows that the HRMR reduces the mean wet troposphere correction by 0.2 mm. As expected, the differences are mainly located on coastal areas (figure 94), with values close to zero over open ocean, and increasing values near the coast (figure 93, right). There are also sub-millimeter variations over time.

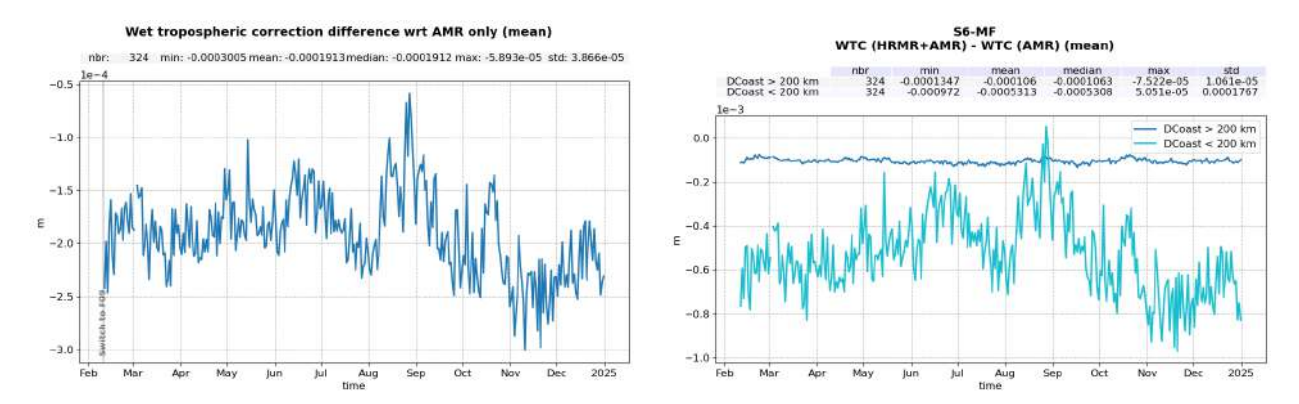


Figure 93: Mean (HRMR+AMR) - AMR wet tropospheric correction difference per day for Sentinel-6 MF in m. Right panel: computed for open ocean (distance to coast larger than 200 km) in dark blue, and for coastal measurement (distance to coast smaller than 200 km) in light blue.

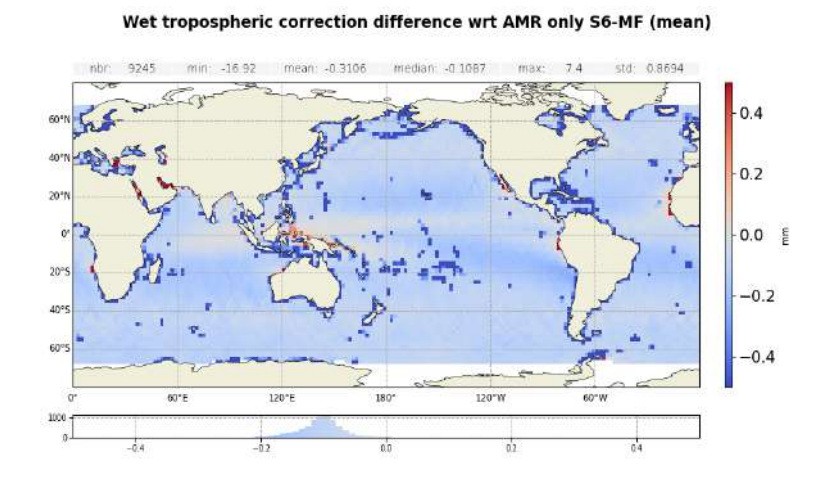


Figure 94: Map of mean (HRMR+AMR) - AMR wet tropospheric correction difference for Sentinel-6 MF in mm.

Figure 95 shows the difference of the variance of SSHA computed with combined HRMR+AMR WTC and the variance of SSHA computed with AMR only WTC as a function of the distance from coast. Variance reduction is only about  $0.35\ mm^2$  when the coast is within a radius of 150 km, and near to zero beyond.

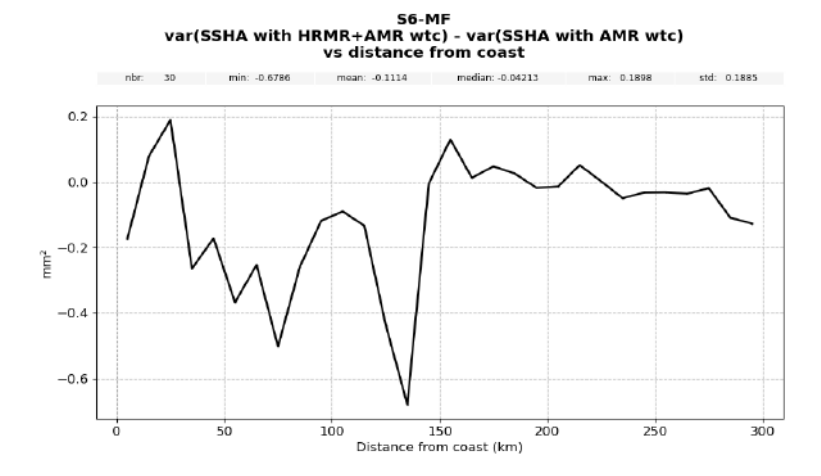


Figure 95: Variance of SSHA computed with HRMR+AMR derived WTC minus variance of SSHA computed with AMR derived WTC, as a function of the distance from the coast for Sentinel-6 MF in  $mm^2$ .

# 6 SSH crossover analysis

#### 6.1. Overview

Sea Surface Height crossover differences are the SSH differences between ascending and descending passes where they cross each other. Sea Surface Heights are computed as follow:

$$SSH = Orbit - AltimeterRange - \sum (Geophysical Corrections)$$

Crossover differences are systematically analysed to estimate data quality and the Sea Surface Height (SSH) performance. SSH crossover differences are computed from the valid data set on a one cycle basis, with a maximum time lag of 10 days, in order to limit the effects of ocean variability which are a source of error in the performance estimation. The mean SSH crossover differences should ideally be close to zero and standard deviation should ideally be small.

Nevertheless, SLA varies also within 10 days, especially in high variability areas. Therefore, an additional geographical selection - removing shallow waters, areas of high oceanic variability and high latitudes (>|50| deg) - is applied.

### 6.2. Mono-mission SSH crossovers

The cycle by cycle mean of SSH crossover differences is plotted in figure 96. All curves follow similar variations and average close to zero, Sentinel-6 MF HR SAMOSA and HR NR having a slightly higher mean at 1.0 mm and 1.2 mm respectively compared to Sentinel-6 MF LR MLE4, LR NR and Jason-3 (0.2 mm, 0.2 mm and -0.4 mm respectively).

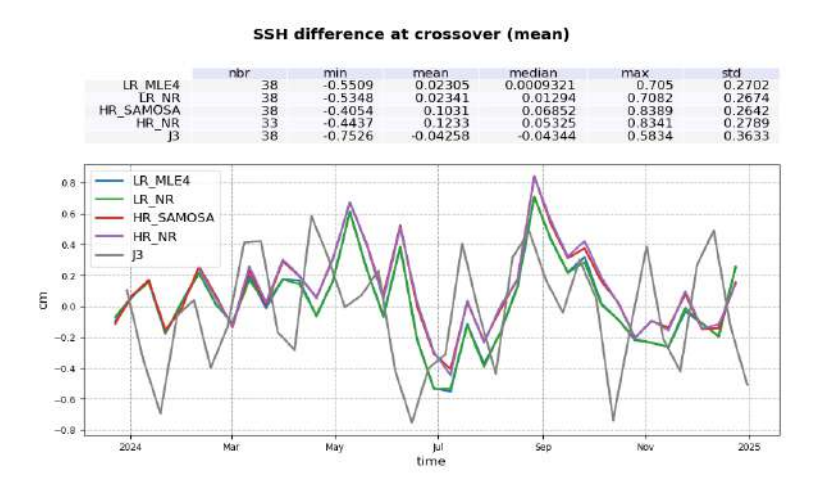


Figure 96: Mean SSH differences at crossovers by cycle for Sentinel-6 MF LR MLE4 (blue), LR NR (green), HR SAMOSA (red) and HR NR (purple) and Jason-3 (black).

Computed on year 2024.

Figure 97 presents the monitoring of the error of crossover SSH differences, for Sentinel-6 MF LR, HR, and Jason-3, computed as the standard deviation divided by  $\sqrt{2}$ . Indeed we consider the error to be measured twice, both on ascending and descending arcs, with supposedly decorrelated differences.

All datasets show very good performance, very similar and stable in time. A slight increase is observed from mid-September to mid-October due to punctual crossover points with higher SSH difference. Sentinel-6 MF LR MLE4, LR NR have similar errors, at 3.4 cm in average, while Sentinel-6 MF HR SAMOSA, HR NR and Jason-3 error is slightly lower at 3.3 cm, partially due to lower noise in HR retrievals. These results are summarized in table 6.

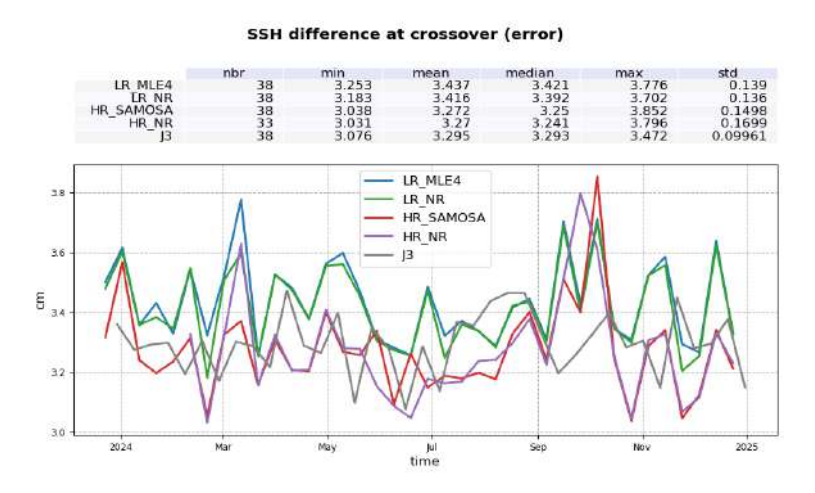


Figure 97: Error of SSH differences at crossovers by cycle for Sentinel-6 MF LR MLE4 (blue), LR NR (green), HR SAMOSA (red) and HR NR (purple) and Jason-3 (black).

Computed on year 2024.

The cyclic monitoring of the crossover differences of the SSH using model wet tropospheric correction is plotted on figure 98. The means of the Sentinel-6 MF LR MLE4, LR NR, HR NR, HR SAMOSA and Jason-3 datasets with model WTC are similar than with radiometer derived WTC, with respective differences not exceeding 0.1mm.

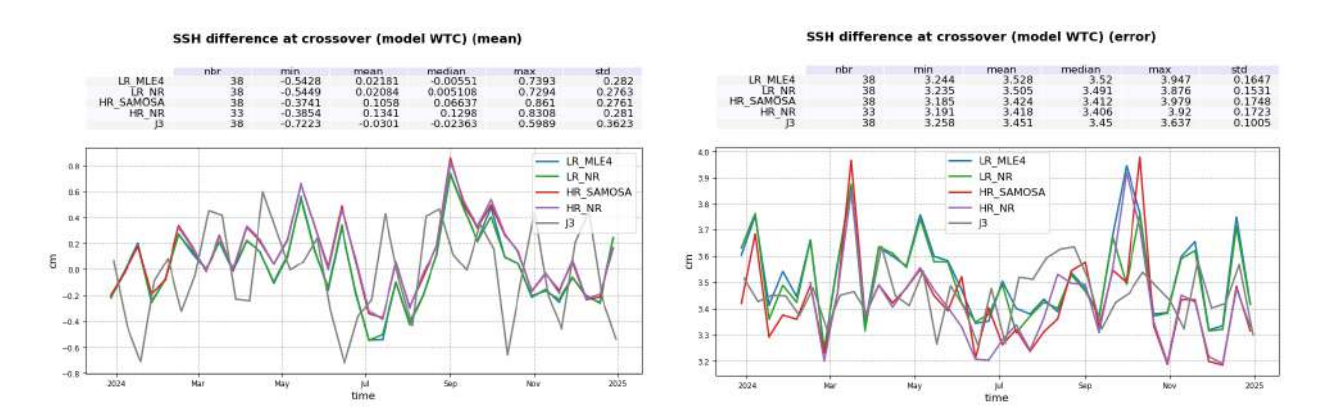


Figure 98: Mean (left) and error (right) SSH differences at crossovers by cycle for Sentinel-6 MF LR MLE4 (blue), LR NR (green), HR SAMOSA (red) and HR NR (purple) and Jason-3 (black), using model wet tropospheric correction. Computed on year 2024.

The differences in errors are slightly higher than with radiometer derived WTC, by about 0.9 mm for LR MLE4, 0.7 mm for LR NR, and 1.5 mm for HR SAMOSA, HR NR and Jason-3. This is expected as the radiometer allows a better restitution of the wet path delay in comparison to the model that is often too smooth. These results are summarized in table 6.

Mission	Mean (mm)		Error (cm)	
	Rad. WTC	Model WTC	Rad. WTC	Model WTC
Sentinel-6 MF LR MLE4	0.2	0.2	3.4	3.5
Sentinel-6 MF LR NR	0.2	0.2	3.4	3.5
Sentinel-6 MF HR SAMOSA	1.0	1.1	3.3	3.4
Sentinel-6 MF HR NR	1.2	1.3	3.3	3.4
Jason-3	-0.4	-0.3	3.3	3.5

Table 6: Mean and error of monomission SSH crossover differences for Sentinel-6 MF LR and HR and Jason-3

The maps of LR and HR SSH differences at crossovers are smooth and do not highlight any strong discrepancies between ascending and descending tracks in terms of SSH (figure 99 top panels).

The map of HR SSH difference at crossover highlight patterns correlated to along-track wind (bottom panel). It is linked to the impact of along-track wind on HR data and more particularly on HR range (see section 5.3.).

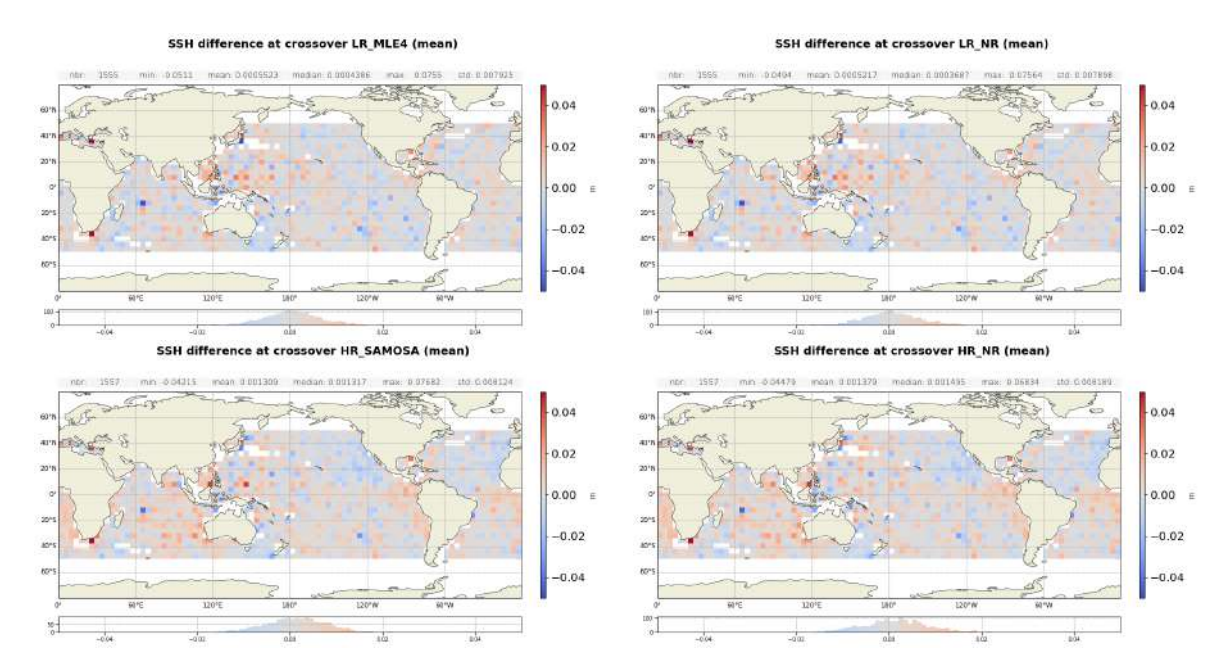


Figure 99: Maps of mean SSH differences at mono-mission crossovers in m for LR MLE4 (top left), LR NR (top right), HR SAMOSA (bottom left) and HR NR (bottom right) computed on year 2024.

### 6.3. Multi-mission SSH crossovers

Mutli-mission crossover analysis is also performed between Sentinel-6MF and Jason-3. The corresponding SSH difference is plotted on figure 100. All four cases, LR MLE4/Jason-3, LR NR/Jason-3, HR SAMOSA/Jason-3 and HR NR/Jason-3, follow the same variations, with means of -1.3 cm, -0.9 cm, -0.1 cm and -1.2 cm respectively.

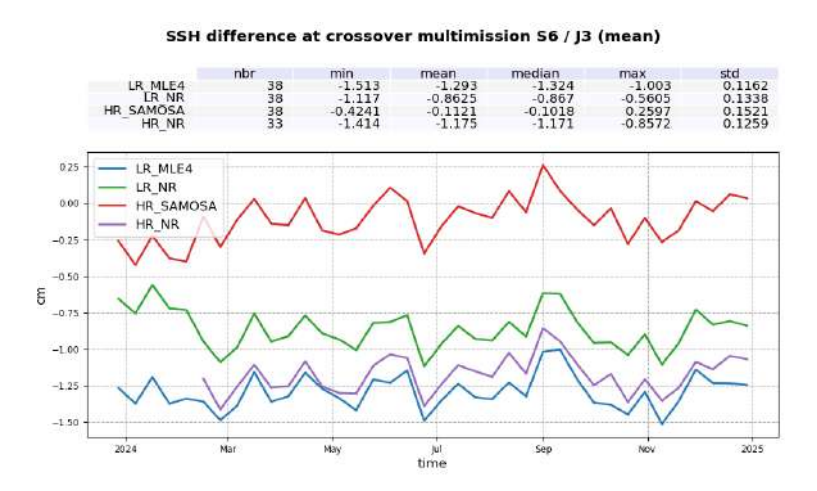


Figure 100: Mean multimission SSH differences at crossovers by cycle for Sentinel-6 MF LR MLE4/Jason-3 (blue), LR NR/Jason-3 (green), HR SAMOSA/Jason-3 (red) and HR NR/Jason-3 (purple). Computed on year 2024.

Figure 101 presents the monitoring of the standard deviation of multimission crossover SSH. All datasets show very good performance at 4.8 cm for LR retrackers and 4.7 cm for HR ones.

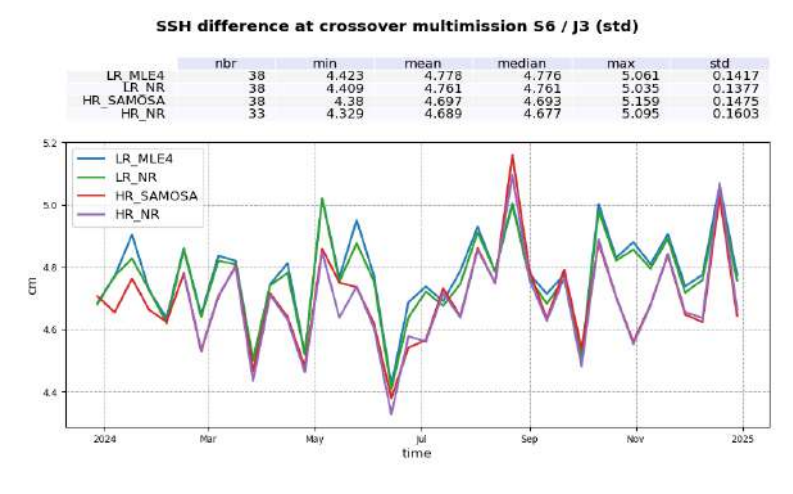


Figure 101: STD multimission SSH differences at crossovers by cycle for Sentinel-6 MF LR MLE4/Jason-3 (blue), LR NR/Jason-3 (green), HR SAMOSA/Jason-3 (red) and HR NR/Jason-3 (purple). Computed on year 2024.

The cyclic monitoring of the multimission crossover differences of the SSH using model wet tropospheric correction is plotted on figure 102. The average SSH crossover difference per cycle follows the same variation as the crossover SSH with radiometer-derived WTC, with only minor value differences. As for monomission crossover differences, however, using a wet troposphere model derived from model degrades the standard deviation of the multimission SSH crossover differences by about 1.4 cm rms in all four datasets.

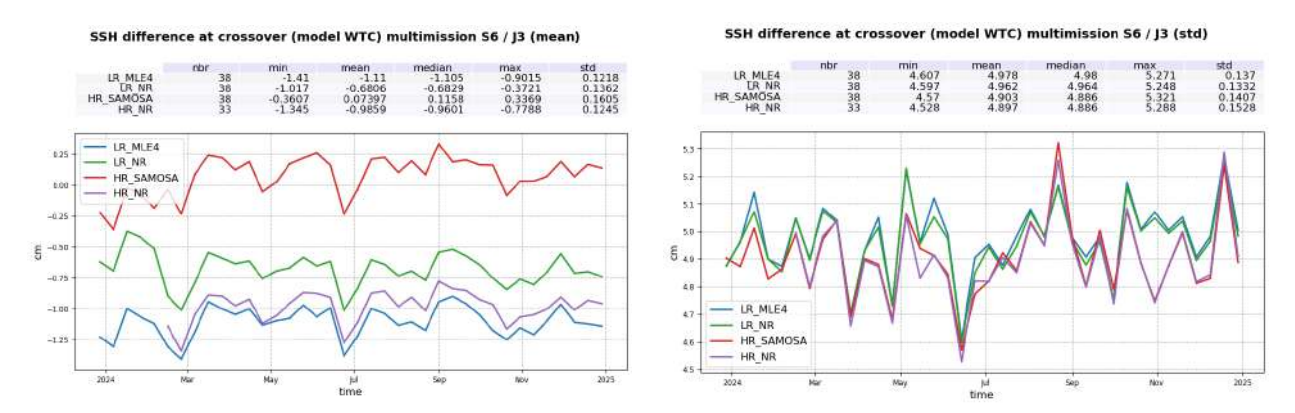


Figure 102: Mean (left) and standard deviation (right) of multimission SSH differences at crossovers by cycle for Sentinel-6 MF LR MLE4 / Jason-3 (blue), LR NR / Jason-3 (green), HR SAMOSA/Jason-3 (red) and HR NR/Jason-3 (purple). Computed on year 2024 using model WTC for SSH.

The corresponding geographical distributions and their differences are presented in figure 103.

While no significant regional pattern can be seen in the Sentinel-6 MF LR/Jason-3 SSH crossovers differences, Sentinel-6 MF HR SAMOSA/Jason-3 SSH crossovers differences are higher at high latitudes. This difference in geographical pattern in clearly visible in the bottom panel, with differences up to about 1 cm at high latitudes, while it is about -2 cm in the equatorial regions. This is expected as no skewness is used in HR SAMOSA processing, unlike for LR, HR NR and Jason-3 processing, leading to a strong correlation of the range to sea state conditions (see section 5.3.).

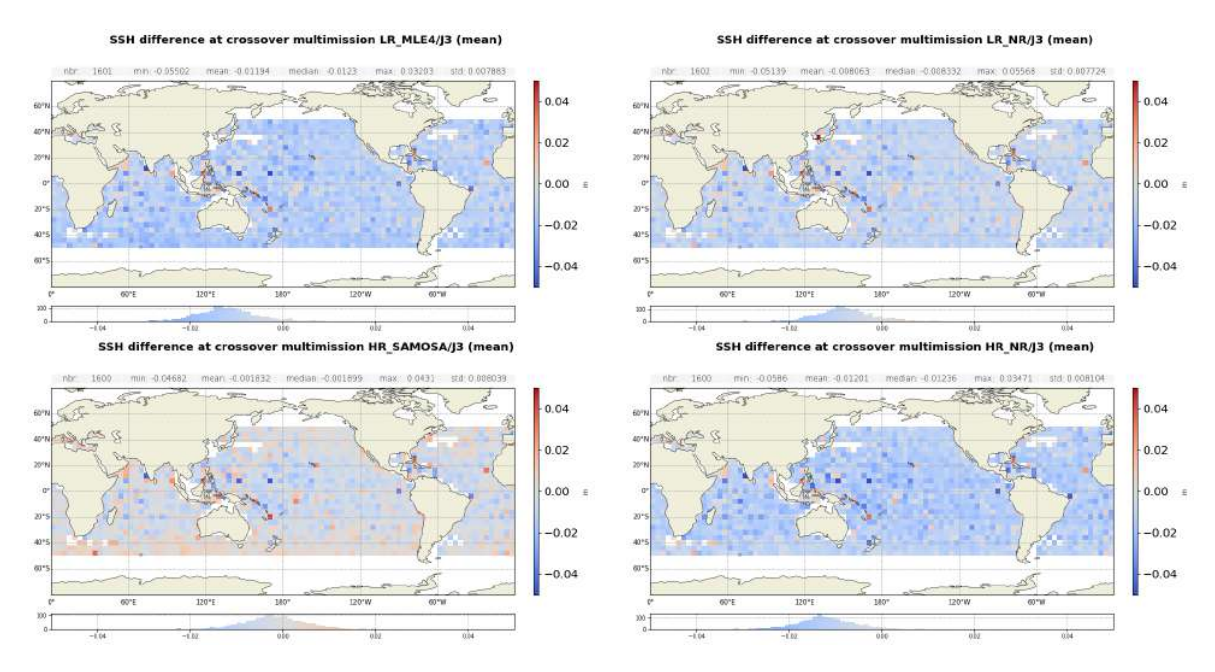


Figure 103: Maps of multimission mean SSH differences at crossovers for LR MLE4/Jason-3 (top left), LR NR/Jason-3 (top right), HR SAMOSA (bottom left) and HR NR (bottom right) computed on year 2024.

## 6.4. Pseudo time tag bias

The pseudo time tag bias  $(\alpha)$  is found by computing at mono-mission SSH crossovers a regression between SSH and orbital altitude rate  $(\dot{H})$ , also called satellite radial speed: SSH =  $\alpha\dot{H}$ . This empirical method allows us to estimate the potential real time tag bias but it can also absorb other errors correlated with  $\dot{H}$ . Therefore it is called "pseudo" time tag bias. The monitoring of this coefficient estimated at each cycle is performed for Sentinel-6 LR and HR in figure 104.

Its mean is -20  $\mu$ s for LR MLE4, -21  $\mu$ s for LR NR, 4  $\mu$ s for HR SAMOSA and 6  $\mu$ s for HR NR mode, and never exceeds a few hundreds microseconds.

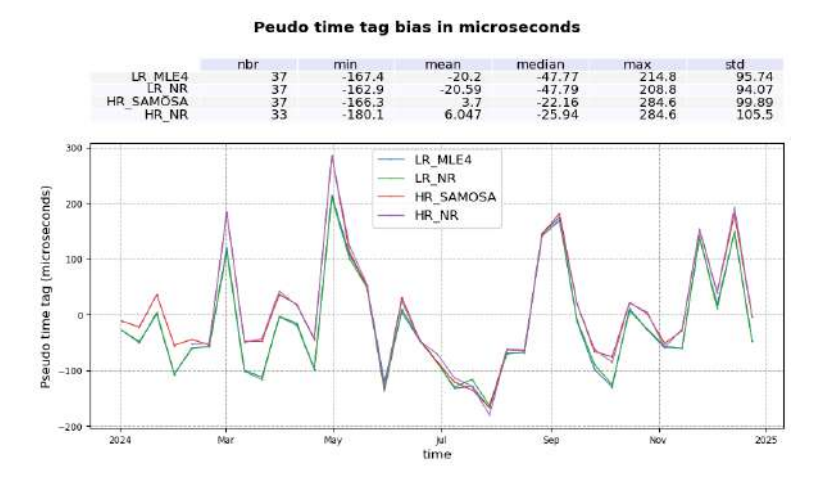


Figure 104: Pseudo time tag bias by cycle for LR MLE4 (blue), LR NR (green), HR SAMOSA (red) and HR NR (purple). Computed on year 2024.

# 6.5. Transponder analysis

An absolute calibration of the Poseidon-4 altimeter is performed over the CDN1 transponder in West Crete mountains for each descending Sentinel-6 MF pass number 18.

The range bias (see figure 105) is calculated for each waveform seeing the CalVal site by taking the difference between the transponder-altimeter distance (accurately determined using a precise positioning of the satellite and the transponder site) and the altimeter range derived from the retracking (based on a sincfunction fit) of the transponder-generated waveform. Note that the altimeter bias is further corrected for transponder and altimeter related errors, the Doppler range shift, and delays through the atmosphere.

The datation bias is also computed and presented on figure 106.

No clear trend is observed but there is remaining significant variability from a cycle to another.

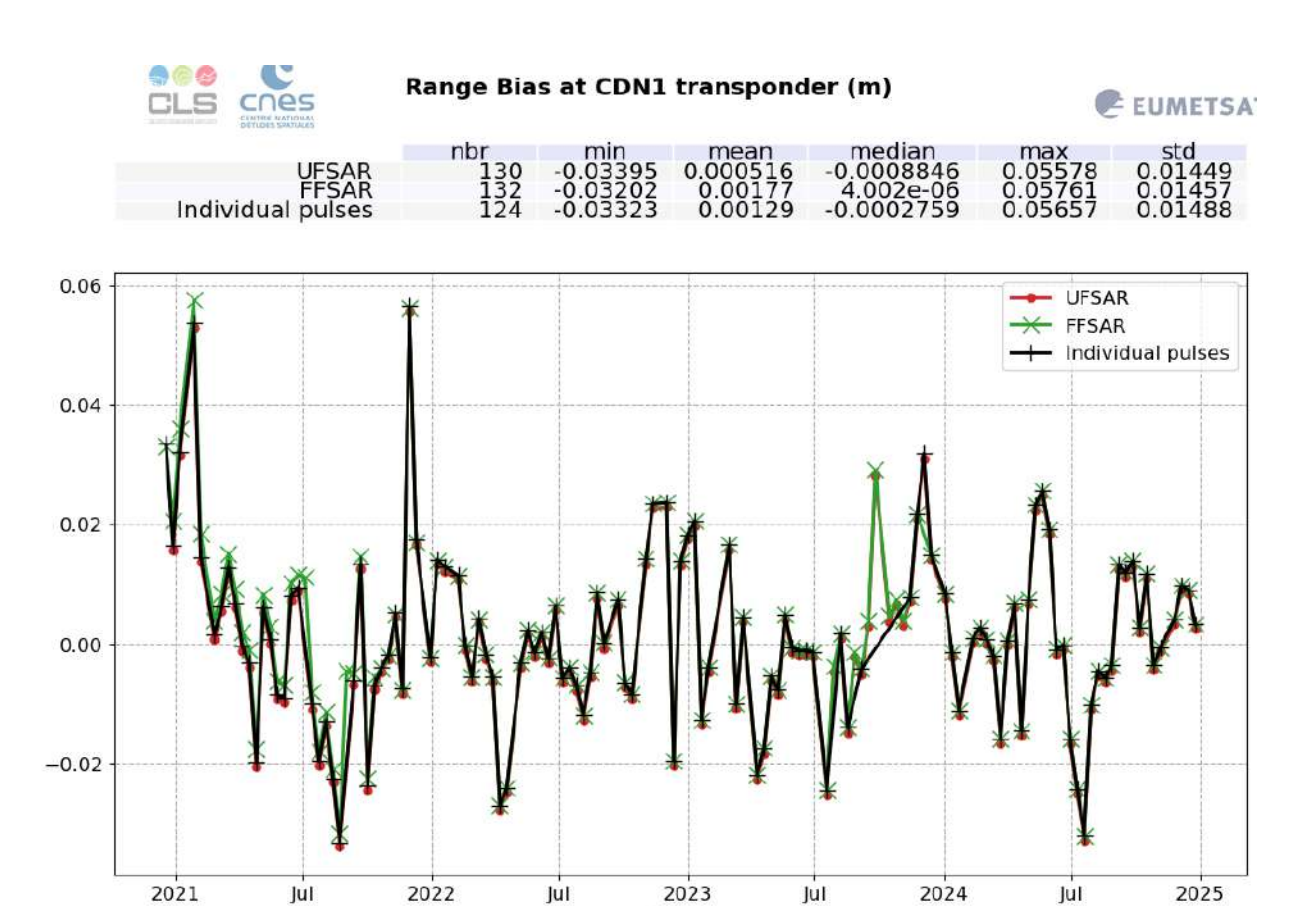


Figure 105: Monitoring of the range bias at CDN1 transponder, up to cycle 152.

time

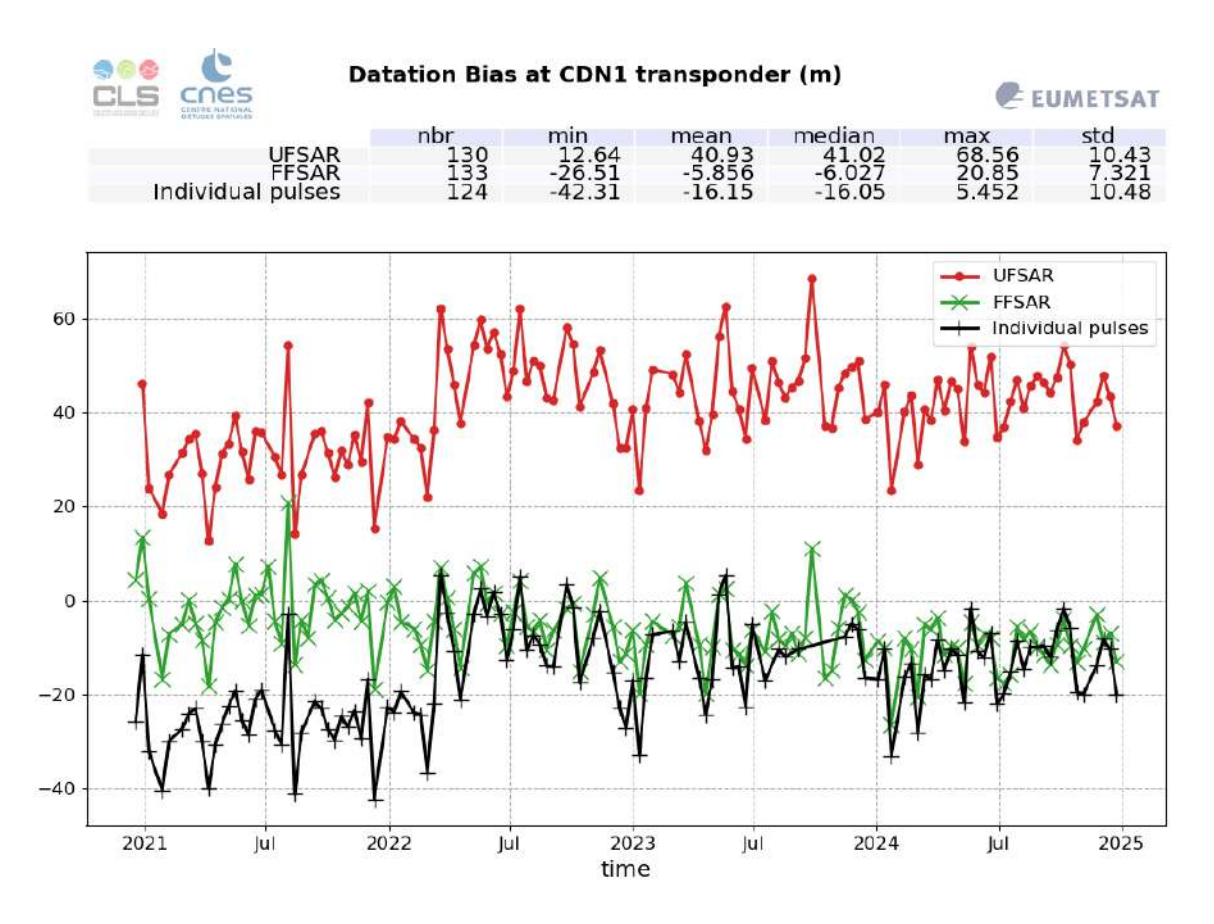


Figure 106: Monitoring of the datation bias at CDN1 transponder, up to cycle 152.

# 7 SSHA along-track analysis

#### 7.1. Overview

The Sea Surface Height Anomaly (SSHA) is the most well-known parameter estimated from altimetry. It corresponds to the elevation of sea surface, with respect to a reference called Mean Sea Surface (MSS), generated by oceanic variability and climatic phenomena (such as Gulf stream current, El Nino, ...). It is computed as follow:

$$SSHA = Orbit - Altimeter Range - \sum (Geophysical Corrections) - Mean Sea Surface$$

The details of the geophysical corrections can be found in Sentinel-6 ALT Level 2 Product Generation Specification [18].

SSHA analysis is a complementary indicator to estimate the altimetry system performance. It enables the study of the evolution of the SSHA mean (detection of jump, abnormal trend or geographical correlated biases), and also the evolution of the SSHA variance highlighting the long-term stability of the altimetry system performance.

The SSHA distributions are plotted on figure 107 for Sentinel-6 MF LR MLE4, LR NR, HR SAMOSA and HR NR as well as Jason-3. Mean values are of 5.9 cm for Sentinel-6 MF LR MLE4, 5.4 cm for LR NR, 4.7 cm for HR SAMOSA and 5.7 cm for HR NR. HR SAMOSA is very close to Jason-3 mean value (4.6 cm).

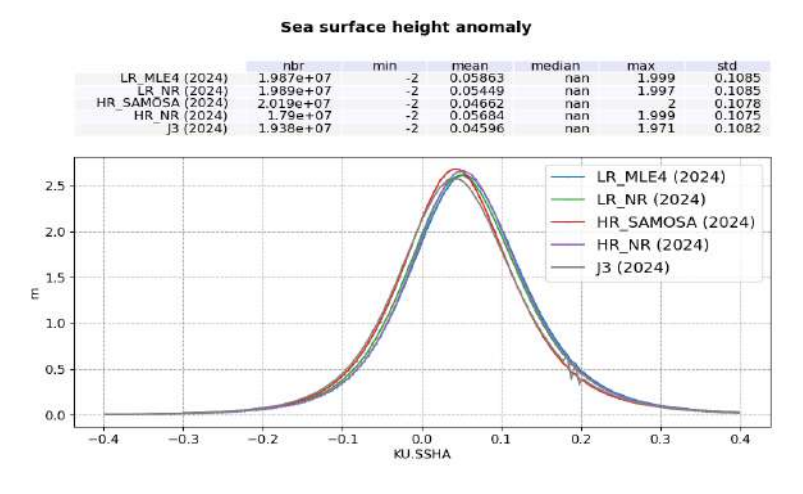


Figure 107: Histograms of SSHA in m for Sentinel-6 MF LR MLE4 (blue), LR NR (green), HR SAMOSA (red), HR NR (purple) and Jason-3 (black).

The monitoring of the SSHA daily mean is presented on figure 108, left panel. Sentinel-6 MF HR SAMOSA and Jason-3 SSHA are very close. As observed on the histogram, Sentinel-6 MF LR SSHA curves as well as HR NR are slightly higher. All curves follow similar seasonal cycles and variations.

On figure 108, right panel, is plotted the daily monitoring of the SSHA standard deviation. The Caspian Sea has been excluded from this monitoring as it creates spikes in the standard deviation on days that this region is observed, reducing the readability of the figure. All curves present similar variations, averaging at 10.4 cm for Sentinel-6 MF LR and Jason-3 and 10.3 cm for Sentinel-6 MF HR.

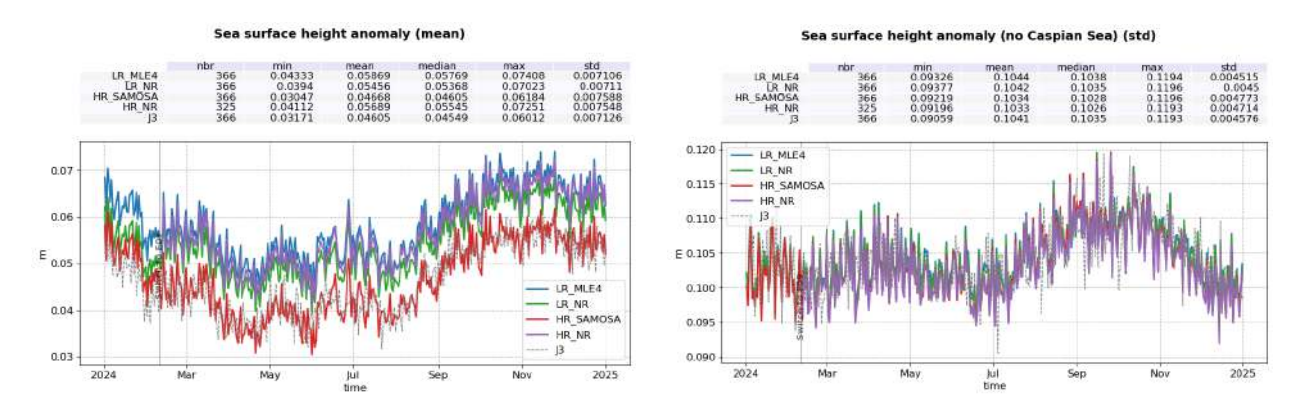


Figure 108: Mean (left) and standard deviation (right) SSHA by day for LR MLE4 (blue), LR NR (green), HR SAMOSA (red), HR NR (purple) and Jason-3 (black).

Figure 109 presents the monitoring of the SSHA computed with model WTC, both in mean (left panel), and standard deviation (right). The use of the model wet tropospheric correction has little impact on the SSHA mean (about 1 mm).

The standard deviation of the SSHA is slightly impacted as well, and increases of about 0.5 mm for all datasets when using the model WTC.

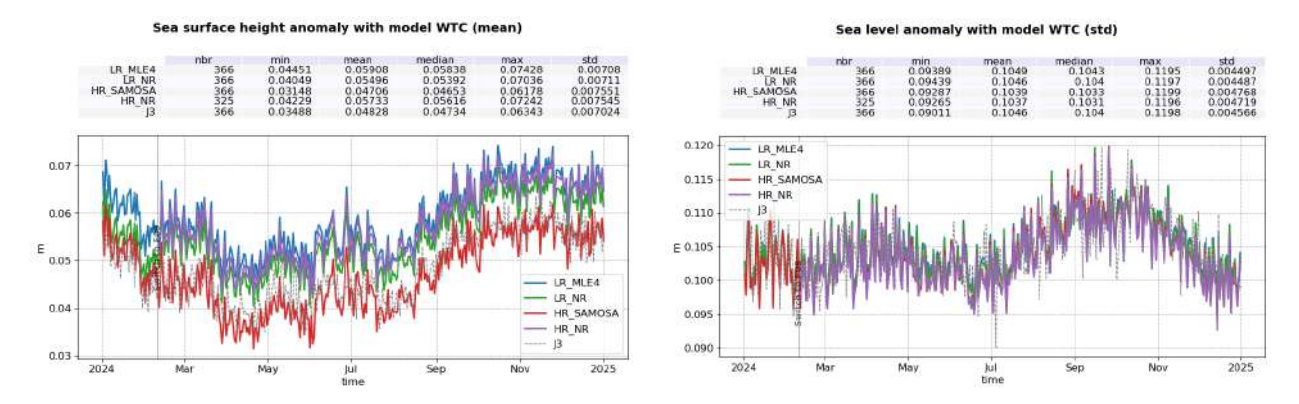


Figure 109: Mean (left) and standard deviation (right) SSHA with wet tropospheric correction from model by day for LR MLE4 (blue), LR NR (green), HR (red) and Jason-3 (black).

### 7.2. SSHA differences between LR MLE4 and NR

The LR NR - LR MLE4 differences monitoring on figure 110 shows an about 2.5mm jump at PB F09 update, resulting from range (section 5.3.) and ionosphere correction behaviours (section 5.8.). This monitoring does not allow to observe the improvement brought by the numerical retracker on the long-term stability of the sea level (no drift is observed). A longer and homogenous time series will be studied in the PB G01 full mission reprocessing planned for 2025.

The standard deviation of the LR difference (figure 110, right panel) is lower with the PB F09 update by about 1mm, highlighting the better consistency between both LR retracking compared to PB F08.

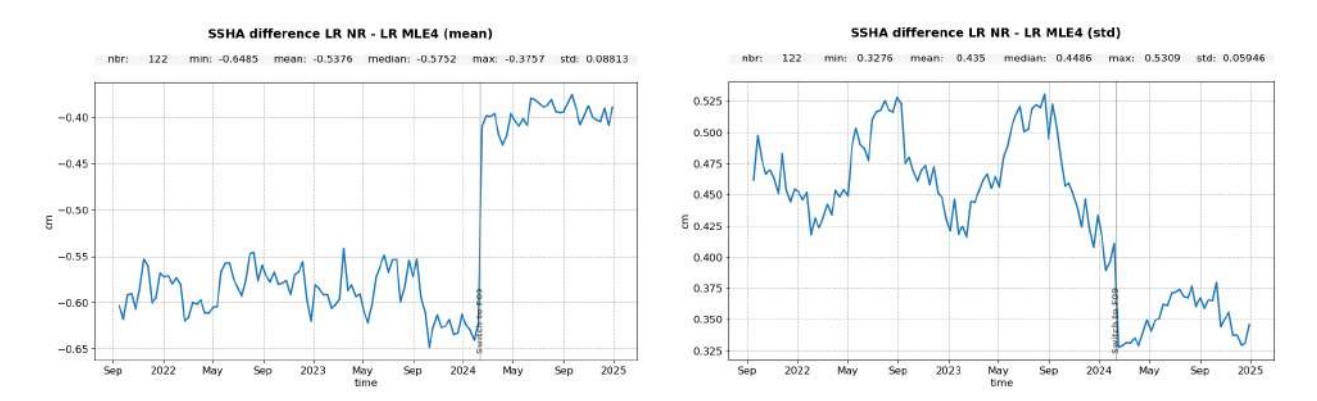


Figure 110: Time monitoring of Sentinel-6 MF LR NR - LR MLE4 SSHA in meters, without the Caspian Sea. Left: mean per cycle, Right: standard deviation per cycle.

The corresponding map on figure 111 highlights a correlation to SWH of about -7 mm between 1 and 7 m SWH. This behavior is expected and is part of the improvement brought by the numerical retracker. Indeed, contrary to MLE4, numerical retracker outputs are not corrected by instrumental LUTs, which are applied as a function of SWH values. Numerical retracker retrievals do not require instrumental LUTs and are thus not sensitive to any approximation in the LUT estimation. Analysis performed in the frame of Sentinel-6 MF commissioning activities have shown that part of the residual bias between Sentinel-6 MF LR MLE4 and Jason-3 can be attributed to Sentinel-6 MF instrumental MLE4 LUT. Using numerical retracker strongly reduces the correlation to SWH in Sentinel-6 MF LR/Jason-3 SSHA bias. Note that with PB G01, deployed in April 2025, LR MLE4 instrumental LUTs have been updated and comparison to LR NR are strongly improved.

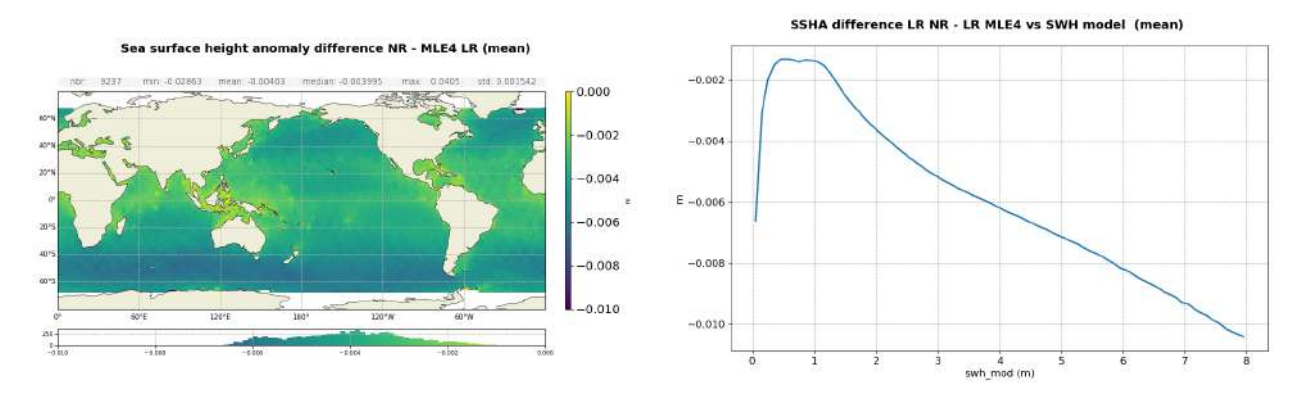


Figure 111: Map of Sentinel-6 MF LR NR - LR MLE4 SSHA in meters (left), and its mean as a function of ERA 5 model SWH (right).

The distribution of SSHA difference is presented on figure 112 for side B. LR SSHA are consistent between retrackings, with only a -4.2 mm bias between LR NR and LR MLE4. This bias is reduced almost by half in PB G01 (2025).

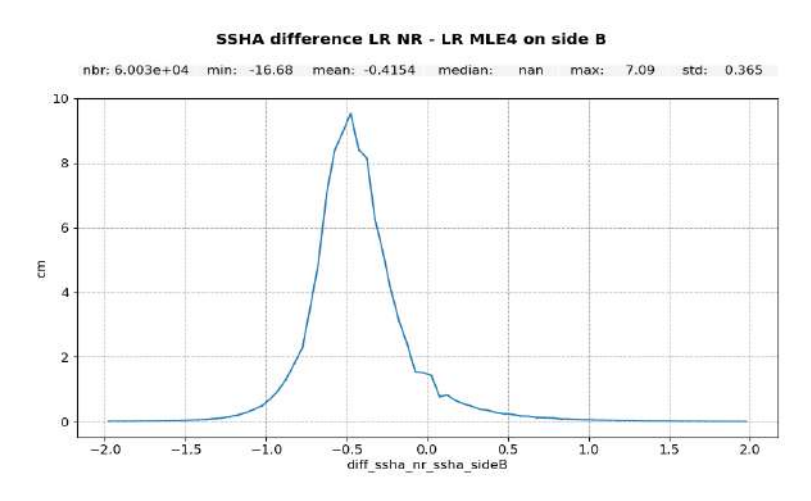


Figure 112: Distributions of Sentinel-6 MF LR NR - LR MLE4 SSHA difference for side B.

## 7.3. SSHA differences between HR SAMOSA and NR

Figures 113 and 114 show the map, correlation to SWH and distribution respectively of HR NR - HR SAMOSA SSHA differences. The bias (+1.1 cm) and correlation to SWH (+1.2 cm between 1 and 7m SWH) are higher than in LR. This is due to the skewness difference between SAMOSA and NR.

The time monitorings (computed 11 months of available F09 data, not shown) are too short to observe any impact of the numerical retracker on the long-term stability of the HR sea level. Further analysis will be conducted with the PB G01 full mission reprocessing (2025).

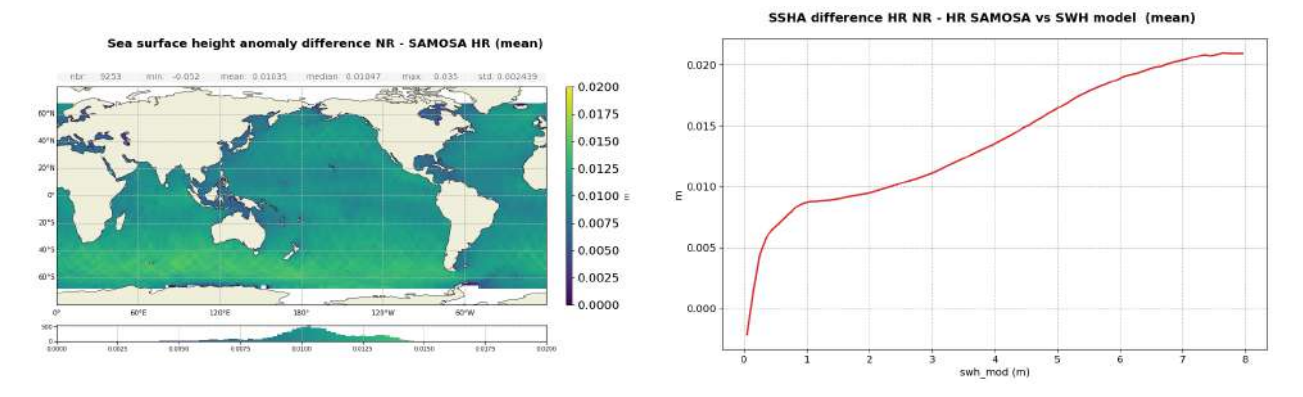


Figure 113: Map of Sentinel-6 MF HR NR - HR SAMOSA SSHA in meters (left), and its mean as a function of ERA 5 model SWH (right).

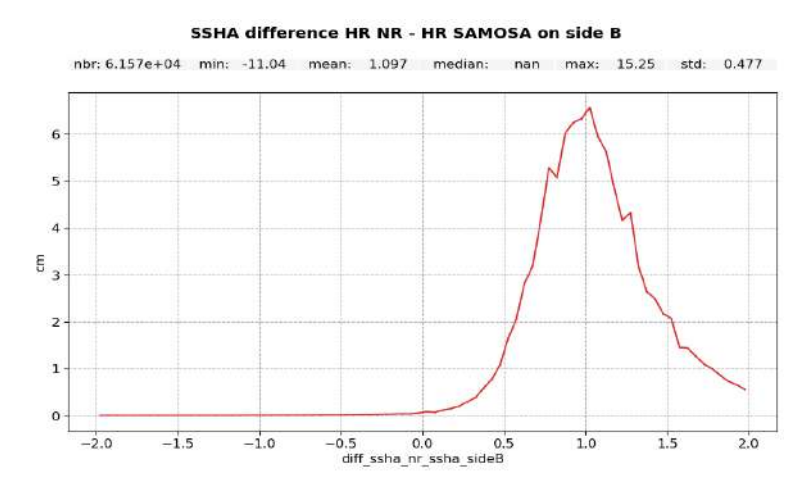


Figure 114: Distributions of Sentinel-6 MF HR NR - HR SAMOSA SSHA difference for side B.

## 7.4. SSHA differences between HR and LR

Figure 115 presents the monitoring of the HR SAMOSA - LR MLE4 (black) and HR NR - LR NR (grey) SSHA differences. These differences are centred around -1.2 cm and +0.2 cm over 2024 respectively. In the HR SAMOSA - LR MLE4 difference, a -2.5 mm jump is visible at the PB F09 update, which is caused by the range walk correction impact on range and SWH (through the SSB). On the long-term monitoring (left panel), a drift is visible on HR SAMOSA - LR MLE4 time series. It is probably caused by the evolution of the PTR shape in the azimuth direction. The range walk correction, implemented in PB F09, aims at correcting from this effect. On 2024, no significant drift is observed since PB F09 implementation, and the upcoming full mission reprocessing (2025) will help us determine if this drift was indeed linked to the absence of this range walk correction in the HR processing.

Similarly, the HR NR - LR NR difference should not present any drift on long-term monitoring, as the numerical retracker is applied on both modes and the range walk correction on HR. The PTR shape evolution should then be entirely accounted for. Once again, dedicated analysis will be performed on the upcoming reprocessing to verify this.

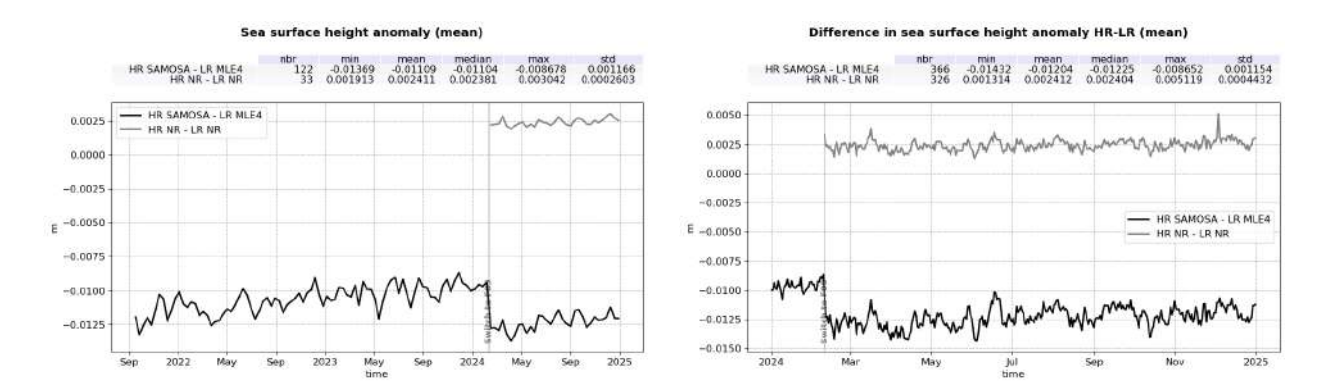


Figure 115: Mean per cycle over side B (left) and per day over 2024 (right) of the HR SAMOSA - LR MLE4 (black) and HR NR - LR NR (grey) SSHA difference.

The geographical distributions of both HR-LR SSHA differences are represented on figure 116. As expected from section 5.3., the HR SAMOSA - LR MLE4 differences are highly correlated with SWH and are mainly due to the absence of skewness parameter in the SAMOSA processing. This correlation is strongly reduced for the HR NR - LR NR difference but not null. The remaining correlation is partly due to the pulse to pulse correlation effect impacting LR data.

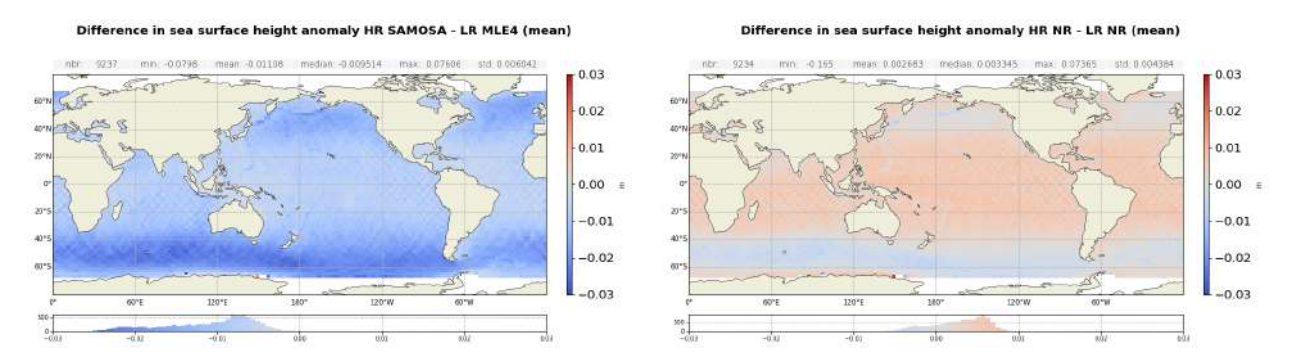


Figure 116: Maps of mean SSHA HR SAMOSA - LR MLE4 (left panel) and HR NR - LR NR (right panel) difference in meters. Computed on year 2024.

# 8 Mean Sea Level trends

## 8.1. Computation of the Mean Sea Level

The Global Mean Sea Level (GMSL) is one of the most important indicators of the climate change. In the past two decades, sea level has been routinely measured from space using satellite altimetry techniques. Since April 2022, Sentinel-6 MF satellite has taken over the responsibility as the reference mission to continue the long-term record of sea-surface height measurements. The role of Copernicus Sentinel-6 MF is not only to extend the GMSL climate record, but also to monitor the changing height of the sea surface with greater precision than before.

Over the tandem phase of Sentinel-6 MF (till cycle 051), both Jason-3 and Sentinel-6 MF satellites flew on the same ground track, only 30s apart. They therefore measured the same ocean, allowing to calibrate Sentinel-6 MF. This allowed linking precisely the MSL time series of Jason-3 and Sentinel-6 MF. The uncertainty of the bias value between the two time series is less than 1 mm. The evolution of the ocean MSL can therefore be precisely observed on a continuous basis since 1993 thanks to the 5 reference missions: TOPEX/Poseidon, Jason-1 (from May 2002 to October 2008), Jason-2 (from October 2008 to May 2016), Jason-3 (from May 2016 to April 2022) and now Sentinel-6 MF (from April 2022 onwards).

Please note that the GMSL presented on figure 117 is computed using DT2024 L2P standards, which uses LR NR data for S6-MF.

Wet troposphere correction, inverse barometer correction, GIA are applied to calculate the MSL and the data series are linked together accurately thanks to the tandem flying phases.

An exhaustive overview of possible errors impacting the MSL evolution is given in [15]. Furthermore, annual and semi-annual signals are removed from the time series and a 2-month filter is applied. For more details about Mean Sea Level (MSL) estimation method, see the dedicated report on the MSL Aviso Website: http://www.aviso.altimetry.fr/msl. This report includes the description of the Mean Sea Level indicator, the comparisons between altimetry and tide gauges measurements, the comparisons between altimetry and ARGO+GRACE measurements and specific studies linked to MSL activities.

Though mean sea level trend is globally positive, it is inhomogeneously distributed over the ocean: locally, sea level rise or decline up to  $\pm 10$  mm/yr are observed as shown on the right panel of figure 117 (note that this map of regional MSL trends is estimated from multi-mission grids (Copernicus Climate Change Service products) in order to improve spatial resolution).

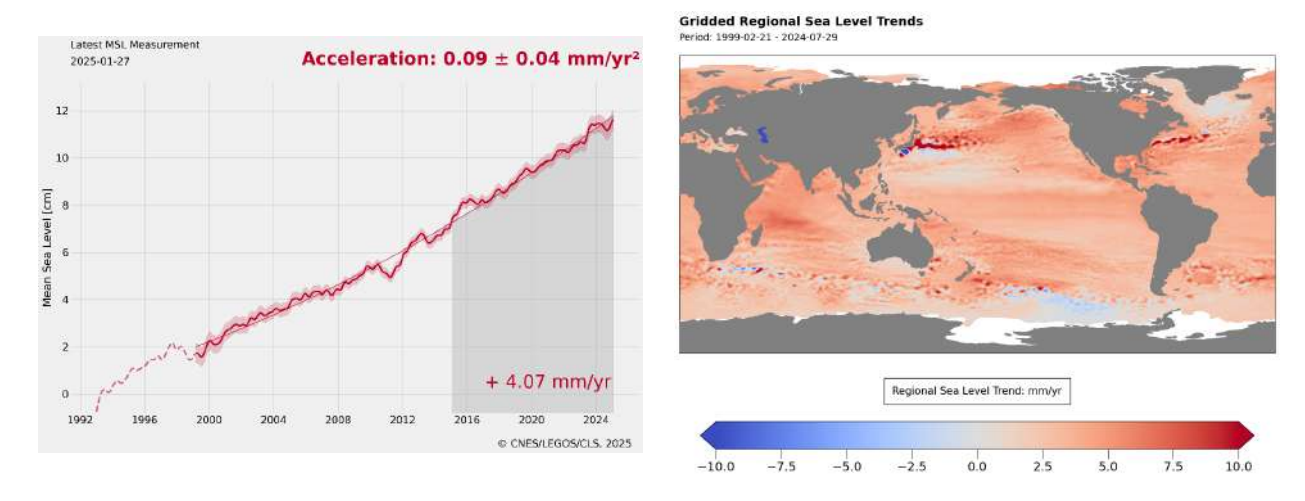


Figure 117: Global (left) and regional (right) MSL trends from 1993 onwards.

## 8.2. Comparison of LR MLE4, LR NR and HR GMSL

This section focusses on GMSL derived from Sentinel-6 MF from the switch to POS4-B to the end of 2024. The GMSL for LR (MLE4 and NR) and HR SAMOSA are plotted on figure 118, along with Jason-3 estimate over the same period. Due to its shorter time serie, GMSL for HR NR is not presented here. This GMSL is computed on a 2-months low-pass filtered data, after having removed the seasonal signals. Such computation is performed with an Ordinary Least Square (OLS) approach, using SSHA from L2 products as input. The details on the computation of the GMSL and its uncertainties are described in Guerou et al. (2022) [15].

Sentinel-6 MF LR MLE4 and LR NR show similar trends with slopes at  $4.43\pm0.95$  mm/yr,  $5.38\pm0.94$  mm/yr respectively. Over the period available here, the improvement brought by the numerical retracker in terms of long term stability cannot be demonstrated. It rather shows the stability of POS-4B retrievals. Over the same time period, Jason-3 GMSL trend is consistent with  $4.66\pm0.95$  mm/yr. HR SAMOSA trend is lower, at  $4.11\pm0.95$  mm/yr. These trends do not significantly change when using model wet tropospheric correction, as shown on the dashed curves of figure 118 and in table 7, suggesting a good stability of the radiometer-derived wet tropospheric correction. Uncertainties are given at the 1 sigma confidence level. From mid-2023 to mid-2024, oscillations can be seen on all GMSL curves. This is linked to the El Niño phenomenon occurring at this period.

Please note that the side B GMSL presented here are computed on a small timescale (less than 28 months) and therefore are impacted by correlated noise leading to significant uncertainties.

Mission/mode	Trend with Rad WTC (mm/yr)	Trend with model WTC (mm/yr)	
Sentinel-6 MF LR MLE4	$4.43\pm0.95$	$4.40\pm0.94$	
Sentinel-6 MF LR NR	$5.38 \pm 0.94$	$\textbf{5.34} \pm \textbf{0.95}$	
Sentinel-6 MF HR SAMOSA	4.11 ± 0.95	$4.08\pm0.95$	
Jason-3 MLE4	$4.66\pm0.95$	$4.87\pm0.94$	

Table 7: GMSL trend values and corresponding 1 sigma uncertainties for Sentinel-6 MF LR, HR and Jason-3 (on the Sentinel-6 MF period), with radiometer and model wet tropospheric corrections. Computed over POS4-B period, i.e. from cycle 32 onwards.

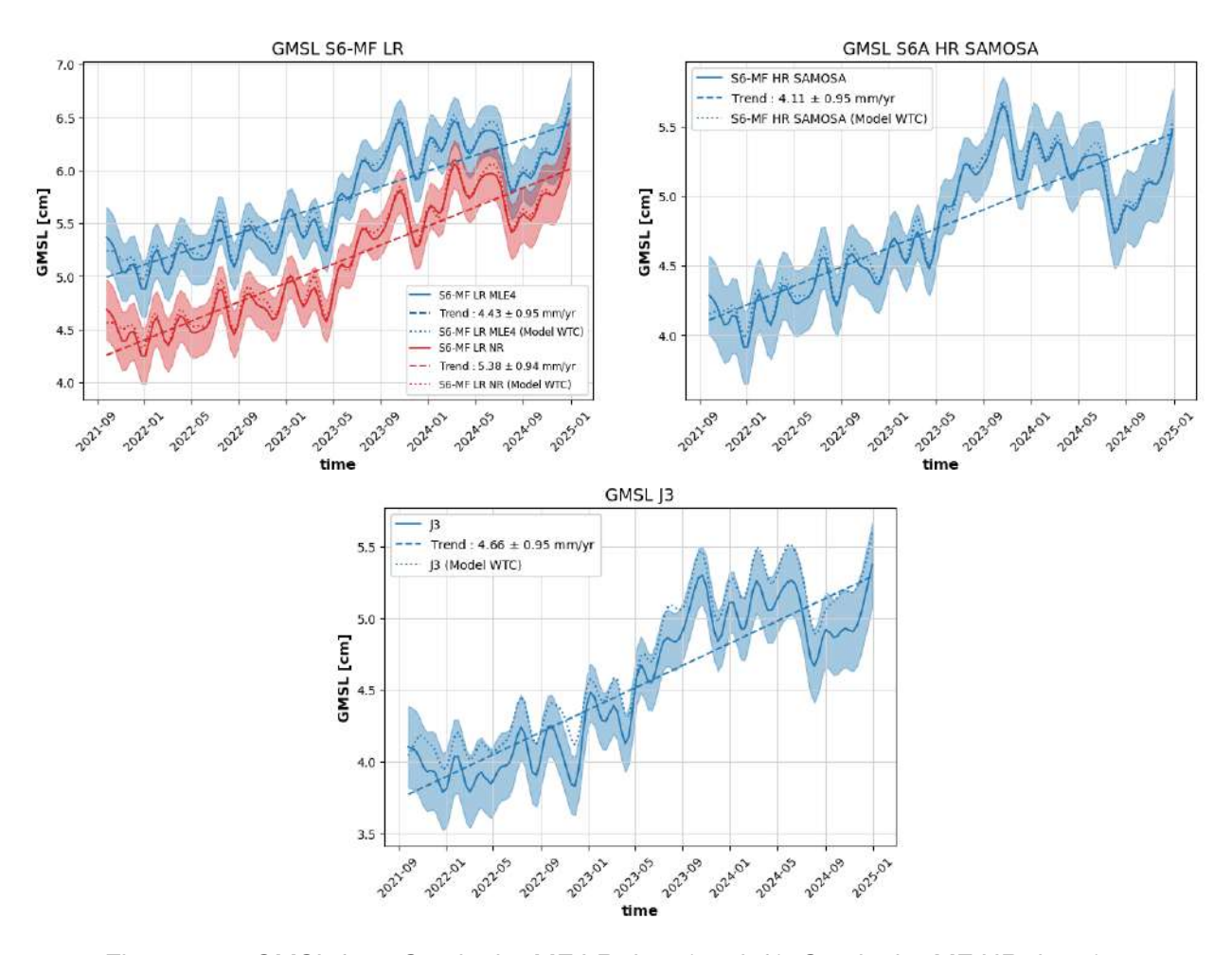


Figure 118: GMSL from Sentinel-6 MF LR data (top left), Sentinel-6 MF HR data (top right) and from Jason-3 GDR-F data with a 1.645 sigma confidence interval. Computed over Sentinel-6 MF POS4-B period, i.e. from cycle 32 onwards.

Sentinel-6 MF GMSL may be impacted by two known effects, none of which are taken into account in the uncertainties computation:

- the evolution of the PTR shape in the range direction. It impacts range (PTR dissymmetry) and SWH estimates (main lobe width) both in LR MLE4 and HR SAMOSA. Numerical retracker allows accounting for the PTR shape evolution thanks to the use of in-flight PTRs.
- the evolution of the PTR shape in the azimuth direction, impacting HR range only. It is corrected
  thanks to the range walk correction, that is available in PB F09. The impact of this correction has
  been estimated at 3.1 mm/yr, based on Dinardo 2022 study [13]. Please note that the Dinardo 2022
  study only covers the first 9 months of side B, from September 2021 to June 2022, and that values
  may be different after the second half of 2022 because of an expected ongoing stabilization.

It is important to note that these results cover a period with several version changes in the data processing (F08 patch version in October 2023 and F09 update in February 2024), and therefore must be considered carefully.

# 9 Conclusions

Sentinel-6 MF was launched on November 21th, 2020 and reaches its operational orbit on December 17th 2020. From this date until April 7th, 2022, Jason-3 and Sentinel-6 MF were flying in tandem formation, with only 30 seconds delay, before Jason-3 was moved to the interleaved orbit. On April 7th 2022, Sentinel-6 MF became the reference altimetry mission, taking on the responsibility to extend the global sea level record on the reference ground track started in 1992 by Topex/Poseidon and continued by the Jason's series.

In 2024, a new Numerical Retracking has been added to Sentinel-6 MF HR processing with PB F09. This retracker uses the in-flight PTR (similarly to LR NR), a skewness parameter identical to LR and Jason-3 (0.1) and includes a vertical wave motion correction applied to SWH. This retracker allows a better alignment of HR data to LR. Additionally, the range walk correction has been added to HR L1B processing, improving the long-term stability of both HR NR and SAMOSA outputs.

The main points of the present performance assessment are summarized below:

- Ocean data availability is excellent with a percentage above 99% in both LR and HR modes.
- Data quality is also very good with 6.4 %, 6.3 %, 4.8 % and 4.9 % of measurements not consistent with altimeter and radiometer parameters threshold criterion in LR MLE4, LR NR, HR SAMOSA and HR NR respectively.
- HR SAMOSA is impacted by the remaining effect of ocean vertical velocity. The next processing baseline G01 (deployed in April 2025) provides a correction for this effect. The absence of skewness parameter in the SAMOSA processing does not allow to properly compare HR range derived parameter to LR or HR NR or Jason-3 data.
- At crossovers, Sentinel-6 MF shows very good performance with errors on SSH differences of 3.4 cm for LR retrackings and 3.3 cm for HR retrackings. Jason-3 standard deviation is similar to HR.
- At crossovers between Sentinel-6 MF and Jason-3, SSH performance presents excellent results with an SLA bias of about -1.3 cm, -0.9 cm, -0.1 cm and -1.2 cm for LR MLE4, LR NR, HR SAMOSA and HR NR respectively.
- The time series is still too short to properly estimate the impact of NR on LR and HR SSHA. Results
  presented in section 7.4 suggest the range walk evolution deployed with PB F09 reduces the trend
  observed between HR SAMOSA and LR MLE4 observed from 2021 (figure 115). This effect will be
  further studied in the 2025 full mission reprocessing that will be performed using the PB G01.

Finally, several recommendations can be made to further refine Sentinel-6 MF data consistency and stability:

- Compute an ice flag from Sentinel-6 MF AMR and altimeter parameters as done for Jason-3.
- Update the alpha-p LUT function for HR SAMOSA retracker to account for the skewness.
- Compute WVM correction from Sentinel-6 MF parameters instead of using model.
- Compute dedicated SSB parametrizations for each retracker, especially SAMOSA.

## 10 References

## References

- [1] Sentinel-6A user handbook available at https://user.eumetsat.int/resources/user-guides/sentinel-6-altimetry-level-2-and-3-data-guide
- [2] Jason-3 product handbook available at https://www.aviso.altimetry.fr/fileadmin/documents/data/tools/hdbk\_j3.pdf
- [3] Product notice for Sentinel-6 MF Processing Baseline F08 available at: https://www.eumetsat.int/media/50743
- [4] Sentinel-6 MF F08 Reprocessing Calval Assessment available at : https://user.eumetsat.int/s3/eup-strapi-media/S6\_A\_F08\_Reprocessing\_Calval\_Assessment\_v2\_1\_c6273b0e23.pdf
- [5] Product notice for Sentinel-6 MF Processing Baseline F09 available at: https://user.eumetsat.int/s3/eup-strapi-media/Copernicus\_Sentinel\_6\_Michael\_Freilich\_Product\_Notice\_Altimetry\_V9\_a5ee70077d.pdf
- [6] 2023 Annual Report of Sentinel-6 MF validation and cross calibration activities available at : https://user.eumetsat.int/s3/eup-strapi-media/S6\_MF\_2023\_annual\_report\_v1\_2\_b5cf5f4d8b.pdf
- [7] 2023 Jason-3 annual validation report available at : https://www.aviso.altimetry.fr/fileadmin/documents/calval/validation\_report/J3/SALP-RP-MA-EA-23692-CLS-AnnualReport\_Jason3\_2024.pdf
- [8] Brown G.S., "The average impulse response of a rough surface and its application", IEEE Transactions on Antenna and Propagation, Vol. AP 25, N1, pp. 67-74, Jan. 1977.
- [9] Thibaut, P. O.Z. Zanif´e, J.P. Dumont, J. Dorandeu, N. Picot, and P. Vincent, 2002. Data editing: The MQE criterion. Paper presented at the Jason-1 and TOPEX/Poseidon Science Working Team Meeting, NewOrleans (USA), 21-23 October.
- [10] Alejandro Egido, Christopher Buchhaupt, François Boy, Claire Maraldi et al.: Correcting for the Vertical Wave Motion Effect in S6-MF Observations of the Open Ocean. Oral Presentation, Ocean Surface Topography Science Team Meeting 2022, Venice. Available at: https://ostst.aviso.altimetry.fr/fileadmin/user\_upload/OSTST2022/Presentations/IPM2022-A\_Significant\_Wave\_Height\_Correction\_to\_Account\_for\_Vertical\_Wave\_Motion\_Effects\_in\_SAR\_Altimeter\_Measurements.pdf
- [11] Emeline Cadier, Bastien Courcol, Pierre Prandi, Victor Quet, Thomas Moreau, Claire Maraldi, François Bignalet-Cazalet, Salvatore Dinardo, Cristina Martin-Puig, Craig Donlon: Assessment of Sentinel-6MF low resolution numerical retracker over ocean: continuity on reference orbit and improvements, Advances in Space Research, Volume 75, Issue 1, 1 January 2025, Pages 30-52
- [12] Raynal et al, Lessons learned from Sentinel SARM missions in preparation of Jason-CS. Oral Presentation, Ocean Surface Topography Science Team Meeting 2019, Chicago
- [13] Dinardo S. poster, Sentinel 6 MF Poseidon 4 main results from the first year of mission from the S6PP LRM and UF SAR chain , OSTST 2022
- [14] Boy F., Callahan P., Desjonqueres J. D., Egido A., Smith W. H. F., Fornari M., Martin-Puig C. (2022): High-Level Instrument Processing Summary for Jason 3 and Sentinel-6 Michael Freilich Tandem Phase. Oral Presentation, Ocean Surface Topography Science Team Meeting(Virtual). Available on-line at https://ostst.aviso.altimetry.fr/fileadmin/user\_upload/OSTST2022/presentations\_mars2022/01-Jason3andSentinel-6MFTandemPhaseInstrumentProcessing\_20220321.pdf

- [15] Guérou, A., Meyssignac, B., Prandi, P., Ablain, M., Ribes, A., and Bignalet-Cazalet, F.: Current observed global mean sea level rise and acceleration estimated from satellite altimetry and the associated uncertainty, EGUsphere [preprint], https://doi.org/10.5194/egusphere-2022-330, 2022.
- [16] Nencioli Francesco, Roinard Hélène, Bignalet-Cazalet Francois. 2021. Filtering ionospheric correction from altimetry dual-frequencies solutions. DOI 10.24400/527896/a02- 2021.001. Available at https:// www.aviso.altimetry.fr/fileadmin/documents/data/tools/NT-Nencioli\_FilteredIonosphericCorrection.pdf
- [17] Obligis, E., L. Eymard, M. Ablain, B. Picard, J.F. Legeais, Y. Faugere and N. Picot, 2010. The wet tropospheric correction for altimetry missions: A mean sea level issue. Oral presentation at OSTST meeting, Lisbon, Portugal.
- [18] Sentinel-6 ALT Level 2 Product Generation Specification available at https://user.eumetsat.int/s3/eup-strapi-media/Sentinel\_6\_Jason\_CS\_ALT\_Level\_2\_Product\_Generation\_Specification\_L2\_ALT\_PGS\_V5\_09f3679da5.pdf
- [19] Collard, F., 2005. "Algorithmes de vent et période moyenne des vagues jason à base de réseaux de neurones." Boost Technologies, BO-021-CLS-0407-RF, 33 pp.